THESIS REPORT

Master's Degree

Design of a Microprocessor-Based Adaptive Control System for Active Vibration Compensation Using PMN Actuators

by G.R. Dold
Advisor: G.M. Zhang

M.S. 96 -4

Sponsored by
the National Science Foundation
Engineering Research Center Program,
the University of Maryland,
Harvard University,
and Industry

Abstract

Title of Thesis:	Design of a Microprocessor-Based Adaptive Control System for Active Vibration Compensation Using PMN Actuators
Name of degree candidate:	George Raphael Dold
Degree and Year:	Master of Science, 1996
Thesis directed by:	Dr. Guangming Zhang, Associate Professor, Department of Mechanical Engineering, and Institute for Systems Research

This thesis is written to address a pressing need in vibration control for machine tools. Machine tools are the platform of machining operations. Precision machining has been the focus to enhance product quality and improve productivity in every sector of the U.S. industry to maintain its competitiveness in the world market.

A mechatronic system is employed in this thesis investigation, incorporating both mechanical and electronic aspects. This thesis focuses on the design of a control system architecture that features a closed feedback loop involving the machining process, a variable-impedance transducer, microprocessor-based parameter adjustment mechanisms, and PMN actuctors. The designed control system serves as a critical part to ensure the success of a previously designed tool post structure. Three basic system components are a sensing system, a phase-shift manipulator and a self-tuning gain adapter. In the sensing system, the high precision variable impedance tranducer detects the tool displacement in micro-scale. Recognizing the time delay between the control action and the detected tool

vibratory motion, an innovative approach to use phase-shift to replicate the time delay is formulated. An information model is incorporated to manipulate the needed phase shift in real time. To balance the need between maintaining system stability and achieving maximum vibration attenuation, a self-tuning mechanism is employed to adjust the level of control energy supplied by the power amplifier to the PMN actuators. Regression analysis is utilized to obtain an empirical relationship between the measured tool vibratory magnitude and the appropriate actuation, thus completing an adaptive control loop. The control system realization, both hardware and software, is completed in this thesis work with success.

Initial results from this thesis investigation have been fruitful. Significant findings include: PMN actuators are excellent electro-mechanical devices for active vibration control; phase shift and self-tuning are two unique mechanisms in controlling time delay and magnification gain; and the microprocessor-based controller developed in this thesis work is a great success and signifies the importance of interdisciplinary research across the mechanical and electrical engineering domains.

Design of a Microprocessor-Based Adaptive Control System for Active Vibration Compensation Using PMN Actuators

by

George Raphael Dold

Thesis submitted to the Faculty of the Graduate School
of The University of Maryland in partial fulfillment
of the requirement for the degree for
Master of Science
1996

Advisory Committee:

Associate Professor Guangming Zhang, Chairman / Advisor
Assistant Professor B. Balachandran
Professor James W. Dally
Professor Andre Tits

DEDICATION

To my father, who always told me not to just think but to know,

and my mother who showed me what patience and love are all about

ACKNOWLEDGMENTS

I would like to sincerely thank Professor Guangming Zhang for his guidance and support throughout this research. I would also like to thank the faculty members at the University of Maryland, especially Professor James W. Dally, Assistant Professor B. Balachandran, and Professor Andre Tits for serving on my committee, and Professor Magrab.

I would also like to thank the members of the Advanced Design Manufacturing Laboratory, especially Huynh Luu, for providing numerous forms of assistance during my research.

I would like to thank Bruce Smith, at the National Institutes of Health, for his dedication in my learning process, and the other members of the Research Services Branch for all of their moral support.

Last but not least, I would like to thank all of my friends for the support they have given me over the years. Thank You!

TABLE OF CONTENTS

List of Tables vii

List of Figures viii

1. Introduction 1

1.1 Background 1

1.2 Scope of Thesis 2

1.3 Outline of Thesis Presentation 4

2. Literature Survey 6

2.1 Introduction 6

2.2 Machining Operations 6

2.3 Dynamics of Machining Systems 7

2.3.1 Derivation of Chatter Loop 8

2.3.2 Cutting Process Equation 8

2.3.3 Vibration and Chatter 9

2.4 Smart Material Actuators 12

2.4.1 Electrostrictive Characterization 13

2.4.2 Actuator Design 15

2.5 Control Systems 16

2.5.1 Open-Loop Control Systems 16

2.5.2 Closed-Loop Control Systems 16

2.5.3 Adaptive Control 17

2.6 Configuration of the Smart Tool Post Structure 18

3. Basic Adaptive Control Methodology **22**

3.1 Introduction 22

3.2 Fundamentals of the Control System Design 22

3.2.1 Design Objectives 22

3.2.2 Destructive Interference 23

3.3 Framework of the Control System Design 28

3.3.1 Design of Sensing System 29

3.3.1.1 Accelerometers and Integrators 31

3.3.1.2 Strain Gage Displacement Sensor 36

3.3.1.3 Non-Contact Displacement Sensor 41

3.3.2 Design of Phase Shift Control System 45

3.3.2.1 R-C Phase Shifting 45

3.3.2.2 Bucket Brigade 46

3.3.2.3 Operation of Microprocessor Controlled Phase Shifter 48

3.3.2.4 Input A/D Conversion 50

3.3.2.5 RAM Storage and Output 51

3.3.2.6 D/A Conversion of Output and Filtering . 53

4. Realization of the Phase Shifter Control System Design **55**

4.1 Introduction 55

4.2 Design of a Signal Conditioner 55

4.3 Information Modeling of Phase Shift 58

4.3.1 Phase Shift of PMN Actuators and Amplification System 58

4.3.2 Phase Shift Criteria 61

5. Realization of the Self-Tuning Gain Adapter **70**

5.1 Introduction 70

5.2 Programming and Communication of Phase Shift Required . . 71

5.3 Design of Automatic Gain Control System 74

5.4 Gain Control for Stability 77

5.4.1 Feedback Gain vs. Frequency and Feedback Amplitude 77

5.4.2 Framework for Automatic Gain Control 80

5.4.2.1 Normalizing Stage 81

5.4.2.2 Input Stage Normalization Calculation 83

5.4.2.3 Peak Detector and Sample and Hold 84

5.4.2.4 Output Attenuation and Gain Stage 85

5.4.2.5 Microprocessor Code Implementation 88

5.5 Discussion of Oscilloscope Plots 92

5.5.1 Phase Shift Output 92

5.5.2 Reduction of Vibration 94

5.5.3 Discussion of Automatic Gain Control and Instability 96

6. Conclusions **100**

6.1 Conclusions 100

6.2 Recommendations 103

Appendices **105**

A Feedback Control System Definitions. 105

B Eight Pole Butterworth Frequency and Step Response 107

References **108**

LIST OF TABLES

Table | Page

Table 3-1 Vibration reduction using signal generator for feedback 39

Table 3-2 Phase Shift and Increments 53

Table 4-1 Phase Shift of Displacement Sensor Electronics 57

Table 4-2 Phase Shift of PMN Actuators 60

Table 4-3 Phase Shifter Phase Shifts 62

Table 4-4 Percent Reduction of Vibration with Manual Phase Shift 65

Table 4-5 Vibration Reduction with Manual Phase Shift 68

Table 5-1 Vibration Reduction Using Automatic Tuning Circuit 73

Table 5-2 PMN Amplifier Voltage vs Frequency and Feedback Amplitude ... 77

Table 5-3 Amplifier Input Voltage Frequency Dependency 79

LIST OF FIGURES

Figure — Page

Figure 2-1 Example of a Typical Lathe 7

Figure 2-2 Block Diagram of Machining System Modeling 8

Figure 2-3 Built-Up Edge phenomenon on Effective Rake Angle 11

Figure 2-4 Stability Chart for a Machine Tool 12

Figure 2-5 Induced Strain versus Polarization 14

Figure 2-6 PMN Actuator Used in thesis work 15

Figure 2-7 Functional Block Diagram of an Open-loop Control System 16

Figure 2-8 Functional Block Diagram of an Closed-loop Control System . . . 17

Figure 2-9 Block Diagram of an Adaptive Control System 18

Figure 2-10 Framework of the Smart Tool Post Structure Project 19

Figure 2-11 Mechanical Structure of Tool Post 20

Figure 2-12 Fabricated Tool Post 20

Figure 2-13 Disassembled Tool Post Housing and Components 21

Figure 3-1 Constructive Interference of Signals 24

Figure 3-2 First Order System Normalized Magnitude and Phase Angle . . . 26

Figure 3-3 Block Diagram of the Designed Parameter Control Adaptive System 27

Figure 3-4 Block diagram of a Parameter Control Adaptive System 28

Figure 3-5 Framework for Control System 29

Figure 3-6 Mechanical Mounting of Toolpost for Experimental Study 30

Figure 3-7 Tool Holder with Accelerometer 31

Figure 3-8 Skewed Accelerometer Output 32

Figure 3-9 Test Assembly without Coupling Bar 32

Figure 3-10 Basic Integrator 34

Figure 3-11 Effect of Offset Voltage and Bias Current in an Integrating Circuit 35
Figure 3-12 Cantilever Beam Sensing System 37
Figure 3-13 Block Diagram of Experimental Set-up 38
Figure 3-14 Graph of Attenuation at Various Frequencies 39
Figure 3-15 Non-Linearity of Sensor 43
Figure 3-16 Sensor Peak-to-Peak Noise 44
Figure 3-17 Diagram of Sensor Electronics 44
Figure 3-18 Phase Relation of R-C circuit 46
Figure 3-19 Bucket Brigade Storage Implementation 47
Figure 3-20 Diagram of Microprocessor Based Phase Shift 48
Figure 3-21 CPU Registers 50
Figure 3-22 Schematic of Microprocessor Based Phase Shifter 54
Figure 4-1 Displacement Sensor Electronics 56
Figure 4-2 Graph of Analytical versus Measured Values for Sensor Electronics. 58
Figure 4-3 Experimental Set-up 59
Figure 4-4 Phase Shift of PMN Actuators 60
Figure 4-5 Feedback System for Reduction of Tool Vibration 61
Figure 4-6 Configuration for Maximum Vibration Reduction 63
Figure 4-7 Interface for Increasing and Decreasing Phase Shift 64
Figure 4-8 Configuration Using Displacement Sensor Feedback 66
Figure 4-9 Comparison between the Theoretical and Empirical Phase Shift . . 67
Figure 4-10 Vibration Reduction with Manual Phase Shift of Sensor Feedback 68
Figure 5-1 Interface Connections between Microprocessor Controlled Circuits 71

Figure 5-2 Capacitor Bypass To Reduce Noise 72
Figure 5-3 Block Diagram of Automatic Phase Control Circuit 73
Figure 5-4 Vibration Reduction Using Analytical Phase Shift 74
Figure 5-5 Schematic of Microprocessor Based Tuning Circuit 76
Figure 5-6 PMN Amplifier Voltage vs. Frequency and Feedback Amplitude .. 78
Figure 5-7 Frequency Dependence of Amplifier Input Voltage 79
Figure 5-8 Block Diagram of Automatic Gain Control System 80
Figure 5-9 Input Amplifier Stage of Gain Control System 81
Figure 5-10 Resolution of Input Signal Compared with LSB Value 82
Figure 5-11 Circuit for Calculation of Parameters of Input Gain Control System 83
Figure 5-12 Peak Detector and Sample and Hold Circuit 85
Figure 5-13 Output Gain Control Amplifier Stage 86
Figure 5-14 Circuit for Calculation of Parameters of Output Gain Control ... 87
Figure 5-15 Comparator Output with Feedback Signal Input 89
Figure 5-16 Compete Adaptive Control System 91
Figure 5-17 Phase Shifts at Various Frequencies 93
Figure 5-18 Oscilloscope Connections for Measuring Phase Shift 93
Figure 5-19 Output of Sensor Without Active Feedback 94
Figure 5-20 Output of Sensor With Active Feedback 95
Figure 5-21 Comparison between Sensor Signal with and without Feedback . 95
Figure 5-22 Output of Sensor without Active Feedback, FFT included 97
Figure 5-23 Active Feedback Present, Two Peaks on FFT 97
Figure 5-24 Maximum Reduction Before Instability 98
Figure 5-25 Onset of Instability 98
Figure 5-26 Unstable System 99

Figure A-1 Block Diagram of Feedback Control System Containing all Basic Elements 106

Figure B-1 Theoretical Butterworth Filter Response 107

Chapter 1 Introduction

1.1 Background

Machining is a manufacturing process in which a cutting tool is used to remove excess material from a workpiece. There are many different machining operations where a variety of tools are used to cut various types of materials. Metal-cutting is a very large segment of the U.S. industry. Machine tools are the platform of machining operations. Precision machining has recently received more and more attention in the machine tools industry as dimensional accuracy becomes a significant means of measuring quality in products. Currently conventional machine tools used on the shop floors dominate the manufacturing community. However, these machines are being pushed to their machining accuracy limits. Therefore, there is a pressing need in this country to revolutionize its machining capability in order to maintain the competitiveness of the U.S. industry in the world market.

In a national effort to raise the competitivness, significant capital investments have been made to install new and precision machine tools, such as computerized numerically controlled (CNC) machines. However, replacement of the conventional machine tools by advanced and new machine tools, if it is not impossible, would be very difficult in terms of the available capital investments. As a result, enhancing the machining capabilities of the conventional machine tools currently being used on the shop floor represents an urgent need to maintain the manufacturing competitiveness in the world market for all business sectors.

Considerable efforts have been spent in updating the capabilities of machine tools. A significant amount of conventional milling machines have been

furnished with digital controllers with great success. These retrofitted machines augment the operational capability through digital control of the tool during machining. However, progress has been slow in efforts to improving machining accuracy. A typical example of the slow progress would be the vibration control during machining. It is well known that vibration is one of the major causes which affect the machining performance. Tool vibration usually leads to poor surface finish, accelerates the process of tool wear, and very often, causes tool breakage during machining. Process control aimed at vibration has been the main focus of research for the entire machine tools industry for decades with limited improvement. The slow progress is mainly due to the complexity of the machining process and the machine tool dynamics, and the lack of interdisciplinary research efforts to take a systematic approach to attack the difficulties currently the machine tools industry is facing.

1.2 Scope of Thesis

This thesis focuses on the research of designing an intelligent system to carry out on-line compensation for vibration. The platform is a mechatronic system, which is composed of a mechanical system and an electronic system. The intelligence comes from the smart material made actuators and the system controller. As part of a team effort, the experimental and analytical investigation conducted in this thesis concentrates on modifying a developed tool post structure by adding a new control system. The developed tool post has six built-in actuators designed for vibration compensation. The added control system is designed in such a way that the control actuation drives the built-in actuators to attenuate tool vibration during machining. Special efforts of this thesis work are in the following three areas:

1. Design of a sensing system. Obtaining accurate and timely information on the tool vibration during machining serves as a gateway to succeed in the control design. Sensors are vital for intelligent processing. Three types of sensors are used in this study. They are accelerometers, strain gage displacement sensors, and a high precision Variable-Impedance-Transducer (VIT). Comparison is made to demonstrate the importance of noise reduction in the feedback loop.

2. Design of a microprocessor based phase-shift controller. To complete the requirement for time response, a MC68HC11 Microprocessor is used as a control device to carry out the proper phase shift which synchronizes the control actuation with the tool vibratory motion. A computer program is written so that the phase shift is manipulated with high accuracy.

3. Design of an automatic tuning and gain control circuit. To overcome the limitation of fixed point controllers in responding to nonlinear machining process dynamics, a microprocessor-based circuit is designed to perform self-tuning of the control gain based on the magnitude and frequency of excitation. A built-in process identification algorithm computes the control gain in real time to adjust the level of control energy supplied by the power amplifier to the PMN actuators, thus ensuring optimal system performance.

In light of these contents, this thesis presents a systematic study of developing an intelligent mechatronic system for tool vibration control during machining.

1.3 Outline of Thesis Presentation

There are six chapters to this thesis. Although each chapter has been written to be self-contained, each chapter builds on the results of preceding chapters. Two appendices are included. The contents of each chapter are summarized below.

Chapter 2 gives an overview of the relevant literature. This review covers vibration of machine tools, smart material and structures, and technical issues related to controller design. The review also characterizes the results of the team efforts in this project and clearly defines the starting point and the scope of this thesis investigation.

Chapter 3 describes the framework of the control design. Two new and innovative ideas are introduced in the conceptual formulation of an adaptive controller to carry out the phase shift compensation and self-tuning control in real time.

Chapter 4 presents the experimental investigation and realization of the designed phase shift control system. It includes the experimental setup, data acquisition, and control system implementation. Details of the controller design are clearly described to demonstrate the fundamentals of controlling the nonlinear dynamic behavior of the PMN actuators during the vibration compensation.

Chapter 5 presents the design and realization of the self-tuning gain adapter control system. It focuses on the development of an algorithm to automate the control action under a variety of machining conditions. Although such a task is very difficult to accomplish, initial results from this analytical study show great potential for effective vibration compensation.

Chapter 6 summarizes the thesis and provides recommendations on continuing research in this field.

Chapter 2 Literature Survey

2.1 Introduction

This chapter presents a background literature survey pertaining to machining operations, dynamics of machining systems, smart materials and actuators, control systems, and configuration of the smart tool post structure. The review is divided into five sections. At the end of this review, an outline of the smart tool structure is presented. The design of a controller for the tool post structure is proposed.

2.2 Machining Operations

There are a variety of machining operations in the manufacturing sectors all over the world. Among them, the screw cutting engine lathe is the oldest and most important of machine tools and from it all other machine tools have been developed. In fact it was the lathe that made possible the building of all kinds of machinery used in industry, such as the locomotive, the electric motor, and the automobile, to name a few. Without the lathe, the great industrial progress of the last century would have been impossible [How 1966]. For this reason, the work completed in this thesis has focused on vibration control of the lathe machining operation.

A typical lathe is shown in Fig. 2-1. The bed, which supports and aligns the other components, is usually of a dovetail design. The carriage (saddle) is where the toolpost is placed, usually on a compound rest, which allows forward and transverse movement of the tool. The headstock contains the power transfer mechanism for the spindle drive. The tailstock is used to support one end of the workpiece, usually with a device called a "live center," or can hold a drill chuck

for drill, and boring operations. The gearing between the spindle and lead screw is arranged in the gear box so that different thread pitches can be obtained.

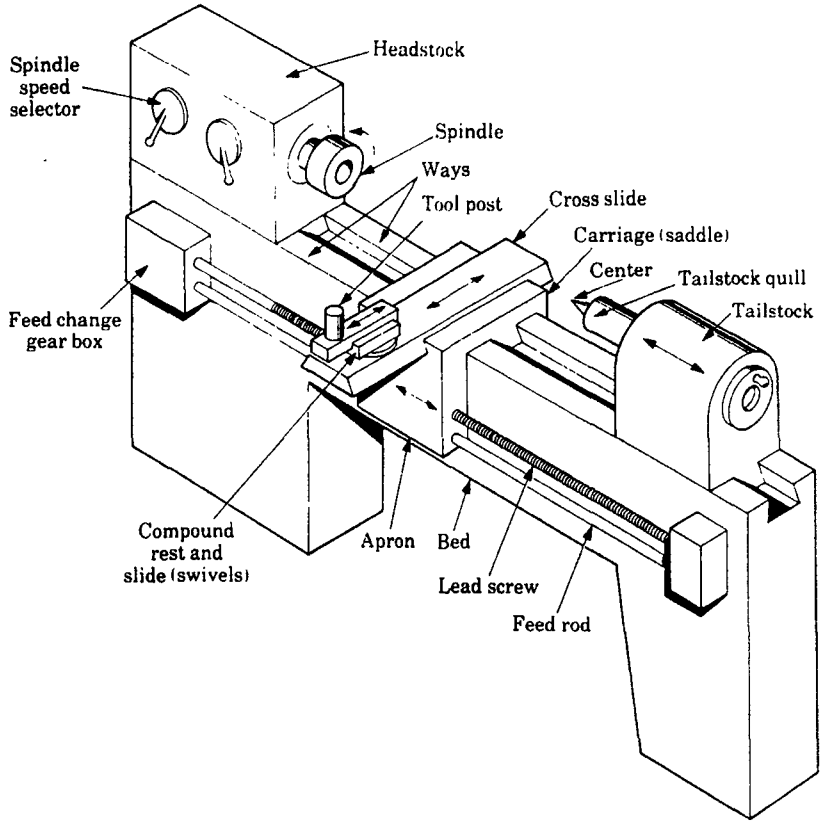

Figure 2-1 Example of a Typical Lathe [Ko 1995]

2.3 Dynamics of Machining Systems

A machining system consists of three major components [Merritt 1965]. They are the cutting process, machine tool structural dynamics, and a set of feedback paths that represent the interactions between the cutting process and structural dynamics. The block diagram that models this system is shown in Fig. 2-2. The closed loop system contains two feedback paths, namely, the primary feedback path and the regenerative feedback path. The input to the cutting process is the chip load, and the output is the cutting force, which serves as the input to

the machine tool structure. The output of the machine tool structure, when subjected to the cutting force, is the tool vibratory motion.

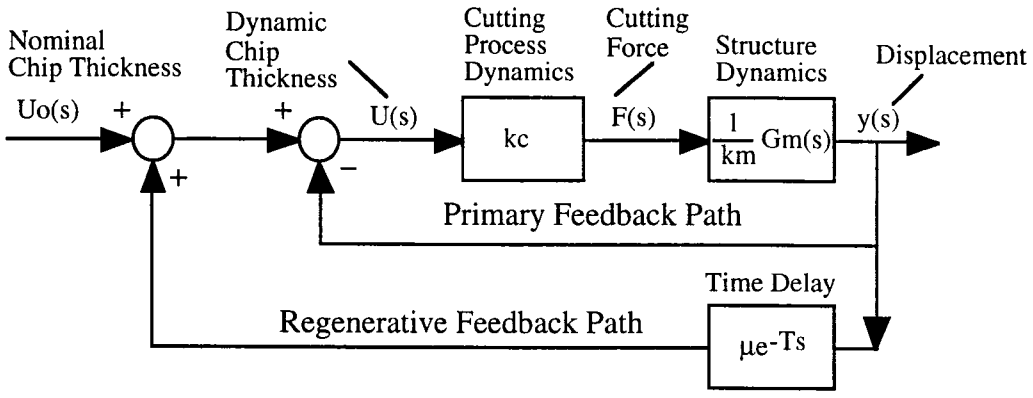

Figure 2-2 Block Diagram of Machining System Modeling [Merritt 1965]

2.3.1 Derivation of Chatter Loop

As illustrated in Fig. 2-2, the instantaneous thickness of cut, $u(t)$, is decreased as the workpiece moves away from the cutting tool. When this happens, a lump is left on the workpiece. This lump increases the uncut chip thickness one revolution of the workpiece later. The instantaneous uncut chip thickness can be written as [Zhang 1991]:

$$u(t) = u_o(t) - y(t) + \mu y(t - T) \tag{2-1}$$

the term μ is called the overlap factor. It accounts for the overlapping of successive cuts, and defines the portion of the previous cut which overlaps the present cut. The overlap factor μ is bounded between 0 and 1, where $\mu=0$ corresponds to the case of threading, and $\mu=1$ corresponds to the case of plunge cutting.

2.3.2 Cutting Process Equation

According to Merchant [Merchant 1944], the resultant cutting force, $F(t)$, is related to the instantaneous uncut chip thickness, $u(t)$, by the dynamics of the cutting process. If the machine tool structural dynamics are neglected, the resultant cutting force relation can be expressed as:

$$F(t) = k_c u(t) \tag{2-2}$$

where k_c is the static cutting stiffness. Here an assumption is made that the cutting stiffness is directly proportional to the width of cut for a given workpiece material and tool geometry. The static cutting stiffness, k_c, can be assumed as

$$k_c = k_a w \tag{2-3}$$

where K_a is the unit cutting force.

2.3.3 Vibration and Chatter

The need to continually improve on machining processes necessitates the identification and modeling of all factors that affect product quality in the machining process. Machine tool vibration during machining has been a focused area in the manufacturing community. A typical example of vibration would be the boring machining process where the slender boring bar is susceptible to vibration. It is often that vibration is observed which is contributed by both the low rigidity of the workpiece and the low rigidity of the tool post structure.

There are two types of vibration which are usually associated with turning operations, forced and self-excited. Forced vibrations can be caused by many

factors, including the vibration of the lathe itself at different resonance frequencies. Non-continuous circular cross sections of the workpiece being machined will also result in forced vibration. Discontinuous geometry, such as holes, key ways, and slots, which are located on the circumference of the workpiece, poses problems for manufacturing. There is an impact between the cutting edge and the workpiece every time the tool passes over the discontinuity and starts to engage in cutting again. An example of this would be turning a square piece of stock to make a round extension or a grooved (keyed) bar. The impact of the edges on the tool will cause vibratory motion of the tool.

Self-excited vibration, also called chatter, is usually caused by the material removal process itself. There are several factors which can influence this. As an example, the cutting tool experiences a phenomenon called Built-up-edge, or BUE, during machining. As illustrated in Figs. 2-3a and 2-3b, the presence of BUE may cause variation of the effective rake angle during machining. A large height of BUE introduces a large effective rake angle, leading to a low cutting force, and vice versa. Such variation of the cutting force can cause tool vibration in a self-excited mode. In cylindrical turning operations, chatter is frequently encountered during the machining of long slender bars. The deflections of bar in the thrust direction increase while the tool moves to the middle of the bar and may initiate the primary or regenerative chatter, leading to self-excited vibration of the workpiece [Tansel 1990].

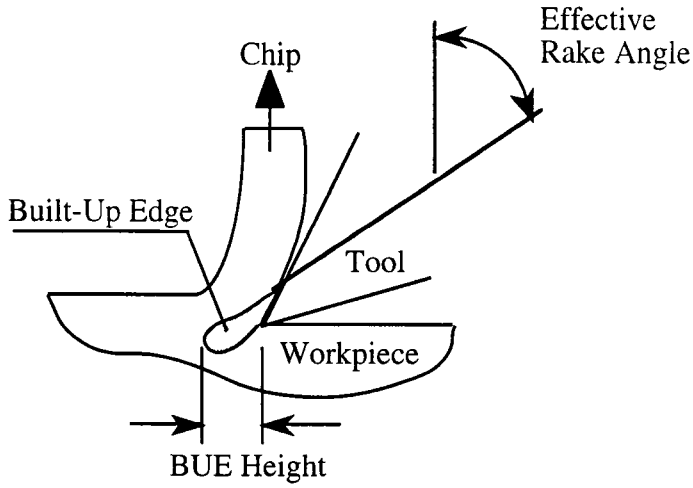

(a) A Larger Height of BUE Corresponds to a Larger Effective Rake Angle

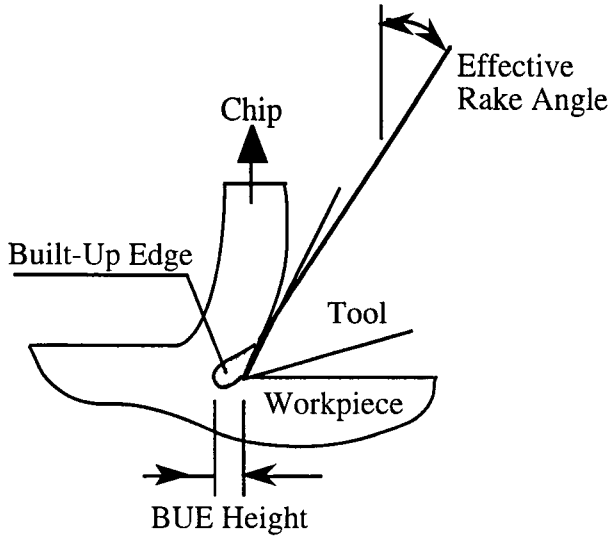

(b) A Smaller Height of BUE Corresponds to a Smaller Effective Rake Angle

Figure 2-3 Built-Up Edge Phenomenon on Effective Rake Angle

A non-homogeneous distribution of the microhardness in the workpiece material can also cause chatter. Because of the difference in hardness of the microstructure, the presence of different phases in the microstructure leads to the cutting force produced during machining to vary instantaneously.

To reduce the effects of chatter, it is usually assumed that by increasing the stiffness of the cutting tool, chatter will be diminished. On the other hand, damping of the entire carriage and of the toolpost holder also reduces chatter, but at the expense of accuracy. Fundamentally, chatter is caused by a lack of adequate dynamic stiffness in the machine structure [Merritt 1965], which can be traced to lack of inherent damping in the structures.

A typical stability chart for a machine tool used by many researchers is shown in Fig. 2-4. Three borderlines of stability can be identified which for classification purposes will be called lobed, tangent, and asymptotic. The lobed borderline of stability is the exact borderline. The asymptotic and tangent borderlines approximate the lobed borderline in two different manners. Calculation of the stability borderlines is very difficult, and many factors complicate the usefulness of the stability charts. However, stability charts present a general picture of vibration patterns observed during machining.

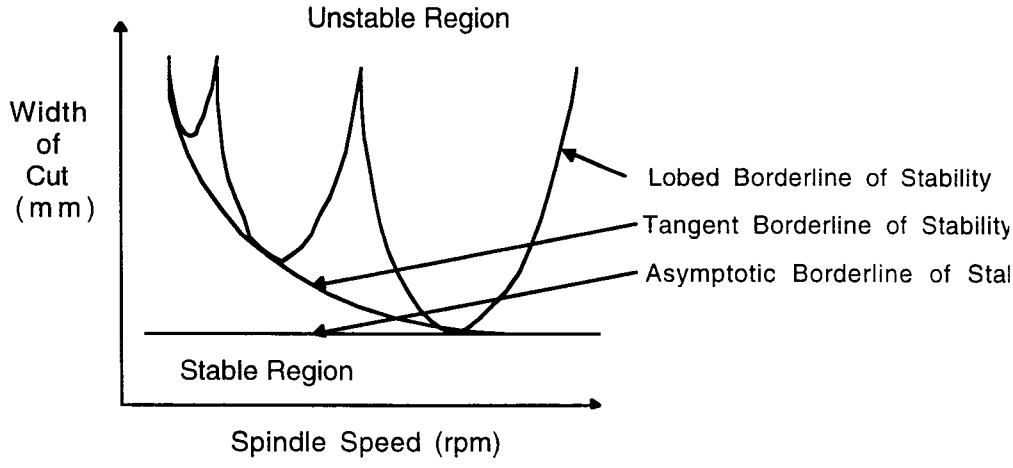

Figure 2-4 Stability Chart for a Machine Tool [Merritt 1965]

2.4 Smart Material Made Actuators

Structures that have the ability to sense and react to their environment are of increasing importance in engineering applications. Due to the advancement of

material processing techniques, smart materials and structures have been developed and applied to active control systems with great success. As a result, strategic material considerations and economic factors are motivating many modern industrial sectors towards the use of smart materials and structures. Where weight, size, and cost are of primary importance, such as in space structures and precision instruments, passive methods for vibration isolation, damping, control and position control have almost reached their limit. Active methods to control structural dynamics have become prime candidates, of which actuators made of smart materials stand out among all of the active devices developed up-to-date.

Actuators have been widely used in control system to drive the plants. Actuators made of smart materials allow a control system to adapt to its environment. The materials that the actuators are made from have the ability to change their mechanical characteristics in response to changes in temperature, electric, or magnetic field. The most common actuator materials are shape memory alloys, piezoelectric materials, magnetostrictive materials, electrorheological fluids, and magnetorheological fluids [Rogers 1992]. In the following, a brief review of electrostriction is presented. A detailed review of smart material made actuators can be found in [Ko 1995].

2.4.1 Electrostrictive Characterization

Ferroelectrics are a type of material that consists of subvolumes, called domains, that have a uniform, permanent, reorientable polarization. The spontaneous polarization is reversible by an electric field. Above a certain temperature, called the Curie temperature, ferroelectrics undergo a transition where the spontaneous polarization disappears. For PZT's, an electric field is introduced at high temperatures to align the polar domains in the crystal. The

subsequent process gives the PZT an induced strain proportional to the induced polarization. Ferroelectric materials are useful materials that can convert electricity into mechanical motion and force.

Electrostrictive ceramics are a class of ferroelectrics. The main difference is that the induced strain is proportional to the square of the induced polarization. They also exhibit less hysteresis, but are more temperature dependent. In electrostriction, the sign of the deformation which occurs with an applied electric field is independent of the polarity of the field, and proportional to even powers of the field [Jaffe 1971]. One type of electrostrictive ferroelectric that is being studied and used in this thesis is based on Lead Magnesium Niobate, $Pb(Mg_{1/3}Nb_{2/3})O_3$-$PbTiO_3$ (PMN). These materials have high electrically induced strains. Also, since the induced strain is proportional to the square of the polarization, the same deformation occurs when the polarization is reversed. The typical response is shown in Fig. 2-5.

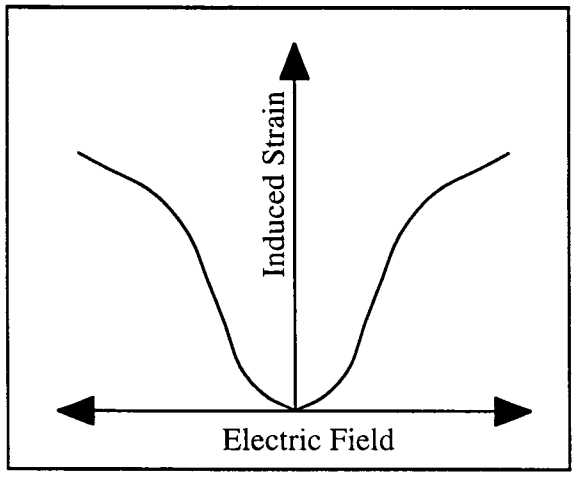

Figure 2-5 Induced Strain versus Polarization [Jaffe 1971]

2.4.2 Actuator Design

The actuators used to drive the toolpost system are multi-layer stack-type actuators made of an electrostrictive Lead-Magnesium-Niobate (PMN) ceramic. In the design of the mechanical structure of the tool post, a provision has been made for changing the number of actuators used to provide various levels of force and displacement, from two to six PMN actuators. A drawing of the PMN actuator is shown in Fig. 2-6.

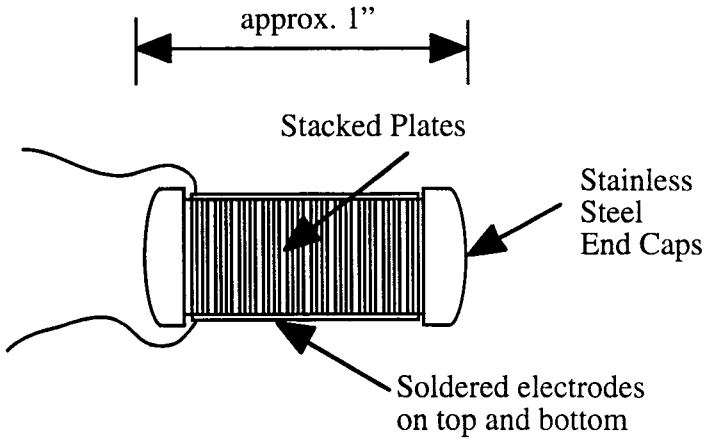

Figure 2-6 PMN Actuator Used in Thesis Work

Multilayer PMN stacks offer high energy densities for actuation over motions of several microns. They are mechanical as well as electrical devices. However, these materials exhibit highly nonlinear transductance and electrical properties. Successful applications of PMN actuators require detailed understanding of these nonlinearities, in order to develop accurate nonlinear performance models for control system designs.

2.5 Control Systems

Control systems have been widely used for industrial applications. In general, control systems are classified into two categories, open-loop and closed-loop systems. The distinction between them is determined by the control action, which is the quantity responsible for activating the system to produce the output. For closed-loop systems, proportional-integral-derivative controllers are typical for linear systems. For non-linear systems, adaptive controller, fuzzy logic controllers, and neural networks controller are a few to name.

2.5.1 Open-Loop Control Systems

An open-loop system is one in which the control action is independent of the output. Such control is termed as passive control. Open-loop systems can be characterized by two outstanding features. First, their ability to perform accurately is determined by their calibration. Second, and most importantly, they are not generally troubled with problems of instability. As described earlier, damping the tool post assembly on a lathe is a form of open or passive control.

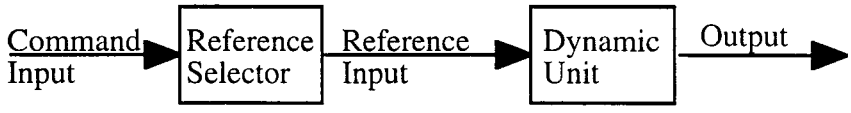

Figure 2-7 Functional Block diagram of an Open-Loop Control System

2.5.2 Closed-Loop Control Systems

A closed-loop system is one in which the control action is dependent on the output of the system. Closed-loop systems are also referred to as feedback control systems. Feedback is the characteristic which distinguishes closed-loop systems from open-loop systems [Phillips 1996]. Feedback is the property which permits the output to be compared with the input to the system (or an input to

some other internally situated component or subsystem of the system) so that the appropriate control action may be formed as some function of the output and input. The feedback action can be continuous or discontinuous. Continuous control implies that the output is continuously being fed back, in time, and compared with the reference input [D'Azzo 1966]. In discontinuous feedback control, the input and output quantities are periodically sampled and compared.

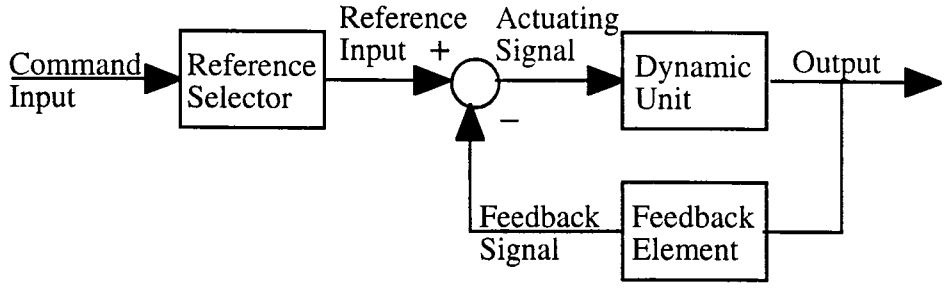

Figure 2-8 Functional Block diagram of a Closed-Loop Control System

In order to accurately classify a control system as open-loop or closed loop, the components of the system must be clearly distinguished from components that interact with, but are not part of the system.

2.5.3 Adaptive Control

It has been well accepted that "to adapt" means to change a behavior to conform to new circumstances. An adaptive control system means that the system has an adaptive controller that modifies the system behavior in response to changes in the dynamics of the process and/or the character of the disturbances. By detecting the dynamic variation, the adaptive controller adjust the settings of some system parameters to ensure that the system conforms or adapts to the new circumstances in terms of meeting the performance specification [Kuo 1982].

In general, an adaptive control system can be thought of as having two loops. One loop is a normal feedback with the process and the controller. Figure 2-9 presents a block diagram of a typical adaptive control system. The other loop is the parameter adjustment loop. As illustrated, real-time estimation is an essential part of adaptive control. Consequently, the parameter adjustment loop is often slower than the normal feedback loop. Computational delay between the measurement and the time the control signal is applied to the process is unavoidable. Special care has to be taken to ensure that the computational delay can be significantly reduced by proper implementation of the controller, because delays can lead to instabilities in feedback systems.

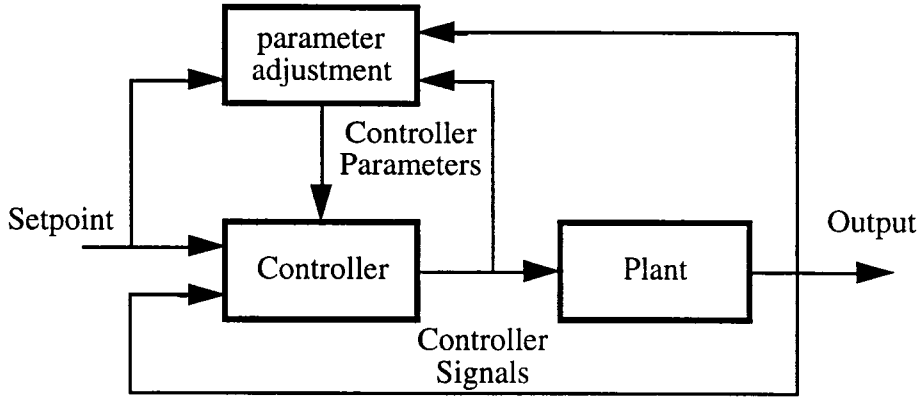

Figure 2-9 Block Diagram of an Adaptive Control System

2.6 Configuration of the Smart Tool Post Structure

On the College Park campus, a project to design a smart tool post structure to control tool vibration during machining has been carried out since 1992. The project is a part of national efforts to revolutionize the machine tool industries competitivness in the world market. For the University of Maryland, the project was initiated in 1993, and represents a three year effort to search for a solution to control the tool vibration during machining [Ko 1995]. During the past three years, a systems engineering approach has been used to develop a system

architecture, under which important system components are defined and their relations to each other are identified. Fig. 2-10 depicts the project framework. As illustrated, this project started from system modeling in 1993. By the end of the second year, the mechanical structural design and the tool post fabrication were completed.

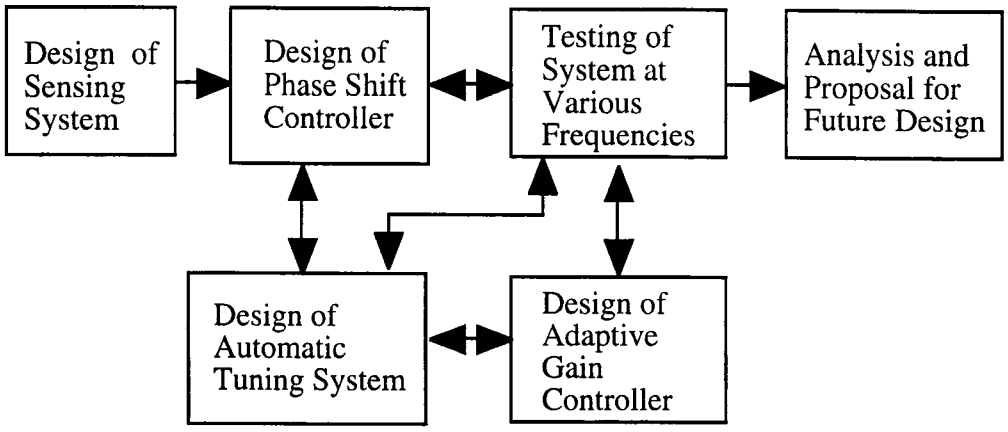

Figure 2-10 Framework of the Smart Tool Post Structure Project

The mechanical structure of the designed tool post is illustrated in Fig. 2-11 and Fig. 2-12. It consists of five components. They are the tool post base, tool insert housing, membranes, actuators, and sensor housing. As illustrated, the cutting force generated during machining will act on the tool insert. With the sensor mounted on the tool insert housing, the cutting force will be transmitted to the sensing element directly. The anti-vibration force will be provided by the built-in actuators. The circular-shaped membranes have direct contact with the actuators and function as energy reservoirs to balance the kinematic-potential energy conversion. The fabricated tool post is illustrated in Fig. 2-13. Detailed information on the design and fabrication of the tool post structure can be found in [Ko 1995].

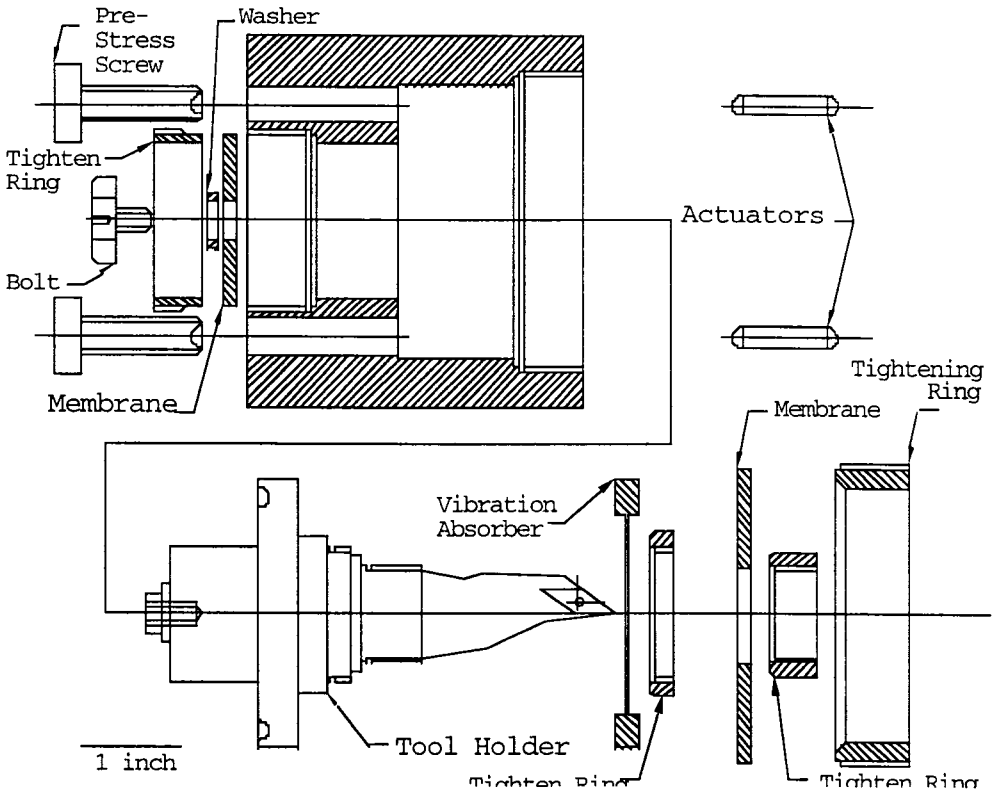

Figure 2-11 Mechanical Structure of Tool Post [Ko 1995]

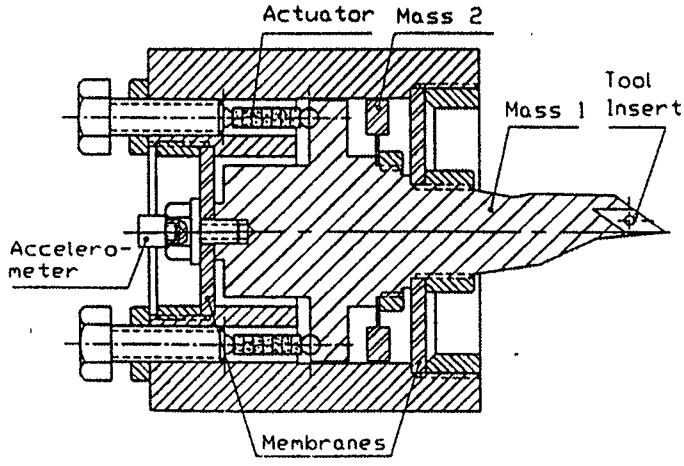

Figure 2-12 Assembled Toolpost Structure [Ko 1995]

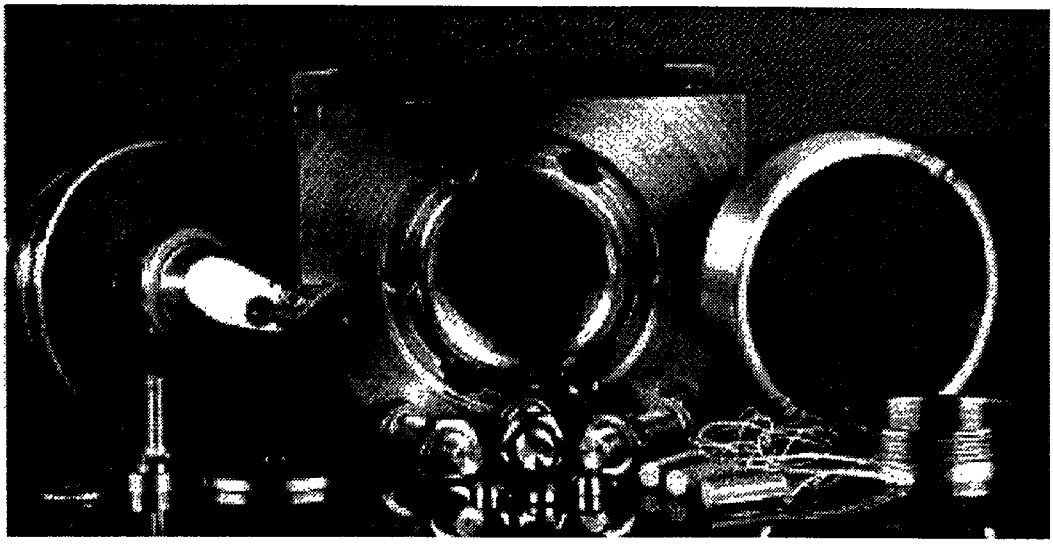

(a) Disassembled Tool Post Showing Various Components

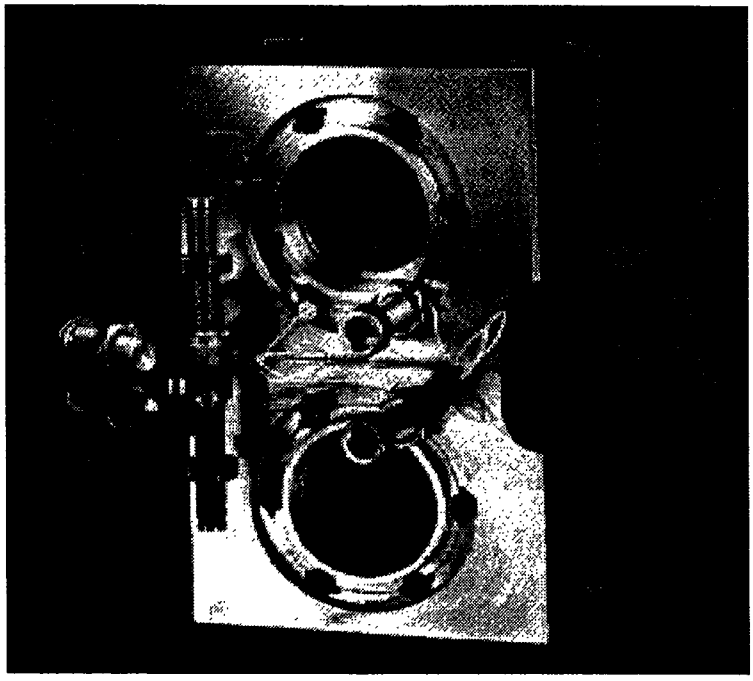

(b) Picture of Tool Post Housing with Pre-stress Bolts and Actuators

Figure 2-13 Disassembled Tool Post Housing and Components

Chapter 3 Basic Adaptive Control Methodology

3.1 Introduction

As stated in Chapter 2, one of the main objectives to design a smart tool post structure is to control tool vibration during machining. Such control will improve the machining performance in terms of surface finish, dimensional accuracy, tool life and machining productivity. In this thesis work, we focus on applying actuators made of smart materials for vibration compensation. Because the actuators are placed in the tool post structure, the control action to attenuate the vibration exciting force, namely, the dynamic variation of the cutting force, is treated as a built-in function of the designed tool post structure. The design of a control system is to implement such a built-in function, to provide on-line compensation in an adaptive manner with the dynamic variation of the cutting force.

3.2 Fundamentals of the Control System Design

In the Engineering domain, there have been a variety of controllers which have been designed, built and utilized. Typical controllers are PID controllers, adaptive controllers, fuzzy logic controllers and neural networks controllers. In this thesis work, the control system design follows the general guideline of adaptive controllers.

3.2.1 Design Objectives

Common sense dictates that tool vibration during machining is due to the dynamic variation of the cutting force generated during machining. Therefore, the objective of the control system design in this study is to compensate the tool vibration using the anti-vibration action provided by the PMN actuators in an intelligent manner.

To attenuate the tool vibration effectively, the acceleration and displacement of the tool from its initial reference position must be under control. This is accomplished by a counteractive force realized through the actuators which bring the tool back to the reference point. In reality, the control system will attempt to provide a counteractive force which will restrict the tool to vibrate about its dynamic equilibrium position within a defined magnitude.

3.2.2 Destructive Interference

To facilitate the study, both analytically and experimentally, the cutting force variation during machining is modeled as a sinusoidal function, generated by a vibration exciter. Under the harmonic excitation, the tool vibrates accordingly. To reduce the tool vibration, the actuators must provide a counteractive force to resist any change of displacement of the tool with respect to its equilibrium position. By using a displacement sensor to provide feedback on the tool position change, for vibration reduction, it is sufficient to provide an equal in magnitude and opposite in phase relation actuation motion which will compensate for any tool position variation produced by the harmonic excitation. Analytically speaking, the vibration the equal and opposite signal for a sinusoidal function must be a signal 180 degrees out of phase of the driving signal. This destructive interference is shown in Fig. 3-1.

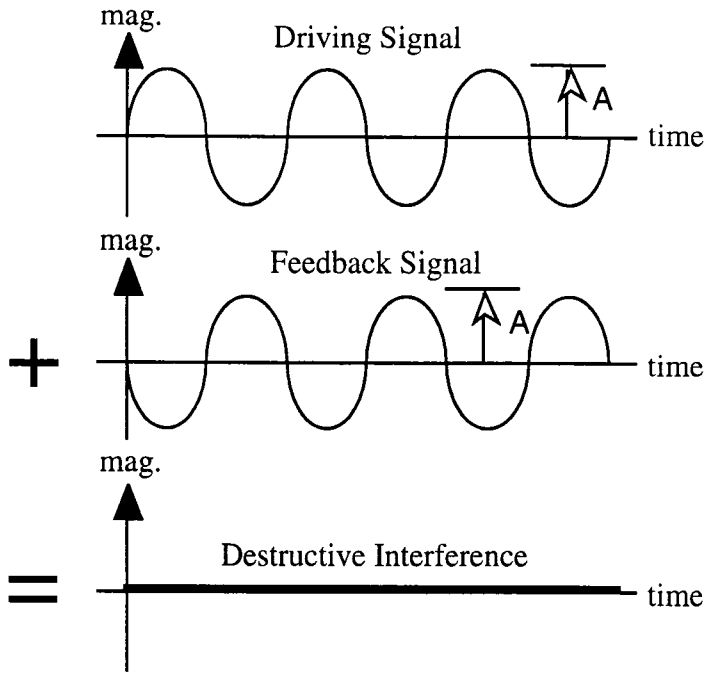

Figure 3-1 Destructive Interference of Signals

The tool vibration observed during machining is characterized by an oscillatory type of motion, with certain frequencies more pronounced than others. This type of oscillation is provided for modeling by the vibration exciter. In this thesis, a control system is designed to reduce the vibration of the tool post at a certain frequency, which has a dominant effect on machining performance. The control system design has several objectives to achieve. However, priorities are assigned to ensure that vibration compensation will be carried out in an effective and efficient manner. Priorities in the control system design in this investigation are given to the following two factors:

1. The magnitude of vibration compensation to implement during machining has to be equal or less than the detected oscillation to ensure that the mechatronic system remains stable.
2. The shift of phase angle between the driving force and anti-vibration force should be compensated in such a way that the anti-vibration

force exerted by the PMN actuators will act to oppose the movement of the tool as closely as possible.

In the control system design, these requirements imply that the locations of the closed-loop system have to be close to the jw axis as nearly as possible, but remain in the left side of the s-plane. However, such a pole-placement design is complicated by the dynamic variation of the cutting force presented during machining. In reality the dominant frequency component of the excitation varies as the machining condition varies. Such variation is typical when the workpiece material is changed, and/or the machining is conducted at different speeds, feeds, and depths of cut The complicity in the control system design is illustrated in Figs. 3-2 and 3-3, leading to the necessity and utilization of adaptive control in the control system design.

Fig. 3-2 is a representative forced response of a second order system where the system is a single mass system and is characterized by

$$m\ddot{x} + c\dot{x} + kx = F_0 \sin\omega t \quad and \quad x(t) = A_0 \sin(\omega_n t + \phi) \tag{3-1}$$

The normalized amplitude and phase shift of the forced response are functions of the excitation frequency and are given by [Inman 1994]

$$\frac{A_0}{F_0/k} = \frac{1}{\sqrt{(1-r^2)^2 + (2\zeta r)^2}} \quad and \quad \phi = tan^{-1}\left[\frac{2\zeta r}{1-r^2}\right] \tag{3-2}$$

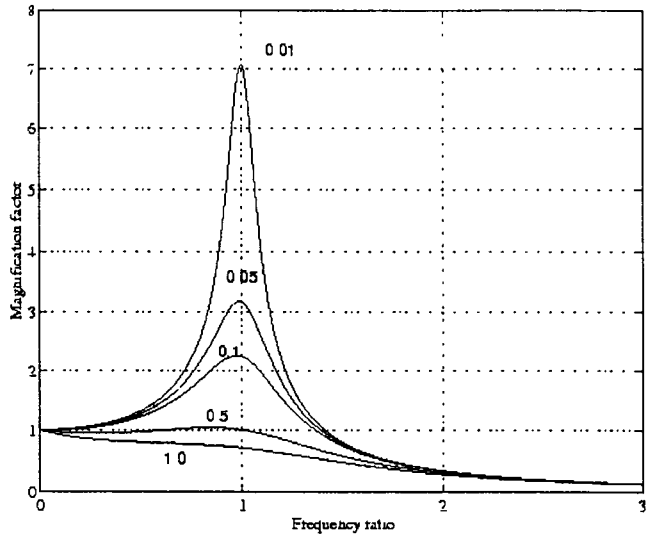

(a) Normalized Magnitude

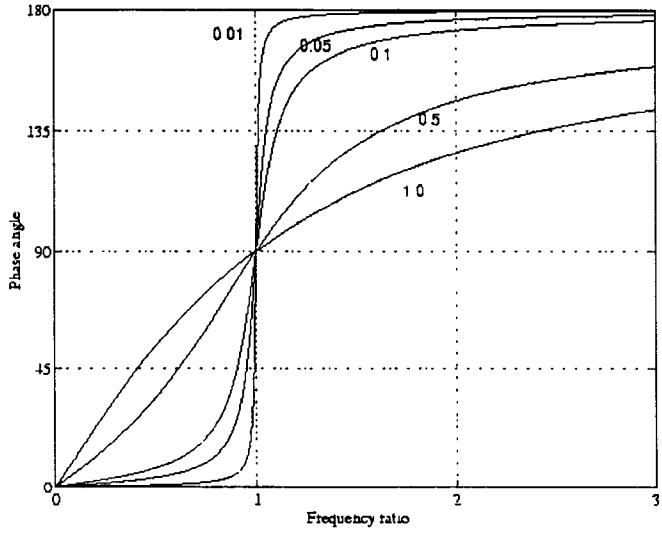

(b) Phase Angle

Figure 3-2 First Order System Normalized Magnitude and Phase Angle

It is evident that, under circumstances where the magnitude of harmonic excitation remains unchanged but its frequency varies, the magnitude of vibration varies. As the excitation frequency approaches the natural frequency of the system, the magnitude of vibration increases significantly, and so does the variation of phase shift. Consequently, the magnitude and phase shift of the anti-vibration force should follow the two variation patterns in order to optimize the vibration compensation. Obviously the fixed point compensation scheme, as discussed in the pole-placement design, is not capable of doing the job. The need for the control system to adapt the variations of external excitation leads to the introduction of adaptive control.

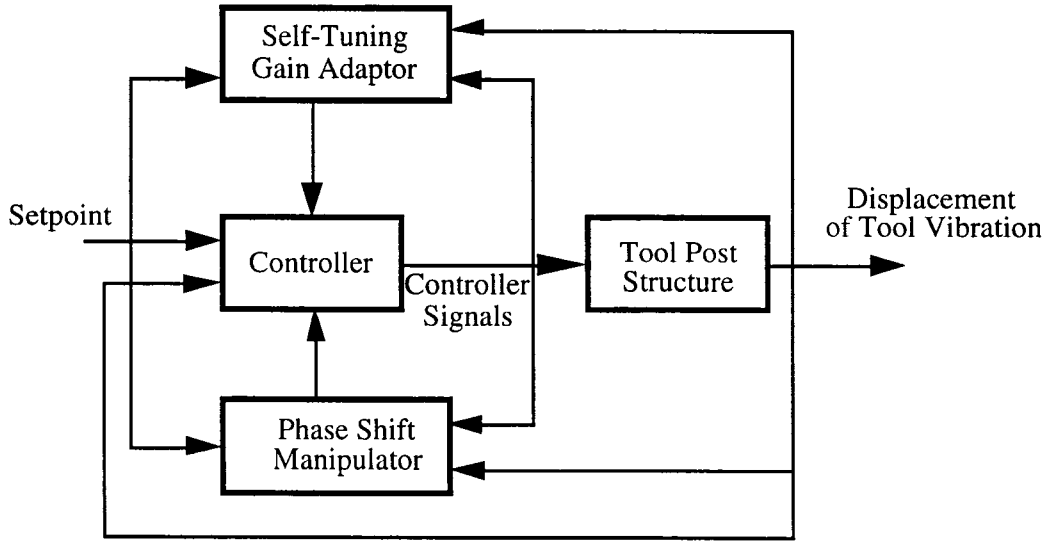

Figure 3-3 Block Diagram of the Designed Parameter Control Adaptive System

An adaptive control system is a controller with adjustable parameters and a mechanism for adjusting the parameters. The controller becomes nonlinear because of the parameter adjustment mechanism. In this thesis investigation, there are two adjustable parameters, namely, the magnitude and phase angle of the actuation exerted by the PMN actuators. Accordingly, two parameter adjustment mechanisms are designed to manipulate the adapted magnitude and phase angle for vibration compensation. However, a meaningful definition of adaptive control, which would make it possible to look at a controller hardware and software and decide whether or not it is adaptive, is still lacking.

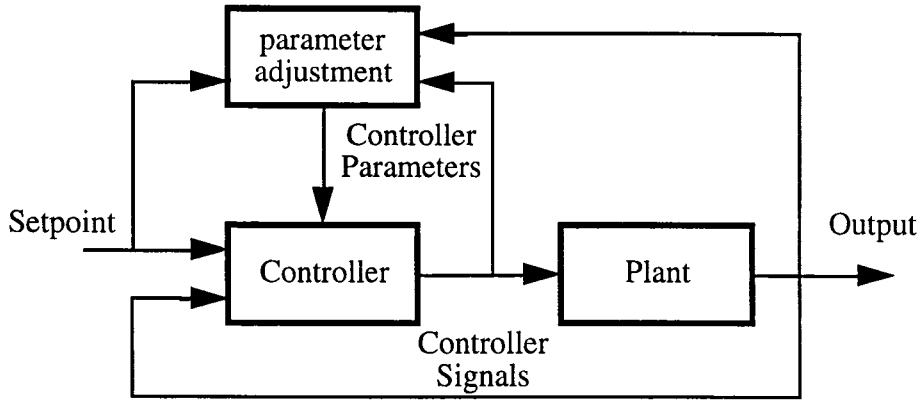

Figure 3-4 Block diagram of a Parameter Control Adaptive System

On-line determination of process parameters is a key element in adaptive control.

3.3 Framework of the Control System Design

In order to achieve the design objective and follow the priority assignment, an adaptive phase-shift manipulator and an automatic tuning and gain adapter is proposed in this investigation. Fig. 3-5 illustrates the framework of the control system design. The adaptive control system consists of three major components,

namely, a sensing system, a phase-shift manipulator, and a self-tuning gain adapter system. The input to the control system is the tool vibration signal which is detected by the sensing system. The output of the control system is the anti-vibration action exerted by the PMN actuators, which will be the input signal to the tool post structure of the machining system, thus closing the control loop.

In the following, descriptions of the three components of the control system are provided with the fundamental theories applied in this investigation.

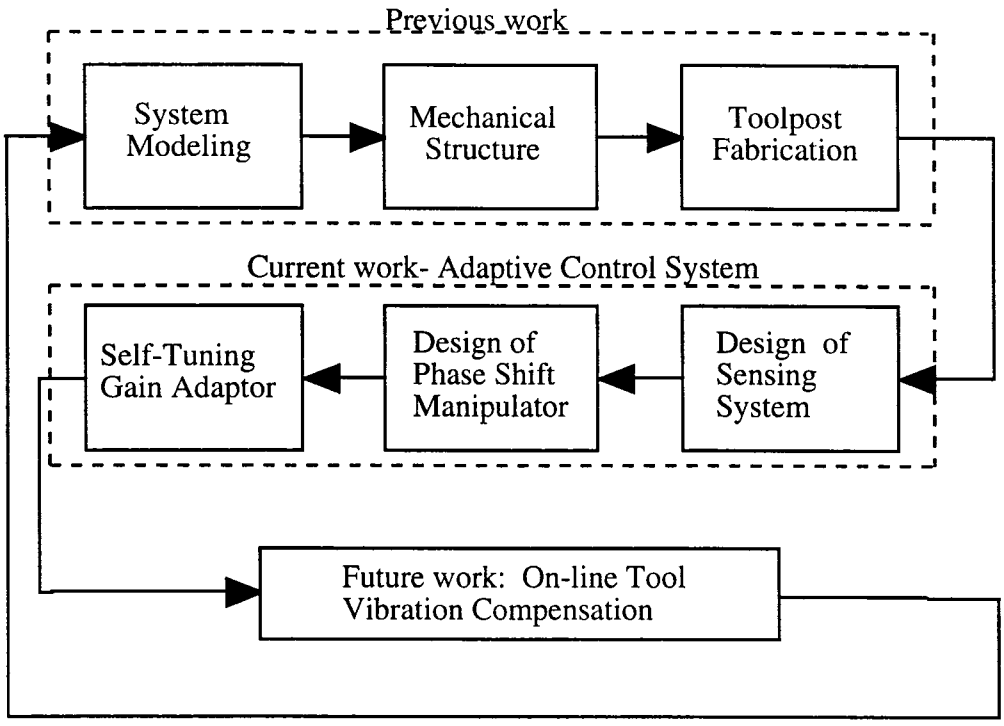

Figure 3-5 Framework for the Control System

3.3.1 Design of the Sensing System

The design of the sensing system is a critical part of the control system design process. To accurately perform any type of control, it is important that the parameters being monitored and used for feedback control are being measured accurately . The difficulty imposed in this investigation is that the displacements

being measured are in the order of microns. The total displacement available by the actuators is 18 μm with a maximum travel of the toolpost being 50 μm [Ko 1995]. To measure these quantities with high accuracy, a platform is built to imitate the oscillatory vibrations produced during the machining process. This platform consists of a vibration exciter, a coupling adapter, the toolpost and base, and an aluminum base to attach the components. This is shown in Fig. 3-6.

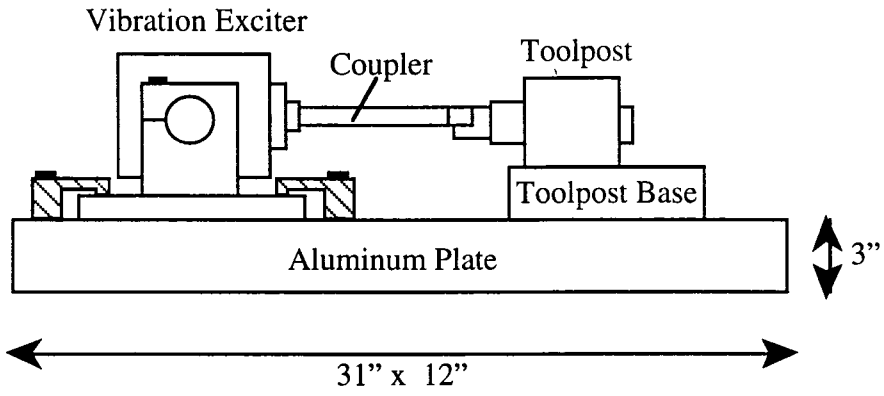

Figure 3-6 Mechanical Mounting of Toolpost for Experimental Study

The vibration exciter is a voice coil driven device, which is powered by an amplifier. It transmits a sinusoidal force through an aluminum coupling bar to the toolpost. To reduce error in measurement, the aluminum base is chosen substantially heavy to insure the presence of a substantial mass for the establishment of a measurement reference. Any force produced by the vibration exciter should be transmitted without damping to the toolpost, so a high order of stiffness and rigidity in the assembly is needed. On the other hand, any secondary harmonics or vibrations that could possibly be transmitted from the vibration exciter to the toolpost through the base should be dampened. A normal lathe used in manufacturing weighs on the order of thousands of pounds. It is very rigid for stability purposes, and provides a high order of damping.

Sensors play a critical role to provide accurate and timely information in this investigation. The sensor design used in this thesis evolved through three stages. Three types of sensors, accelerometers, strain gages, and multi-VIT (Variable Impedance Transducer), are implemented in these stages.

3.3.1.1 Accelerometers and Integrators

The first approach to the design of the sensor system is to directly couple an accelerometer to the back of the tool holder. This is shown in Fig. 3-7.

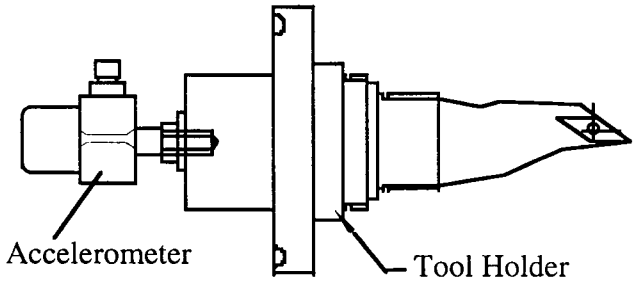

Figure 3-7 Tool Holder with Accelerometer

Accelerometers are piezoelectric transducers. The transducer is an oscillator with a very high natural frequency, and it is used to measure the acceleration of a vibrating element to which it is attached. The accelerometer used in this thesis work is a Dytran model 3101A3. The reference sensitivity is calibrated at 10 mV/G. There are three drawbacks encountered when using the accelerometer:

1. Noise in the signal. Under high amplification, the sensor system produces a high frequency noise riding on the accelerometer output. A high level of filtering is needed to compensate for this.

2. Secondary Vibration Output. As testing progressed, it was observed that at several frequencies, with the vibration exciter producing a sine wave forcing function, the accelerometer output was not a smooth sine wave. The output sine wave appeared skewed. This is shown in Fig. 3-8.

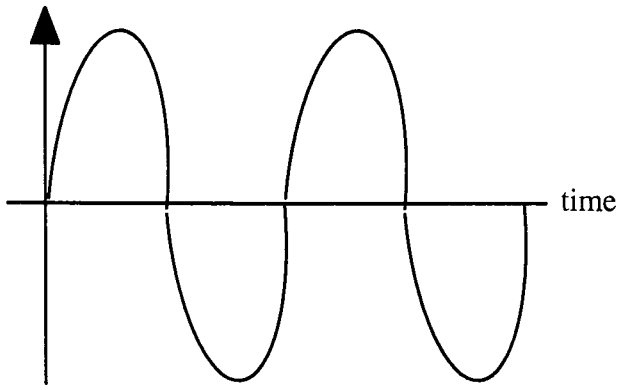

Figure 3-8 Skewed Accelerometer Output

It was speculated that the accelerometer was picking up the movement of the entire assembly including the base and the table the base was placed upon. High silicone content anti-vibration padding was placed between the aluminum base and the table. This changed the skewing effect, but did not eliminate it. The coupling rod between the vibration exciter and the toolpost was then removed, as shown in Fig. 3-9.

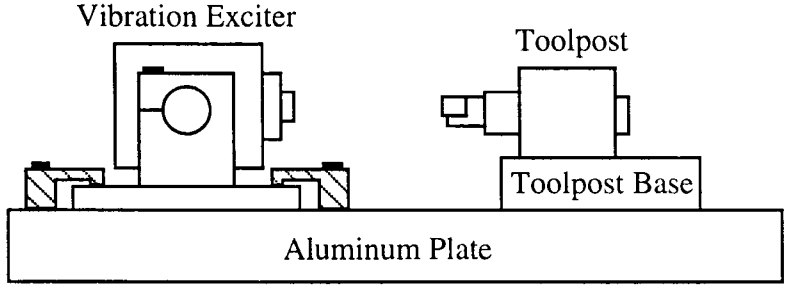

Figure 3-9 Test Assembly without Coupling Bar

Without being coupled, the accelerometer could pick up the vibration of the vibration exciter through the vibration of the aluminum mounting plate, with a large enough amplitude to effect the system. The coupling bar presents a high level of stiffness to transmit force to the toolpost from the vibration exciter, but the mounting system also has high stiffness, so it also provides a means to transmit vibration to the toolpost assembly. A system that would measure the displacement of the tool holder relative to the toolpost frame or base would eliminate this problem, because any vibration induced in the toolpost housing would also act on the sensor mounting plate.

3. Integration of accelerometer signal. The signal from the accelerometer has to be used to drive the feedback system. Directly applying the acceleration signal to the feedback system could complicate the gain control in the feedback loop since the magnitude of acceleration-related signals has its root with frequency. Very often system instability caused by oscillation occurs. A more robust and stable control system would use displacement instead of acceleration as the criteria for feedback compensation. To obtain the displacement from the acceleration, two integrators are needed. Integrators have been designed with op-amps, as shown in Fig. 3-10.

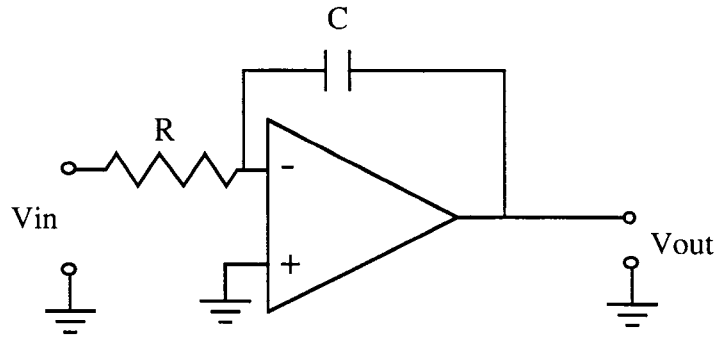

Figure 3-10 Basic Integrator

Input current V_{in}/R flows through the capacitor C. The output voltage is given by

$$V_{in}/R = -C(dV_{out}/dt) \tag{3-1}$$

or

$$V_{out} = -\frac{1}{RC}\int V_{in}dt + constant \tag{3-2}$$

With an ideal operational amplifier, dual integration to extrapolate the displacement from the acceleration would produce a useful displacement signal. The problem with this approach is when a more realistic model is taken for the operational amplifier, and the dc offset and bias current of the amplifier are taken into account. Because these dc errors exist, the output of the integrator now consists of two components, the integrated signal and the error term [Graeme 1971], and is given as

$$V_{out} = -\frac{1}{RC}\int V_{in}dt + \frac{1}{RC}\int V_{OS}dt + \frac{1}{C}\int I_B dt \tag{3-3}$$

The more realistic model for this integrating circuit is shown in Fig. 3-11.

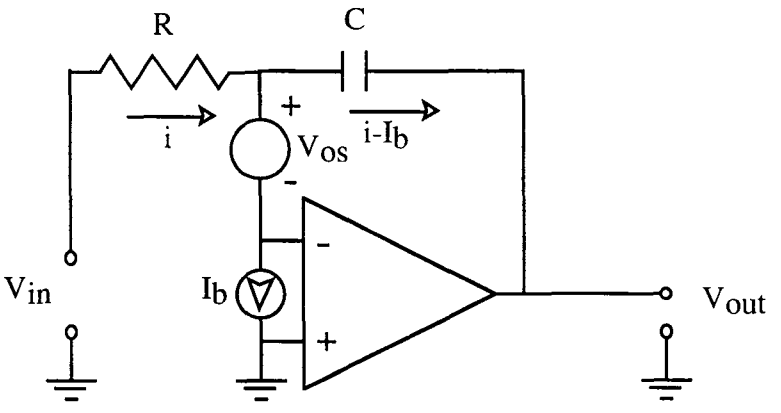

Figure 3-11 Effect of Offset Voltage and Bias Current in an Integrating Circuit

The integral of the dc offset voltage results in a ramp voltage, a linearly increasing term whose polarity is determined by the polarity of the input offset voltage [Graeme 1971]. In addition to this ramp voltage error, the input offset voltage creates an output offset voltage equal to it in value. The bias current flows almost entirely through the feedback capacitor, also charging it in a ramp fashion. These two ramp voltage errors will continue to increase until the amplifier reaches saturation. These error components usually set the upper limit on the feasible length of integration time. The feedback capacitor and type of operational amplifier used also are determined by the integration time. The feedback capacitor must have a dielectric leakage current less than the bias current of the amplifier. Chopper stabilized amplifiers are used in applications where long term integration is required, and FET amplifiers are used for medium length applications because of their low bias current. For this thesis work, no integration circuits were used due to the difficulty in implementation, consequently accelerometers were not adapted for the feedback control sensing system.

3.3.1.2 Strain Gages

Recognizing the need to obtain information on displacement directly from the sensing system, instead of integrating the acceleration signal to indirectly estimate the tool displacement, strain gages were used in the design of a sensing system. Figs. 3-12a and 3-12b illustrate the design of a cantilever beam strain gage assembly attached to the toolpost to directly measure the tool displacement. As shown in Fig. 3-12a, two strain gages were attached to the base, which were used in two legs of a wheatstone bridge as shown in Fig. 3-12b. A calibration curve was also used to convert the measured voltage signal to the displacement in micro-scale. It should be noted that the resolution of the sensing system is limited by two important factors:

1. Low resonant frequency of the strain gage sensing system. This is caused by the flexibility of the cantilever beam required to ensure the sensitivity to obtain sufficiently large strains. The dynamics of the cantilever beam, when subjected to the cutting force, represent a significant amount of undesirable signals mixed with the true displacement signal.
2. Accuracy of the calibration curve. In order to obtain measurable signal for manipulating the tool displacement, wheatstone bridges and amplifier circuits are used. Noise in electronic devices is unavoidably induced to the sensing system because of the high amplification required.

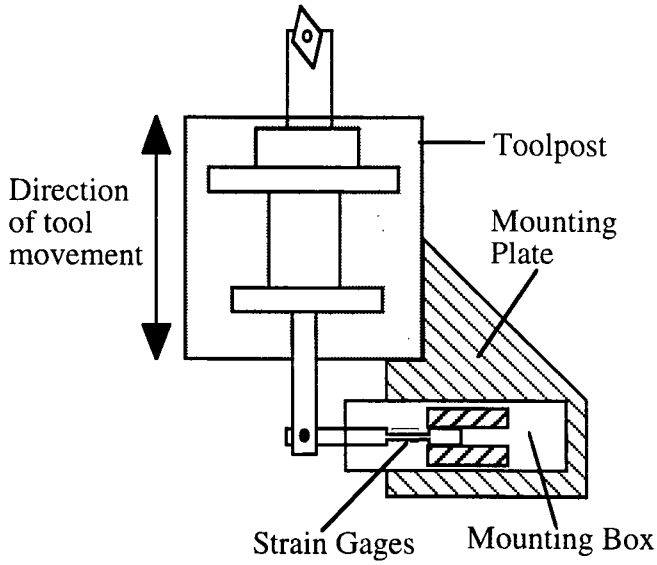

(a) Cantilever Beam Mechanical Sensor

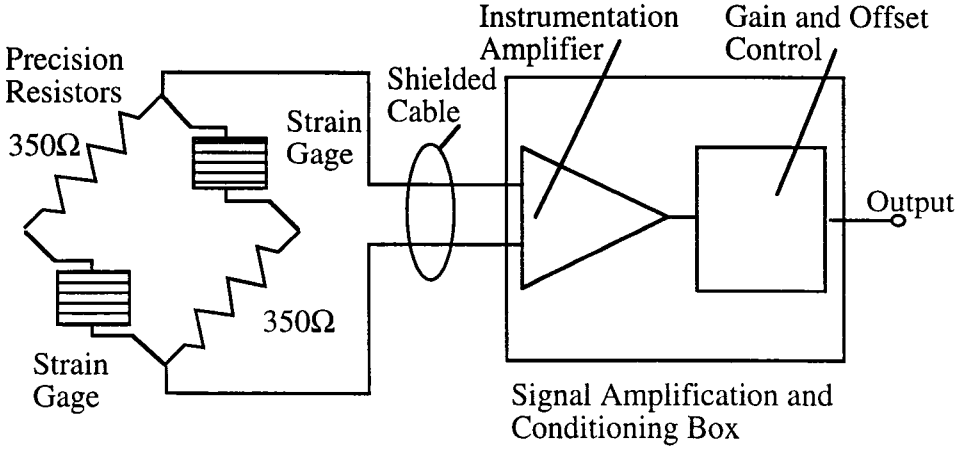

(b) Electrical Configuration of Wheatstone Bridge

Figure 3-12 Cantilever Beam Sensor System

The data detected by this sensor system provided many insights as to problems which would be encountered in this design process. Using this system to test the feasibility of using the actuators to provide compensatory control, an

experiment was performed to test the vibration reduction. The set-up is shown in Fig. 3-13.

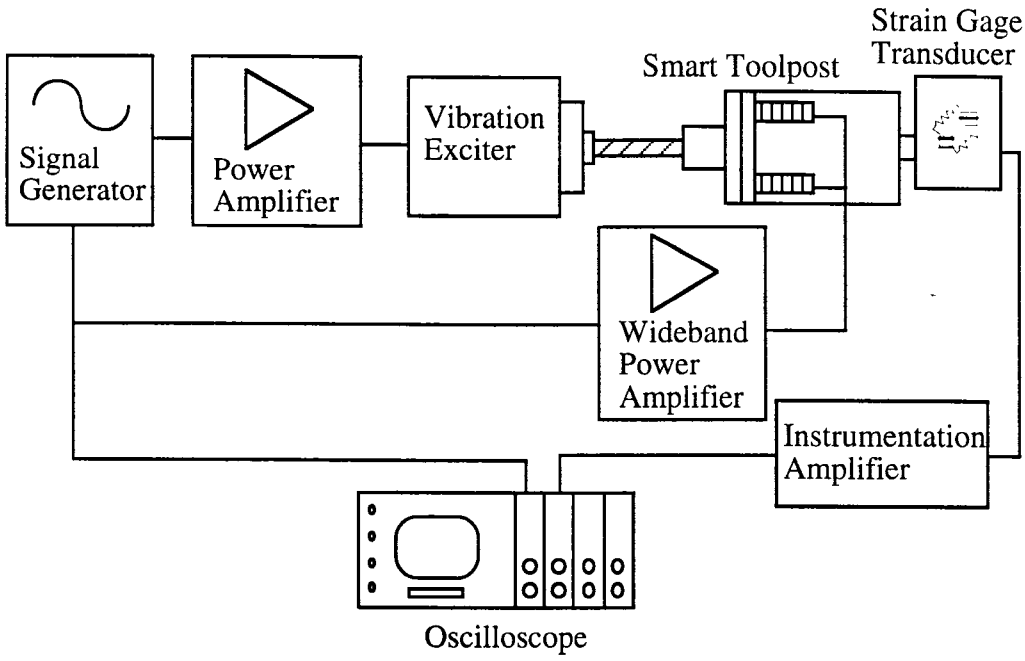

Figure 3-13 Block Diagram of Experimental Set-up

A signal generator was used to drive both the vibration exciter and the PMN actuators, and the signal from the strain gage displacement sensor output was used for monitoring purposes only. The data recorded from this experiment for a frequency range between 100 Hz and 300 Hz are shown in Table 3-1 and the graph of the listed data is shown in Fig. 3-14. The presence of a power amplifier is to adjust the level of the driving voltage to the vibration exciter so that the amplitude from the displacement sensor without feedback is normalized at 20, 40, and 80mV, respectively. Comparison is made between the amplitude of the measured displacement without the feedback loop and the amplitude of the measured displacement with the feedback loop to demonstrate vibration compensation.

Table 3-1 Vibration reduction using signal generator for feedback

Driving Frequency (Hz)	DC Offset (V)	AC Voltage to Actuators (Vp-p)	Displacement w/o feedback (mVp-p)	Displacement with feedback (mVp-p)	% Reduction
100	0	0	20	20	0
125	-92	43	20	16	20
150	-203	15	20	7.4	63
200	-203	8	20	4	80
250	0	0	20	20	0
300	-153	43	20	7	65
100	0	0	40	40	0
125	-88	54	40	31	23
150	-197	26	40	22	45
200	-202	15	40	4.5	89
250	0	0	40	40	0
300	-153	86.3	40	11	73
100	0	0	80	80	0
125	-96	73	80	30	63
150	-195	33	80	54	33
200	-203	26	80	9	89
250	0	0	80	80	0
300	-119	98	80	43	46

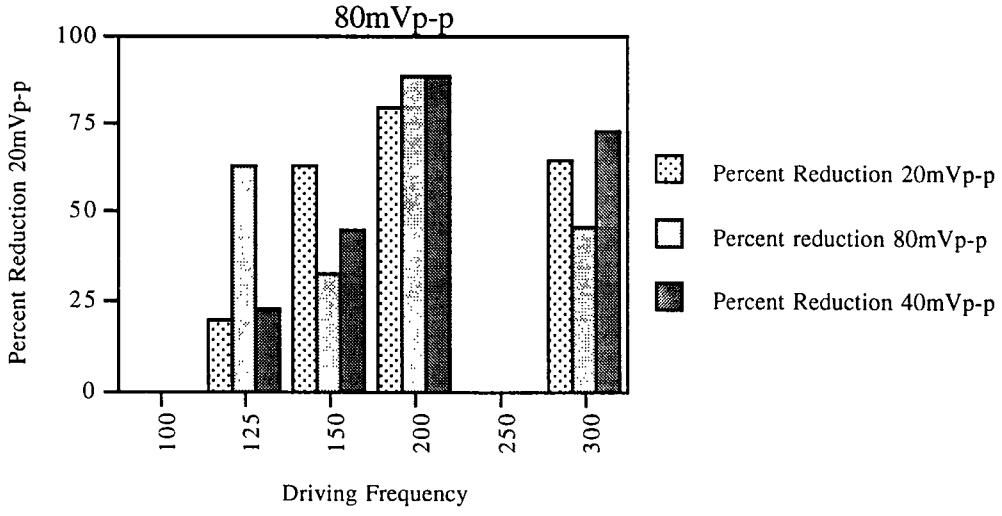

Figure 3-14 Graph of Attenuation at Various Frequencies

As can be seen by the results, at different frequencies, different attenuation levels could be achieved due to different factors. However, at certain frequency settings, the attenuation can be hardly observed. The influencing factors are summarized as follows:

1. By looking at the first six rows, with a range of frequencies from 100Hz to 300Hz, the percent reduction varies from 0% to 80%. A maximum reduction is achieved with the driving frequency set at 200 Hz. Therefore, the reduction is a function of the frequency.
2. The effect of AC voltage setting can be evidenced by examining the three vibration reduction levels achieved at 125 Hz and 200 Hz. The non-linear nature is clearly displayed. At 125 Hz, the reduction levels are 20%, 23%, and 63% for the AC voltage setting at 43, 54, and 73 Vp-p, respectively. On the other hand, the reduction levels are 80%, 89%, and 89% at 200 Hz, respectively. The percent reduction corresponding to the initial displacement can also be seen as a function of the feedback level. The compensation pattern varies so dramatically that an adaptive control mechanism has to be considered in order to maximize the vibration reduction while maintaining the control system stable during the compensation.
3. There are five cases among the 18 cases where vibration reduction can not be achieved. It is interesting to observe that, for any effort to adjust either the DC offset or AC voltage, or both, the vibration magnitude will increase, instead of decreasing. Very often such adjustment leads to an unstable system if the adjustment level increases. These phenomena strongly indicate that the phase relation between the excitation and the force exerted by the PMN

actuators is out of phase. The control action is not in the position to compensate, but promote the existing vibration.

These observations are so critical that they have provided a foundation for the controller design. The attainable reduction is subject not only to the mechanical interaction of the tool post system, but also subject to the previously described factors and their interaction. It is evident that a phase shifter control unit is required to adjust the phase of the feedback signal for proper attenuation at all frequencies, and for attenuation without oscillation. In addition, a gain control is also required to accommodate the variation of initial displacement. The most important conclusion derived from the experiments is that an adaptive control mechanism must be implemented for both the phase shift control and the gain control because these two parameters displayed strong non-linear nature. Without a self-tuning system, an optimal vibration control action can never be realized.

While performing the experiments with the strain gage sensor, it was determined that the resonant frequency of the sensing system was too low, and that the data being received by the sensor was not entirely correct. To determine the effect of the resonance of the cantilever beam on the measurements, the vibration exciter was decoupled from the toolpost as was done for the accelerometer and the system was again tested. The output of the sensor showed that it was also picking up vibrations transmitted through the base.

3.3.1.3 Noncontact position measuring system

To overcome the limitations imposed by the strain gage sensor, efforts have been made to introduce noncontact sensing systems. Two noncontact position sensors with different sensitivities are used in this thesis work. After comparison, a better one is selected.

The first attempt is to use a noncontact position measuring system manufactured by Kaman Instrumentation corporation in the design. The KD2300-1S system consists of a variable impedance bridge with an active coil and a reference coil. Variation in impedance results from the eddy currents induced in nearby conductive surfaces. The sensitivity is dependent upon the material and shape of the target. The KD 2300-1S has a resolution of 100 μm, with an output of 1000 mV/mm. This system performed well at high amplitude excitation by the vibration exciter, but did not produce enough output at lower amplitudes. The gain of the unit was then raised to compensate for the low output, but the noise level produced necessitated in filtering at a frequency lower than 1000Hz, thus modifying the feedback signal too much.

The Kaman Smμ-9100 Microinch System is then designed into the system. This system is similar to the KD2300-1S, with much higher resolution. This system consists of a sensor and a special SMU-9000 signal conditioning unit. It has high resolution, excellent temperature stability, low non-linearity, single supply operation, and low power consumption. The unit is pre-calibrated at the factory to an aluminum target for an output of zero to one volt over a .001" (25.4μm) range with a .010" (254μm) offset from the sensor face. A plot of the non-linearity and absolute error versus distance is shown in Fig. 3-15.

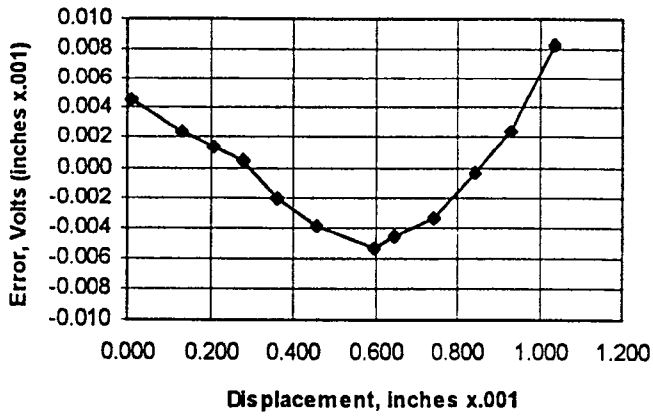

Figure 3-15 Non-Linearity of Sensor

From the range of 600μinch to 1000μinch, the error has a range of 13 mV. The measurement accuracy at such a high level allows a linear relationship between the output voltage and the displacement. This accounts for an error of 32μV per 1μInch of displacement. Note that the linear relation is characterized by 1000 μV per 1μInch of displacement. Therefore, the error level in measurement is limited to below 1%.

Temperature performance is a key issue with regards to the sensing equipment. When the cantilever beam strain gage system was implemented, semiconductor strain gages were not used due to their temperature dependence. The SMμ-9100 has a temperature coefficient specified as less than +/-1 μinch/degree F. The SMμ-9100 has excellent resolution with a frequency response from 0 to 10kHz, with a peak-to-peak noise as shown in Fig. 3-16.

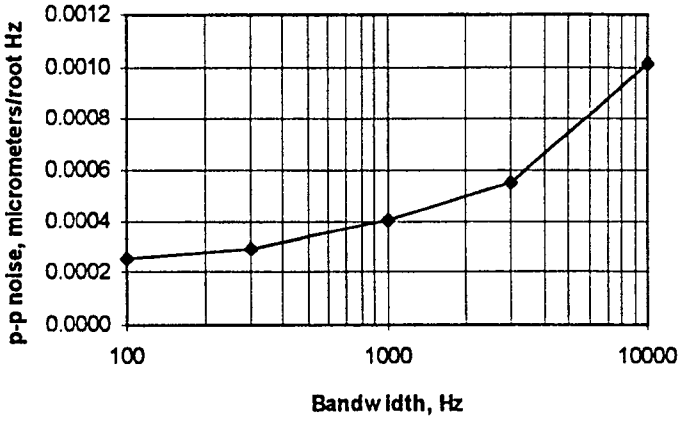

Figure 3-16 Sensor Peak-to-Peak Noise

To ensure minimal noise from the sensor unit, the sensor unit and the amplifier are powered by a dual 12V battery system to keep the system isolated from 60-cycle noise. An isolation transformer is used to keep noise from corrupting this isolated system, shown in Fig. 3-17.

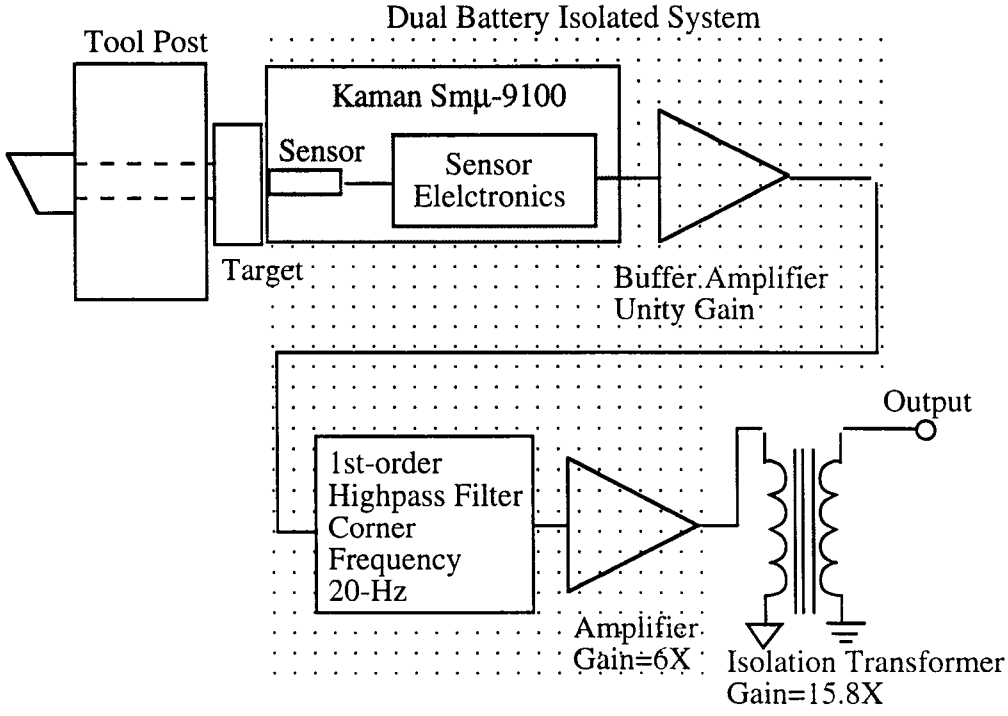

Figure 3-17 Diagram of Sensor Electronics

3.3.2 Design of Phase-Shift Control System

To reduce the tool vibration, the actuators must provide a counteractive force to resist any change of displacement of the tool. As shown previously, the signal to the actuators has to be such that the actuator produces a signal 180 degrees out of phase with the driving signal. Because the analog-to-digital (A/D) and digital-to-analog (D/A) conversions and model-based computations required by the control system design take a finite amount of time, there will always be a delay between the signal detection and the time the control action is applied to the PMN actuators. This means that the measured tool displacement at time t_k is used to compute the control signal applied at time t_{k+1}. The length of the time interval must be shorter than 1/100th of a second if the vibration compensation is performed at a frequency of 100Hz. This time interval is reduced to 1/400th of a second if the frequency is at 400Hz. In order to implement the destructive interference principle and consider the computational delay, a combined information [Agogino 1996] modeling and microprocessor-based approach is introduced.

3.3.2.1 R-C Phase Shifting

As illustrated in Fig. 3-18, a simple phase shifter can be constructed with a single resistor-capacitor circuit. By filtering with a corner frequency close to that of the driving frequency, a phase shift can be obtained. A schematic of this circuit is shown in Fig. 3-18.

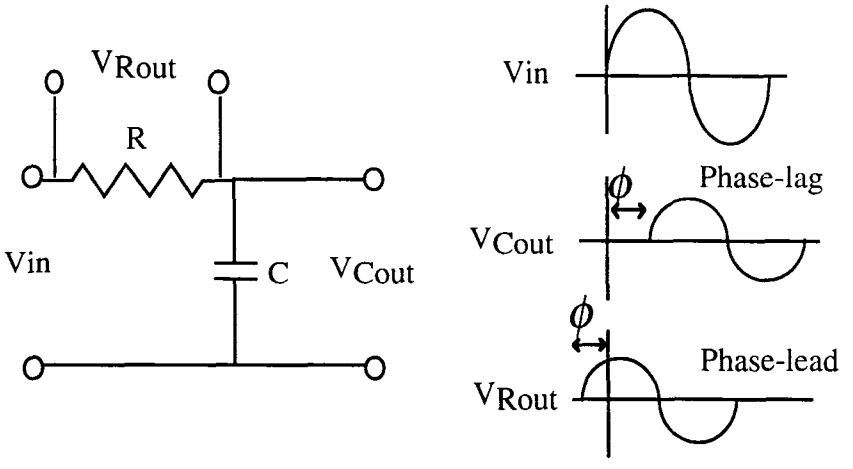

Figure 3-18 Phase Relation of R-C Circuit

Depending on the location where the voltage is taken, phase-lag and phase-lead can be obtained. The phase shift given by this circuit with phase-lead or phase lag is given by

$$\phi = tan^{-1}(\omega RC) \tag{3-4}$$

If a variable resistor or capacitor is used, a phase shifter can be designed. However, in the process of shifting the phase, the output from this circuit also attenuates. The attenuation level varies at different frequencies. To compensate for this, a gain control circuit should be designed with an amplifier to keep the output level constant, regardless of the frequency. The drawback to this is that at high phase shifts, large amplification is necessary. Any noise introduced by the gain control circuit is also be amplified and will be present in the output. Therefore, a different approach for a delay line is proposed and implemented.

3.3.2.2 Bucket Brigade

The phase shifter employed in this thesis work is based on a "bucket brigade" principle. This principle uses a series of storage locations to shift a known quantity, and in the shifting process, delay it in time. Figure 3-19 illustrates this principle.

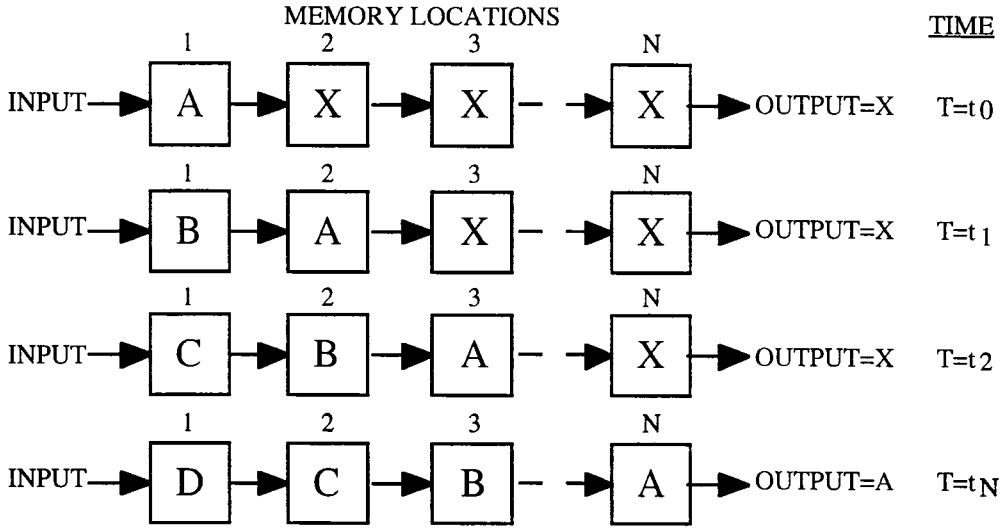

Figure 3-19 Bucket Brigade Storage Implementation

The value "A" is input into the system at time t_0, and at a specific time interval, the value of all of the registers are shifted once to the next memory location. To accomplish this digitally, a specific value of amplitude is first converted to a binary representation using an A/D converter. It is then stored in a memory location, successively shifted through a series of memory locations, and is then shifted out at a later time. As this process continues, a delayed representation of the input signal is output from the bucket brigade. The diagram for the phase delay designed for this thesis is shown in Fig. 3-20. To implement the "bucket brigade" principle, two key factors are:

1. Fast and accurate calculation or retrieval. Implementation of a bucket brigade is accomplished accurately by a dedicated microcontroller. The storage and retrieval process can not be subject to any interruptions which can affect the precise timing of the process loop, which might happen if using an A/D board on a computer due to internal computer interrupts.
2. The relationship between the phase shift angle and frequency has to be available before implementation. Such a relationship can be obtained by a analytical model or empirical model.

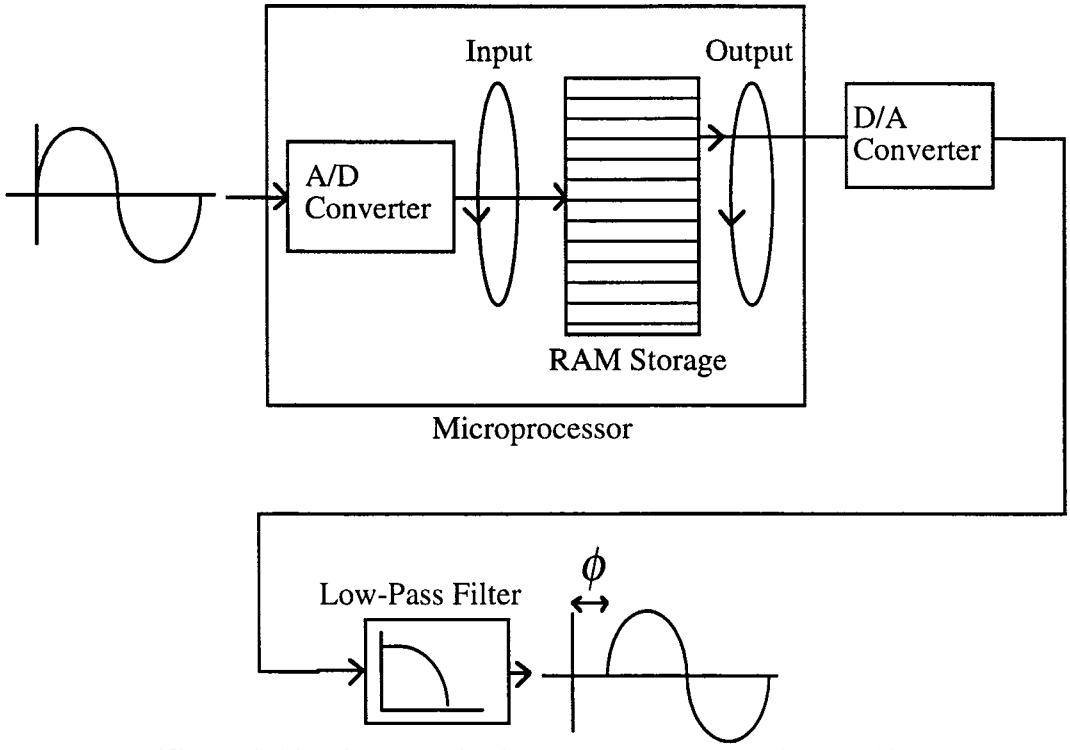

Figure 3-20 Diagram of Microprocessor Based Phase Shift

As is shown in Fig. 3-20, the key components for the bucket brigade are an A/D converter, a RAM storage area, a D/A converter, and an output low-pass filter.

3.3.2.3 Operation of Microprocessor Controlled Phase Shifter

The microprocessor used for the phase shifter is a Motorola MC68HC11F1. The Motorola MC68HC11F1 is a high-density complementary metal-oxide semiconductor (HCMOS) advanced 8-bit microcontroller (MCU) with highly sophisticated, on-chip peripheral capabilities [HC11 1990]. It has a nominal bus speed of 2MHz, with a fully non-multiplexed address/data bus. The fully static design allows for operation at frequencies down to dc to reduce power consumption. The HCMOS technology used on the MC68HC11 combines smaller size and higher speeds with the low power and high noise immunity of CMOS. In addition to the non-multiplexed bus, on-chip memory systems for the MC68HC11F1 contain 512 bytes of electrically erasable and programmable ROM (EEPROM), and 1K bytes of random-access memory (RAM), and intelligent chip selects for simple connection to external program memory without the need for any external logic chips.

Major peripheral functions are provided on chip. An eight channel analog-to-digital (A/D) converter is included with eight bits of resolution. An asynchronous serial communications interface (SCI) and a separate synchronous serial peripheral interface (SPI) are included. The main 16-bit, free running timer system has three input capture lines, five output compare lines, and a real time interrupt function. An 8-bit pulse accumulator subsystem can count external events or measure external periods.

The MC68HC11 instruction set includes 110 opcodes. Fig. 3-21 shows the seven CPU registers available to the programmer. The two 8-bit accumulators (A and B) can be used by some instructions as a single 16-bit accumulator called the D-register, which allows a set of 16-bit operations even though it is technically an 8-bit processor. With the index registers X and Y, 16-bit arithmetic can be used, with a 16-bit divide function and an eight bit multiply function.

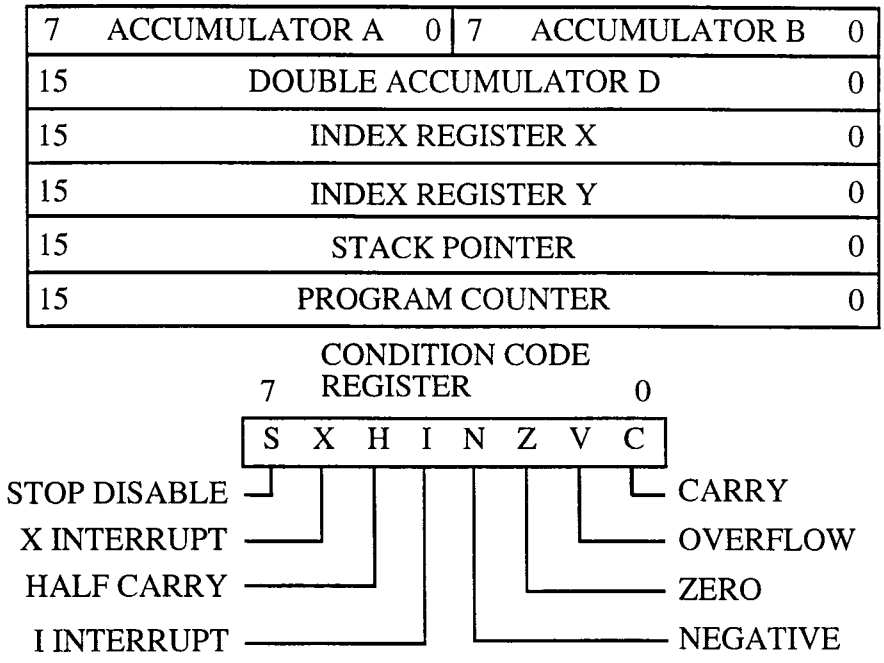

Figure 3-21 CPU Registers

The basic operation of the microprocessor controlled phase shifter can be divided into three areas:

1. Input A/D conversion
2. RAM storage and output
3. D/A conversion of output and filtering

3.3.2.4 Input A/D conversion

The Motorola MC68HC11F1 analog to digital (A/D) converter system uses an all-capacitive charge redistribution technique for conversions. The A/D system is an 8-channel, 8-bit, successive approximation converter with +/-1/2 least significant bit accuracy. Because of the charge-redistribution technique, no external sample and hold circuits are required. With respect to timing conversion speed, the system E-clock, which is one fourth the crystal frequency, is used as the conversion clock. The earliest availability of valid data in the result register 1 is 34 E-clock cycles after the initiation of the conversion process.

3.3.2.5 RAM storage and output

To perform the operation of the bucket brigade, a storage area is needed to successively store the converted values during the conversion process. The size of the storage area and the sampling rate determine the maximum time delay obtainable. The delay process is implemented as follows. The MC68HC11 has two pointers, index register X and index register Y. Index Y is set to the address corresponding to the start of the memory storage, and index X is set at some specified offset ahead of index Y in the memory space. During the loop process, the data which has been converted by the A/D converter is stored in the memory location pointed by index X, and the data corresponding to the position pointed to by the index Y is read and sent to the D/A converter. Both of the values of the index registers are then incremented, thus pointing to the next data location. During the loop process, a check to see if either index register is at the end of the memory allocation. If it is, then the index register is reset to the beginning memory location. The timing of the loop is very critical to ensure a precise delay time.

The complete conversion and output process loop takes 54 cycles to implement. With a clock rate of 4.9152MHz, each instruction cycle takes .8138μSec. Therefore, the total loop process of 54 cycles takes 43.945μSec, which corresponds to a sampling rate of 22.756 kHz. With this microprocessor, the maximum clock rate is 8.0 MHz, which would correspond to a sampling rate of 37.037 kHz.

The MC68HC11 has a multiplexed address and data bus which facilitates external memory addressing with minimum address time. At a sampling rate of 22.756 kHz, with an input frequency between 100Hz and 400Hz, the conversion memory storage area should have no less than 228 bytes. There are 1024 bytes of internal RAM incorporated into the MC68HC11. The memory allocation used for

the conversion storage was located in the internal RAM, from 0100Hex to 030FHex, which corresponds to a memory size of 767 bytes. The maximum delay time is given by

$$Max\ Delay = \frac{(\#\ bytes\ memory)(clock\ cycles\ per\ loop)}{(clock\ speed)/4} \tag{3-5}$$

At the clock rate of 4.9152Mhz used, this corresponds to a maximum time delay of 33.7mSec, as shown below.

$$Max\ Delay = \frac{(767)(54)}{(4.9152Mhz)/4} = 33.7mSec \tag{3-6}$$

The resolution of the degrees of phase shift is determined by the clock speed of the microprocessor, which determines the sampling rate, and the frequency of the input signal. The phase shift resolution possible is given by

$$Max\ Phase\ Shift(degrees) = MaxDelay \times Frequency \times 360 \tag{3-7}$$

The phase angle resolution is also a function of the microprocessor clock speed and the frequency of the input signal. This is given as

$$Phase\ angle\ resolution = \frac{(\ clock\ cycles\ per\ loop)}{(clock\ speed)/4} \times Freq \times 360 \tag{3-8}$$

At a clock rate of 4.9152 Mhz, this corresponds to

$$Phase\ angle\ resolution(degrees) = 43.945\mu Sec \times Frequency \times 360 \quad (3\text{-}9)$$

Table 3-2 gives the phase shifts possible and phase angle increments for various frequencies.

Table 3-2 Phase Shift and Increments

FREQUENCY Hz	PERIOD mSec	Phase shift possible degrees	Phase angle increments degrees
100	10	1213.2	1.58202
150	6.667	1819.8	2.37303
200	5	2426.4	3.16404
250	4	3033	3.95505
300	3.333	3639.6	4.74606
350	2.857	4246.2	5.53707
400	2.5	4852.8	6.32808

As can be seen from the table, ensuring that the timing of the A/D conversion and RAM storage loop is kept to a minimum is very critical, even at higher clock speeds. The resolution of the phase shift as the frequency increases becomes coarser for a given microprocessor clock speed.

3.3.2.6 D/A Conversion of Output and Filtering

The value that is read by the index register Y, the shifted value, is sent over the data bus to an 8-bit D/A converter, an Analog Devices AD558. Since the output at this stage is stepped representation of the input, the signal must be filtered to smooth it out. This filtering is done in the feedback loop of an operational amplifier. The circuit diagram for the phase shifter is shown in Fig. 3-22.

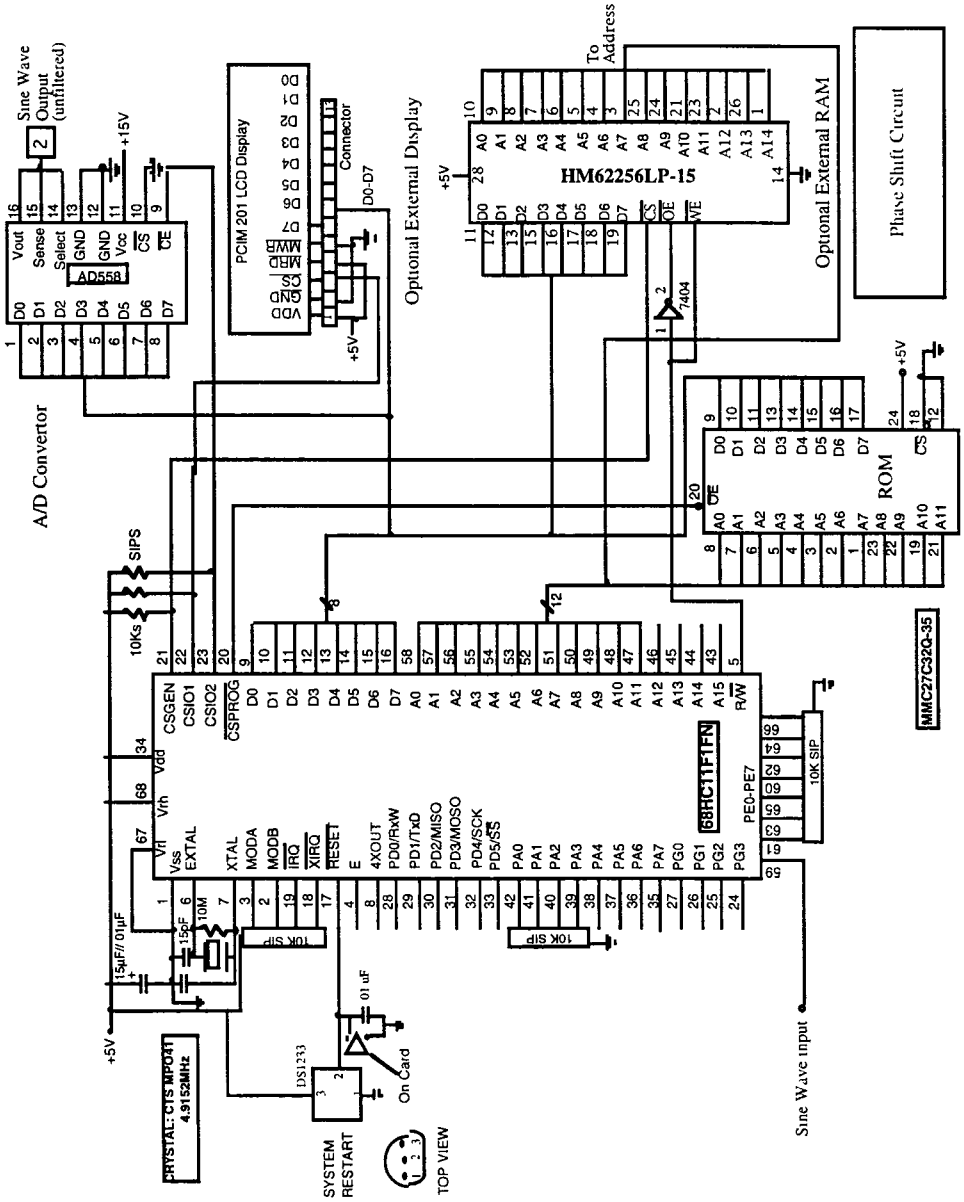

Figure 3-22 Schematic of Microprocessor Based Phase Shifter

Chapter 4 Realization of the Phase Shifter Control System Design

4.1 Introduction

Following the control system design, efforts to realize the phase shift control design are made to build the control system. The built control system is tested and results from tests are compared with the design specifications to verify that the performance of the designed control system accomplishes the objective to control the tool motion during machining. In this chapter, the work done in the realization of the phase shift process is presented. The realization process consists of four steps:

1. Designing a signal conditioner to amplify and filter the feedback signal;
2. Establishing an empirical model for the phase shift vs. frequency relationship for the control system;
3. Implementing the real-time estimation for the feedback signal; and
4. Testing of the control system performance.

4.2 Design of a Signal Conditioner

A circuit diagram for the electronics associated with amplification and filtering of the signal provided by the displacement sensor is given in Fig. 4-1.

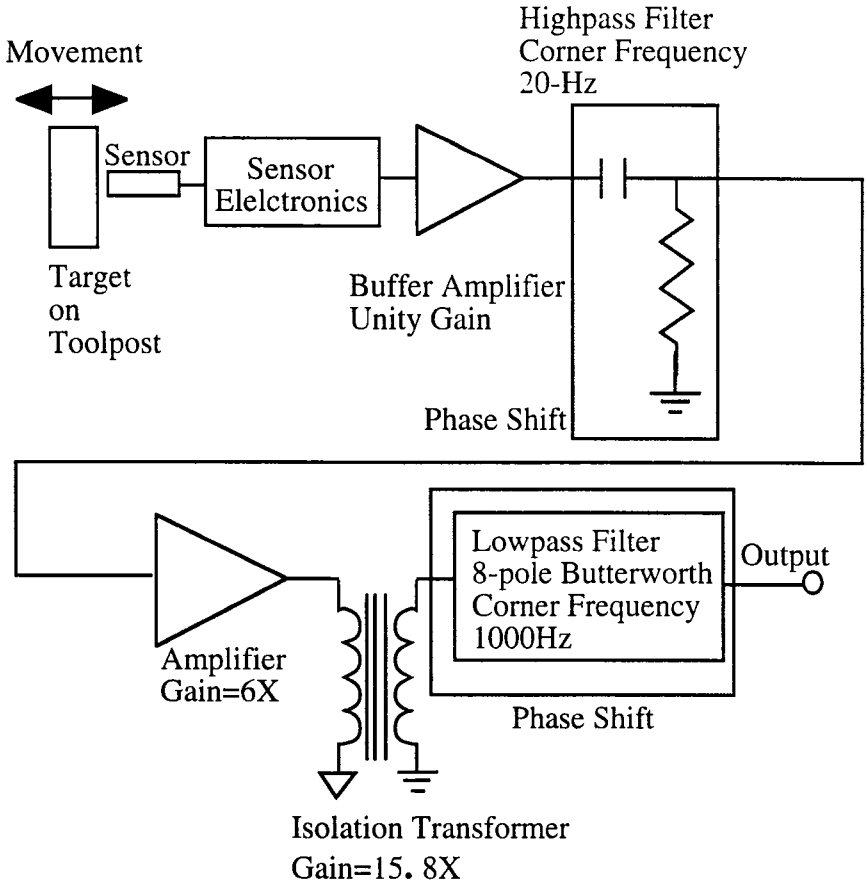

Figure 4-1 Displacement Sensor Electronics

The input stage consists of a buffer amplifier connected to a high pass single pole R-C filter. The buffer amplifier is a J-FET input precision operational amplifier, used to protect the sensor in case of any electrical problems. The highpass filter is used to AC-couple the output of the displacement sensor signal, because this output has a DC level ranging from 0V to 1V. The corner frequency of this filter is set at 20 Hz, to reduce low level signal fluctuations produced by the displacement sensor. The analytical phase shift for this filter is given by, for the frequency range of interest:

$$\phi = 90^{o} - tan^{-1}(\frac{1}{2\pi RCf})$$

(4-1)

The signal is then amplified by an operational amplifier by a factor of 6. After passing through an isolation transformer with a gain of 15.8, the signal passes through an eight pole butterworth filter with a corner frequency of 1000Hz. The amplification is required to raise the signal level within the dynamic range of the A/D converter. The corner frequency is chosen through experimentation as the best trade off between phase shift and reduction of noise from the displacement sensor. The analytical response for this filter is given in appendix B. The phase shift given by this complete system was measured by using a sine wave input and comparing it with the output signal. Table 4-1 shows the data, and Fig. 4-2 shows the comparison between empirical and analytical values. The slight discrepancy can be attributed to signal noise error and measurement capabilities.

Table 4-1 Phase Shift of Displacement Sensor Electronics

Frequency	Phase Shift electronics degrees	Analytical Phase shift degrees
100	18.72	17.5
120	23.328	
140	33.264	
160	41.472	
180	47.952	
200	54.72	53
220	60.984	
240	67.392	
260	73.944	
280	80.136	
300	86.94	85
320	93.312	

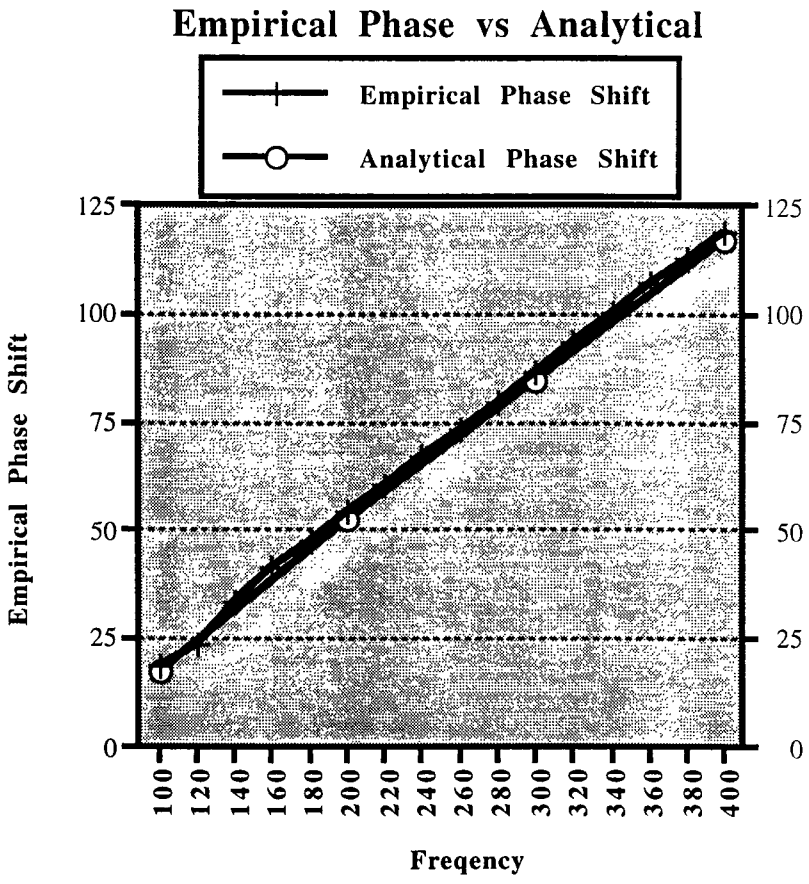

Figure 4-2 Graph of Analytical versus Measured Values for Sensor Electronics

4.3 Information Modeling of Phase Shift

The control system realization starts in identifying the phase shift vs. frequency relationship for the control system. Figure 4-3 presents the experimental setup used in this investigation.

4.3.1 Phase Shift of PMN Actuators and Amplification System

The next step in the experimental process is to characterize the phase shift of the PMN actuators and the actuator amplifier. The two phase shifts of the actuators and amplifier are measured as a combined phase shift unit. The experimental set-up is shown in Fig. 4-3.

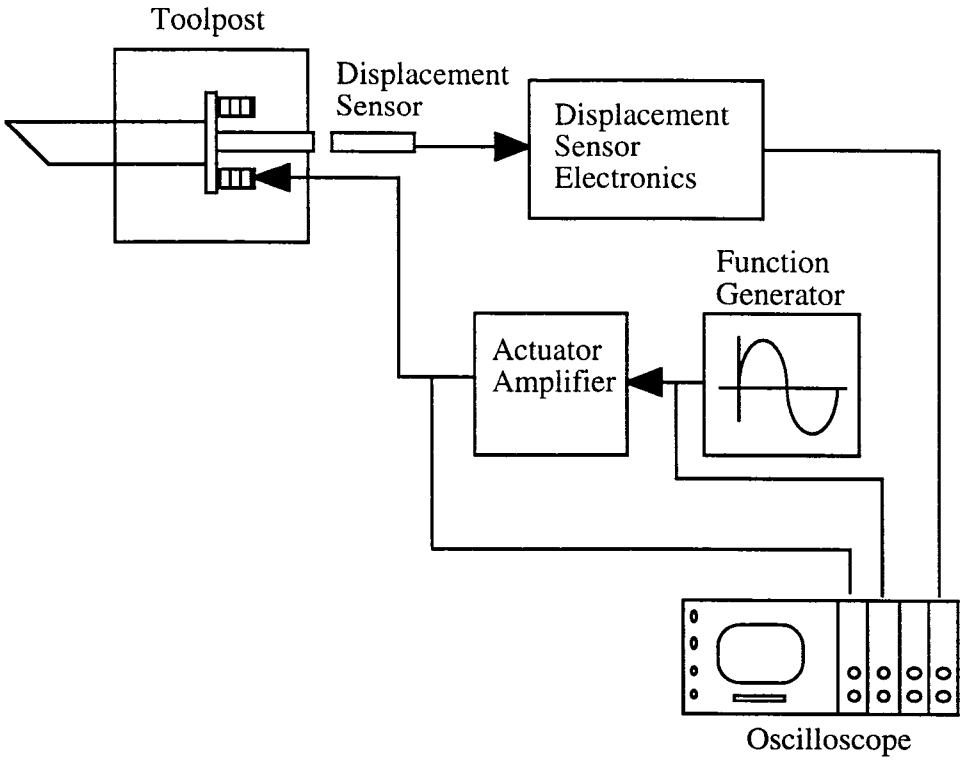

Figure 4-3 Experimental Set-up

Table 4-2 shows the tabulated data from this experiment, and Fig. 4-4 the graphical results. The phase shift given in column 2 of Table 4-2 is from experimental data with units in seconds, and column 3 is the phase shift values converted to the corresponding degrees based on the following formula:

$$Phase\ Shift\ (degrees) = Phase\ Shift\ (sec) \times \frac{1}{Frequency} \times 360 \qquad (4\text{-}2)$$

Table 4-2 Phase Shift of PMN Actuators

Frequency	Phase shift amplifier and actuator (mSec)	Phase shift amplifier and actuator (degrees)
100	0.78	28.08
120	0.78	33.696
140	0.73	36.792
160	0.61	35.136
180	0.64	41.472
200	0.6	43.2
220	0.61	48.312
240	0.62	53.568
260	0.57	53.352
280	0.535	53.928
300	0.495	53.46
320	0.48	55.296
340	0.46	56.304
360	0.475	61.56
380	0.454	62.1072
400	0.424	61.056
420	0.402	60.7824
440	0.402	63.6768

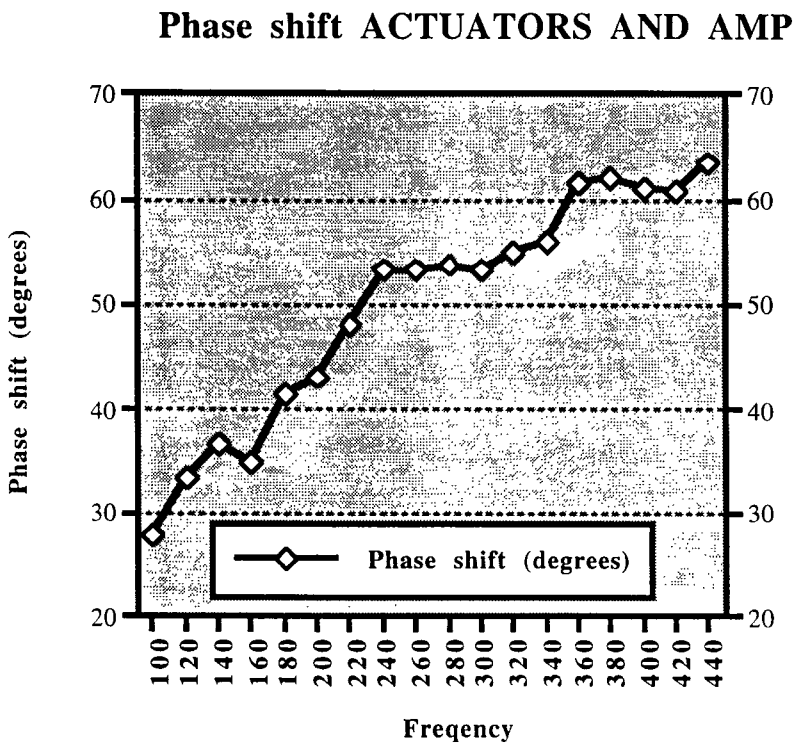

Figure 4-4 Phase Shift of PMN Actuators

4.3.2 Phase Shift Criteria

A concept is now presented on the proper phase shift needed for proper reduction of tool vibration. Figure 4-5 shows a block diagram of the simplified feedback system necessary for tool vibration reduction.

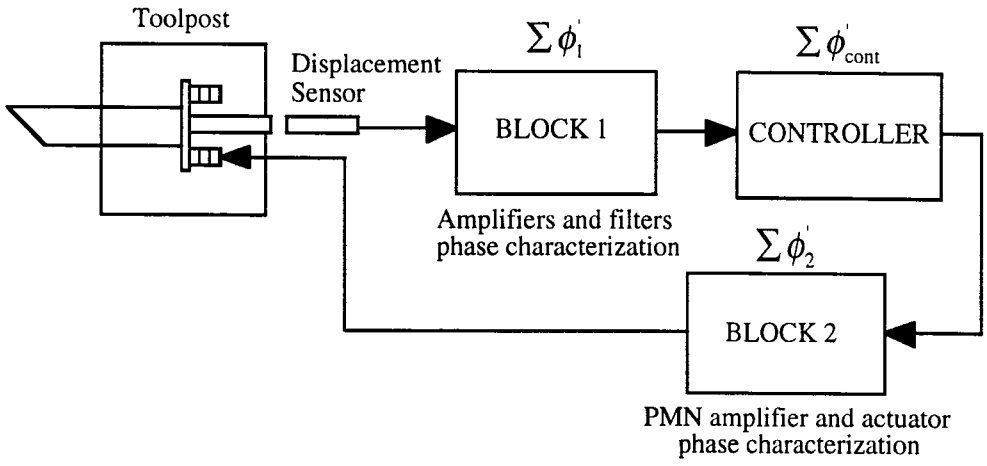

Figure 4-5 Feedback System for Reduction of Tool Vibration

For proper attenuation, the force imposed by the actuators must be the displacement sensor signal shifted 180 degrees. Therefore, the system must follow Equation 4-3.

$$\phi_{Act} = \Sigma\phi_1' + \Sigma\phi_{cont}' + \Sigma\phi_2' = 180^{o} \tag{4-3}$$

The phase shift introduced by the control system should then be

$$\Sigma\phi_{cont}' = 180^{o} - (\Sigma\phi_1' + \Sigma\phi_2') \tag{4-4}$$

Table 4-3 shows the needed phase shifts for adjusting the phase angle of the voltage signal which drives the PMN actuators for active vibration compensation. Note that the values obtained previously for block 1, the amplifiers and filter, and block 2, the PMN amplifier and actuators, are used in the calculation. Table 4-3 gives the analytical and analytical corrected values in columns two and three.

Table 4-3 Phase Shifter Phase Shifts

Frequency Hz	Analytical phase shift from microprocessor 180-actuator-electronics	Corrected Analytical phase shift	Empirical Measured Phase	Corrected Empirical feed back phase
100	133.2	133.2	139.2019	139.20192
120	122.976	122.976	119.5871	119.587104
140	109.944	109.944	106.2996	106.299648
160	103.392	103.392	93.64493	93.644928
180	90.576	90.576	74.03011	74.030112
200	82.08	82.08	82.25568	82.25568
220	70.704	70.704	66.12091	66.120912
240	59.04	59.04	60.74266	60.742656
260	52.704	52.704	61.69176	61.69176
280	45.936	45.936	31.00406	31.004064
300	39.6	39.6	18.98208	18.98208
320	31.392	31.392	30.37133	30.371328
340	23.328	23.328	5.378256	5.378256
360	11.52	11.52	11.38925	11.389248
380	355.104	-4.896	342.6265	-17.373456
400	360	0	329.0227	-30.97728

In column 1, the analytical phase shift is calculated by Equation 4-3, substituting in the values from Tables 4-1 and 4-2. As an example, the analytical phase shift at 100 Hz is given by 180 - 18.72 - 28.08, which is equal to 133.2 degrees. The corrected analytical phase shifts, as listed in column 3, are the same as the analytical phase shifts listed in column 2 except for those few values above 180 degrees which have been subtracted from 360 degrees to give a linear graph. A

least squares or higher order curve fit of the frequency to phase shift relation is then possible.

To determine the effectiveness of applying the adjusted phase shift to reduce vibration, an experiment was conducted to determine the proper phase shift for maximum vibration reduction by using on-line manual adjustment. This set-up is shown in Fig. 4-6.

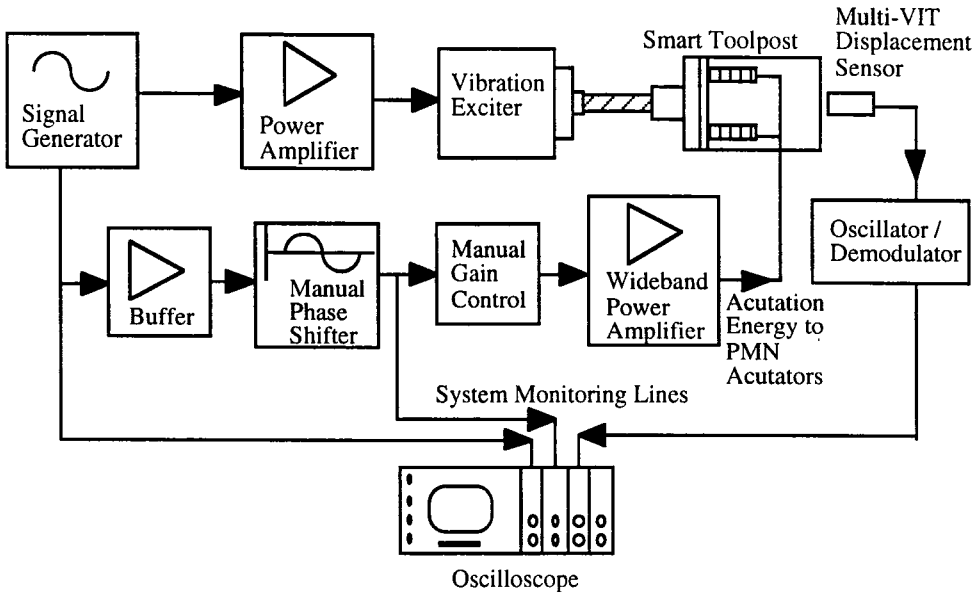

Figure 4-6 Configuration for Maximum Vibration Reduction

As can be seen in the diagram, the signal generator was used to drive both the vibration exciter and the PMN actuator systems. The feedback value from the displacement sensor was used only for monitoring purposes. A two button interface for increasing or decreasing the relative phase shift was incorporated into the microprocessor phase shifter. This was accomplished by using one push-button switch to trigger the pulse accumulator input, pin PA7, creating an

interrupt in the delay loop process. The microprocessor then polls PORT(A) and inputs the value of pin PA0 to determine whether to increase or decrease the delay time. A high level (5V) on pin PA0 increased the delay, a low level (0V) decreased the delay. Fig. 4-7 shows the pin configuration for this manual controlled phase shifter.

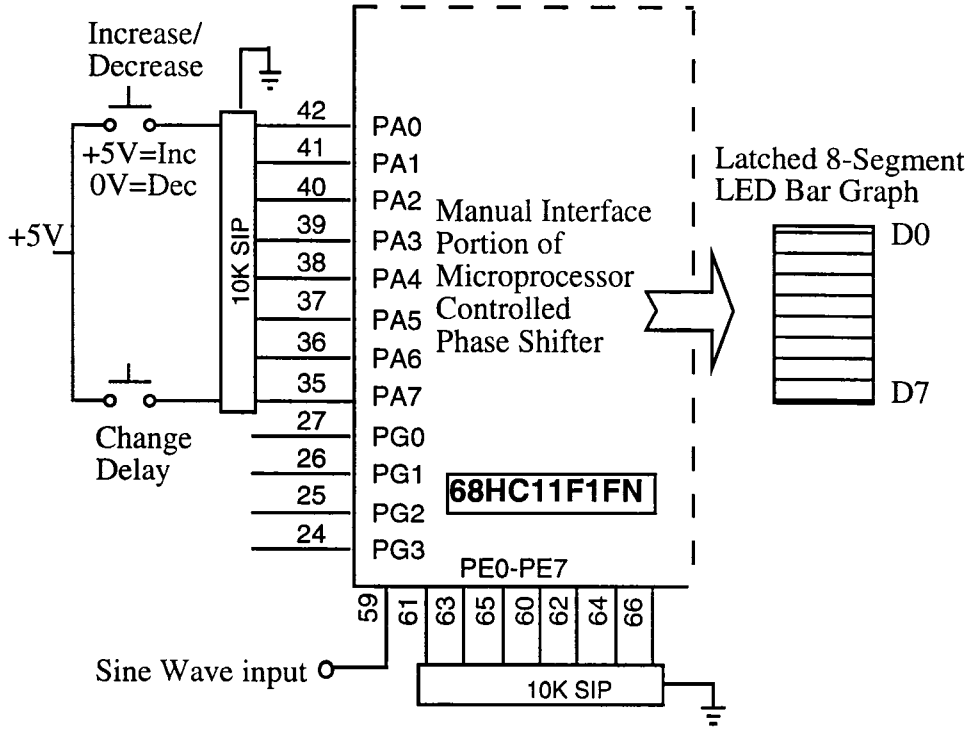

Figure 4-7 Interface for Increasing and Decreasing Phase Shift

The proper phase shift is found by changing the phase shift and monitoring the output of the displacement sensor. The number of time shifts used between the input and output of the signal by the phase shift control system (as explained in section 3.2.2) is displayed on an 8-segment latched bar graph as a binary value, and the phase shift time and degrees are calculated from this value. The percent reduction that is achievable in this process and the phase shift necessary are shown in Table 4-4.

Table 4-4 Percent reduction of Vibration with Manual Phase Shift

Frequency (Hertz)	Amplitude (Volts) without feedback	Amplitude (mV) with feedback	Percent Reduction
100	4.93	484	90.183
120	3.82	368	90.366
140	3.7	480	87.027
160	3.9	531	86.385
180	3.94	520	86.802
200	4.1	520	87.317
220	3.9	430	88.974
240	3.78	440	88.36
260	3.58	480	86.592
280	3.74	480	87.166
300	3.62	440	87.845
320	3.58	440	87.709
340	3.54	480	86.441
360	3.42	327	90.439
380	3.61	440	87.812
400	3.54	445	87.429
420	3.5	440	87.429
440	3.7	480	87.027

As can be seen by the percent reduction, the actuators can provide a counteractive force which gives a substantial reduction of vibration. PMN actuators are excellent candidates for producing large forces at small displacements. This test is only an indication of the use of the actuators to provide counteractive force for vibration reduction, since feedback is not used.

The experimental set-up was then changed to used the feedback from the displacement sensor to drive the actuators. This is shown in Fig. 4-8.

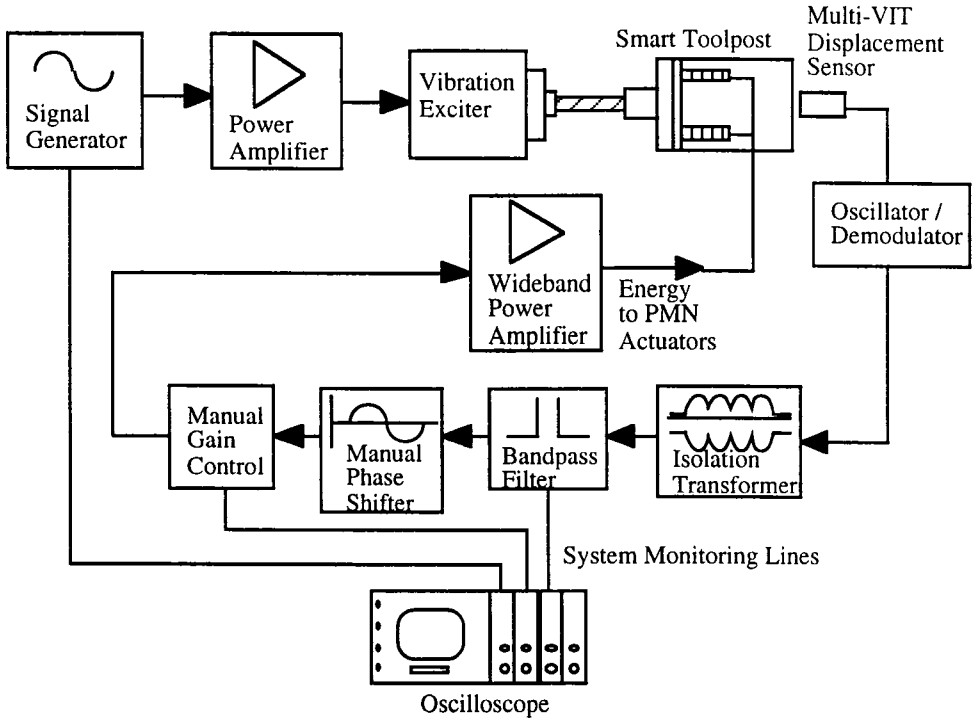

Figure 4-8 Configuration Using Displacement Sensor Feedback

The feedback signal was shifted by hand so that the delay was the same amount as was recorded previously with the sine wave generator driving both systems. This is accomplished by using the cursors on the oscilloscope. One cursor is placed at the start of the cycle of the sine wave produced by the function generator going to the vibration exciter. The second cursor is then placed at the time delay (delta-T) needed for the proper phase shift, and then the feedback signal is shifted by hand so that the start of its cycle is at the position indicated by the second cursor. The phase delay being produced by the phase shift control system is then read from the binary latched output and converted into degrees. This data is shown in columns three and four in Table 4-3.

The comparison between the analytical phase shift and the empirical phase shift for best reduction is shown in Fig. 4-9. The data in columns three and four in Table 4-3 have been shifted 360 degrees to give a continuous graphical representation. As can be seen by the graph, the analytical and empirical data matched very closely.

Using the signal from the sensor to drive the feedback loop resulted in reduction of vibration between 32%-47%, with an average of 37%. This is seen in Table 4-5, and graphed in Fig. 4-10.

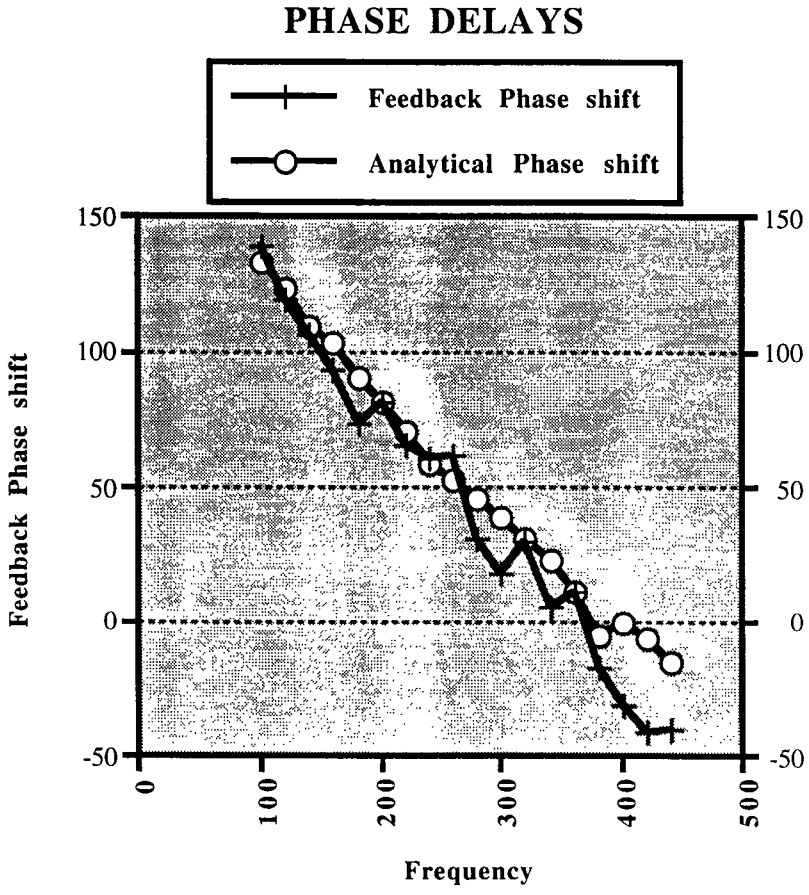

Figure 4-9 Comparison between the Analytical and Empirical Phase Shift

Table 4-5 Vibration Reduction with Manual Phase Shift

Frequency	Amplitude (Volts) w/o feedback	Amplitude (mV) with feedback	Percent Reduction
100	1.15	657	42.86957
120	1.12	593	47.05357
140	1.01	577	42.87129
160	0.92	568	38.26087
180	0.895	530	40.78212
200	1.47	870	40.81633
220	1.32	850	35.60606
240	1.3	880	32.30769
260	1.19	790	33.61345
280	1.23	790	35.77236
300	1.18	768	34.91525
320	1.14	768	32.63158
340	1.15	770	33.04348
360	1.12	743	33.66071
380	1.12	730	34.82143
400	1.14	714	37.36842
420	1.11	750	32.43243
440	1.2	715	40.41667

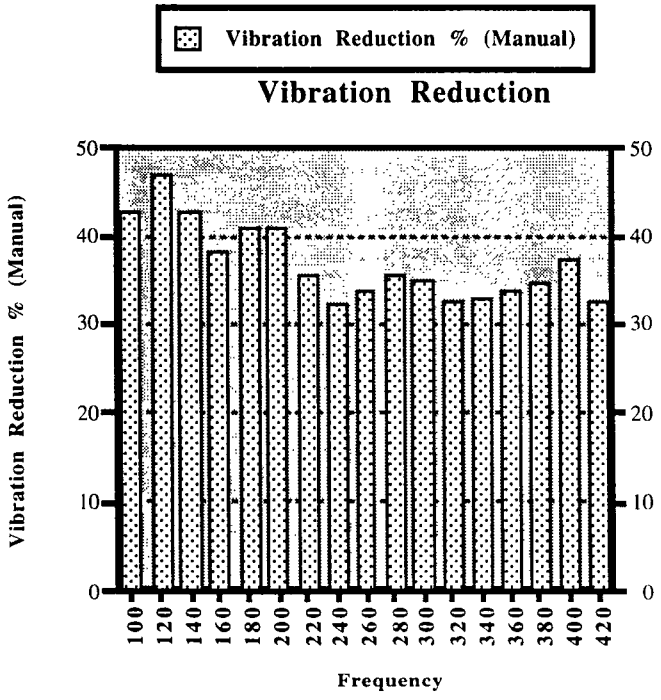

Figure 4-10 Vibration Reduction with Manual Phase Shift of Sensor Feedback

Using the data calculated from the analytical phase shift, an equation was modeled for the correct frequency to phase shift conversion. This is given by

$$PhaseShift(degrees) = 191.252 - .613 \times Frequency \tag{4-5}$$

This equation is used as the basis for modeling the algorithm of the self-tuning system given in Chapter 5.

Chapter 5 Realization of the Self-Tuning Gain Adapter

5.1 Introduction

As stated before, an intelligent mechatronic system for vibration control should have the capability to compensate the tool vibration by providing a counteractive force to resist any change of displacement of the tool. The actuating force must meet two requirements:

1. Synchronizing: The phase relationship between the actuating force and vibration action must be 180°, or out of phase so that the actuating force and the vibration action will be in the destructive interference. This requirement has been achieved through the design of the phase shift control system discussed in this chapter.
2. Appropriateness: The amplitude of the actuating force must be maintained at a certain level to insure effective vibration compensation can be achieved without instability.

Common sense dictates that a large gain factor will generate a powerful actuating force. However, overcompensation, in which the magnitude of the actuating force is larger than the magnitude of the vibration action, will lead the mechatronic system going to another end - unstability. Therefore, a compromise has to be reached at such a critical point that an actuating force has reached its peak value under the condition that stability of the mechatronic system is maintained. Precaution has to be taken because the peak value of the actuating force is a function of frequency and the original magnitude of the vibration action. A fixed gain mechanism can do an optimal control job, but will not be able to do the job if either frequency or the original magnitude of the vibration varies. Under circumstances where both frequency and the original magnitude of the vibration vary, which are the reality observed on the shop floor, an

automatic tuning system is needed. It will not only trace the frequency variation, but also detect the variation of the magnitude of the vibration action, which is before the compensation. Consequently, an intelligent mechanism has to be designed to accomplish such a two-fold task. Chapter 5 is mainly devoted to the design of an automatic gain adapter.

5.2 Programming and Communication of Phase Shift Required

The basis for the modeling of the self-tuning algorithm is given by equation 4-5, given in section 4.3.2. The automatic tuning circuit was programmed with an algorithm to determine the frequency of the feedback signal, and convert this frequency to the proper phase shift required by the phase shifter circuit, as given by equation 4-5. The automatic gain control system calculates the number of time shifts needed between the input and output of the signal by the phase shift control system (as explained in section 3.2.2), and converts it to a binary number. This information is then sent from the tuning circuit to the phase shifter circuit, automatically updating the phase shift. The communications between the two circuits are shown in Fig. 5-1.

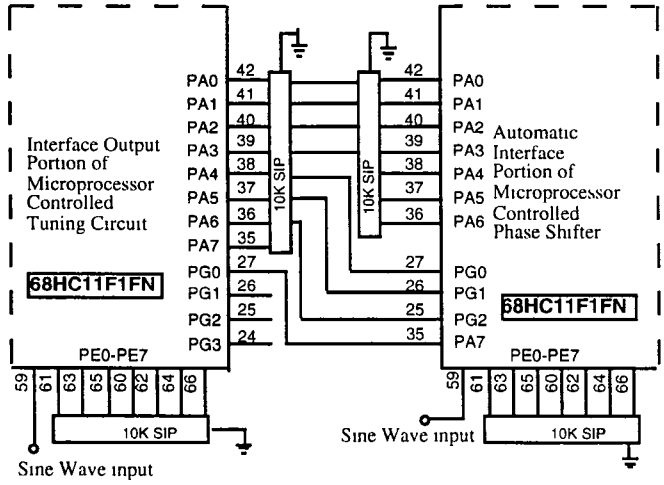

Figure 5-1 Interface Connections between Microprocessor Controlled Circuits

Each microprocessor radiates a certain amount of high frequency noise, which is radiated from the parallel data bus and address lines. This noise is transmitted on the digital ground of the circuit. Bypass capacitors are placed on the circuit board to reduce this noise. Initially, when both microprocessors were connected together, the noise level became larger, since separate crystals were being used to generate the clock signals for both microprocessors. This noise, which is tied in with the clock frequency driving the microprocessor, appeared on the output of the D/A converter. The ribbon cable interconnecting the two systems also became a source of noise. One solution to this problem would have been to place optically isolated line drivers between the two microprocessor circuits. A quick acceptable solution to this problem was to place filter capacitors at the junction point of the ribbon cable. This is shown in Fig. 5-2.

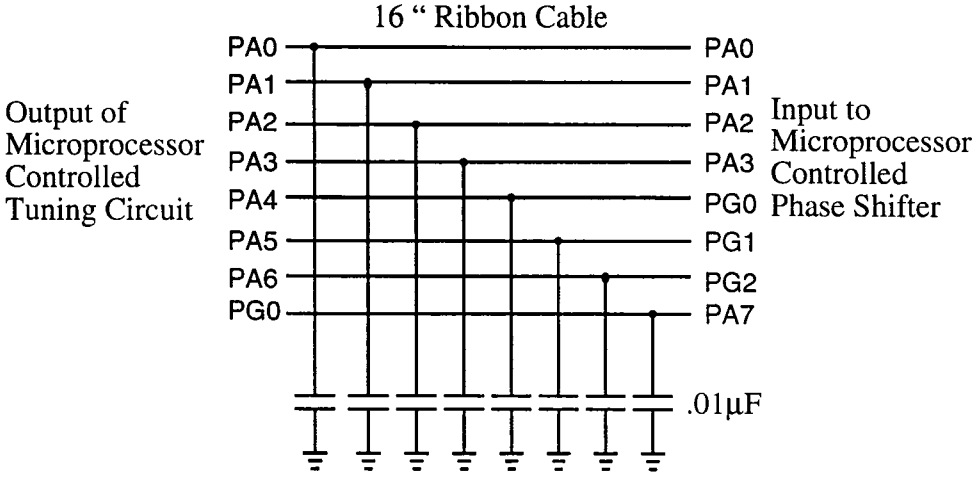

Figure 5-2 Capacitor Bypass To Reduce Noise

The completed circuit was tested as shown in Fig. 5-3, with the automatic tuning circuit using the analytical frequency to phase shift conversion factor. The data is shown in Table 5-1 and graphed in Fig. 5-4.

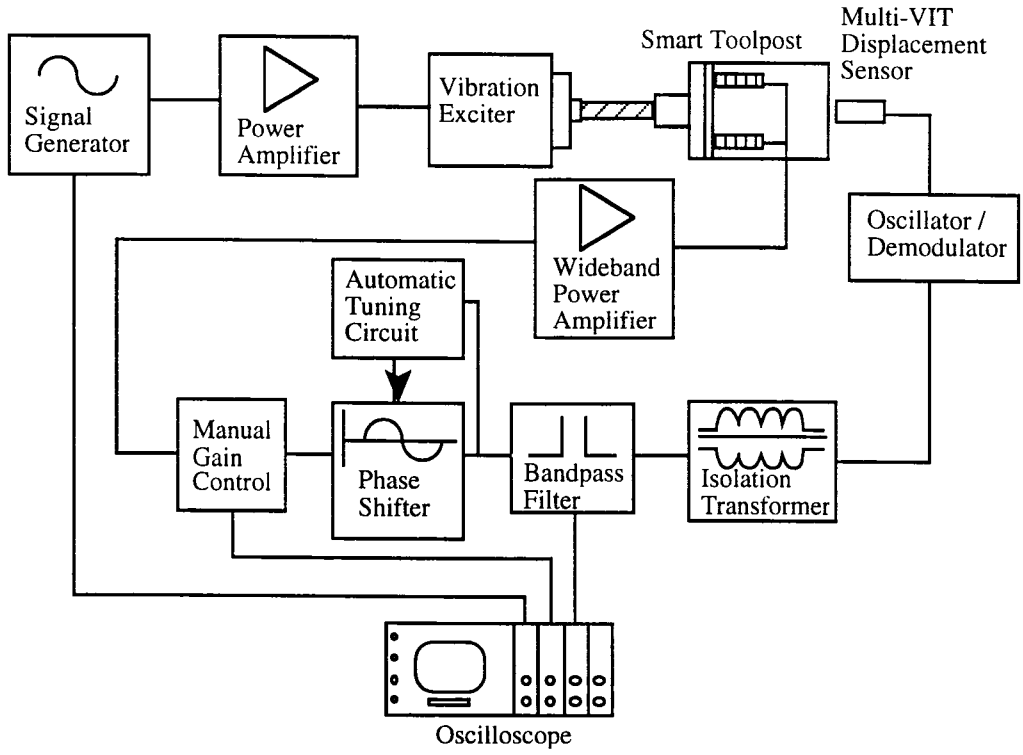

Figure 5-3 Block Diagram of Automatic Phase Control Circuit

Table 5-1 Vibration Reduction using Automatic Tuning Circuit

Frequency	Amplitude (Volts) w/o feedback	Amplitude (mV) with feedback	Percent Reduction
100	1.15	728	36.696
120	1.12	667	40.446
140	1.11	668	39.82
160	1	630	37
180	0.953	628	34.103
200	0.897	580	35.34
220	0.775	503	35.097
240	1.35	890	34.074
260	0.929	656	29.386
280	0.83	608	26.747
300	1.06	742	30
320	1.56	1100	29.487
340	1.44	1030	28.472
360	1.34	945	29.478
380	1.21	881	27.19
400	1.17	841	28.12
420	1.12	825	26.339

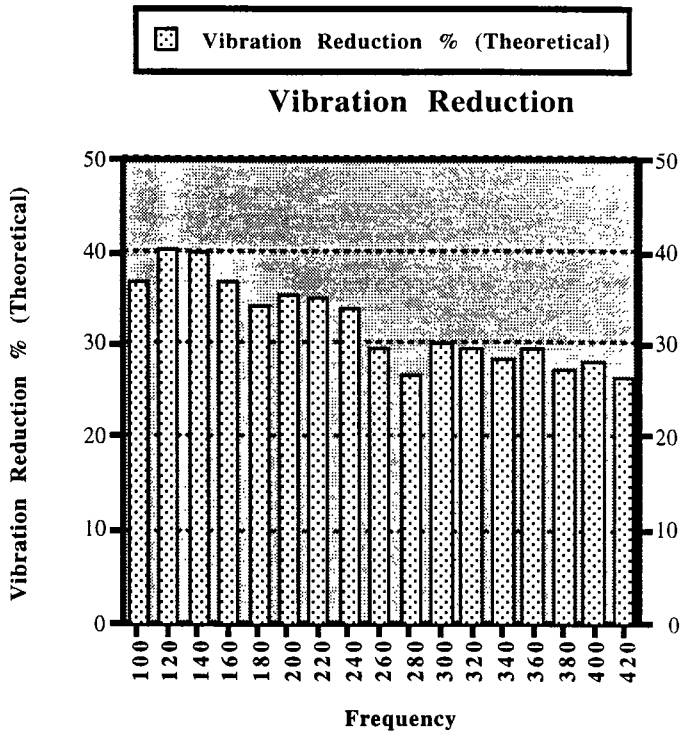

Figure 5-4 Vibration Reduction Using Analytical Phase Shift

The vibration reduction attainable using the analytical phase shift criteria was slightly less than that of using manual tuning, with a range of 26%-40% and an average of 32%.

5.3 Design of Automatic Gain Control System

As is proposed in the testing section, a certain phase relation exists between the components at different frequencies, and a phase shifter must be used in the feedback circuit to attenuate the tool vibration effectively. The timing of the conversion loop in the phase shifter must be as fast and precise as possible, so a separate circuit is needed to adjust the phase delay automatically at different frequencies. The purpose of this system is to sense at what frequency the feedback is set, calculate the correct delay for the phase shift in the feedback loop

at the given frequency, and transmit the information to the phase shifter. This automatic tuning system was also accomplished using a MC68HC11F1 microprocessor. The central element of the main timer system in the MC68HC11 is a 16-bit free running counter. This counter starts from a count of $0000 and then counts up continuously. When the maximum count is reached, $FFFF, the counter rolls over to a count of $0000, sets an overflow flag, and continues to count up. The counter increments once for every E-clock cycle.

A zero-crossing comparator is used to convert the sinusoidal feedback signal into a square wave, which is sent to the pulse accumulator pin on the microprocessor. An interrupt is established in the microprocessor that is triggered by the rising edge of an input to the pulse accumulator. After the first rising edge interrupt, the value of the free running counter is stored into a register. The second rising edge creates another interrupt, which again loads the free running counter into a register. The microprocessor then computes how many counts have taken place between the first and last interrupts, and since the time base for the free running counter is known, the period is then computed. The value for the period is then manipulated to produce the value for the inverse of the period, which is the frequency. The value for the phase shift is a linear function of the frequency in the frequency domain, so the phase shift is calculated for the corresponding frequency. This value is then converted into the correct time delay needed, and then converted directly to the correct number of loops the phase shifter must delay the input signal to achieve the proper phase shift. The data is then put on a latch, and the tuning microprocessor sends an interrupt request to the phase shifter to read this calculated value for the index X offset. The schematic of the automatic tuning circuit is shown in Fig. 5-5.

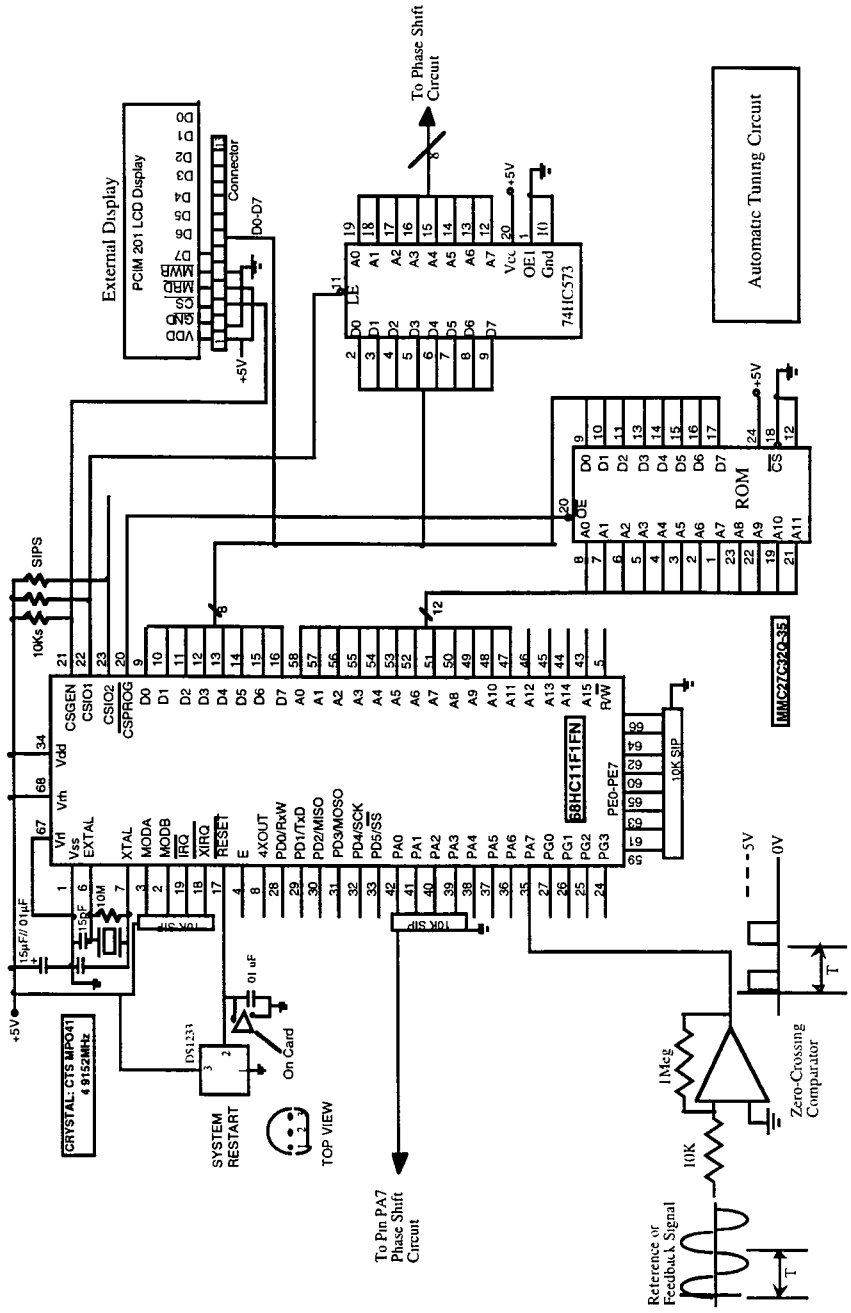

Figure 5-5 Schematic of Microprocessor Based Tuning Circuit

5.4 Gain Control for Stability

The design of an automatic gain control system which provides the proper feedback gain is the next setup in the realization of the controller. If the feedback level is set too high, oscillations and instability occur, which must be avoided.

5.4.1 Feedback Gain versus Frequency and Feedback Amplitude

The first step in the process to design an automatic gain control system is to determine the peak-to-peak voltage signal that is needed to be input to the PMN amplifier versus the frequency and amplitude of the feedback signal for vibration control without instability. Using the experimental set-up shown in Fig. 5-3, the peak-to-peak voltage being supplied to the PMN amplifier (wideband power amplifier) was recorded for various frequencies and feedback amplitudes. The data are given in Table 5-2.

Table 5-2 PMN Amplifier Voltage vs. Frequency and Feedback Amplitude

Frequency	Amplitude without Feedback (V)	Amplitude with Feedback (V)	AC Voltage to Amplifier (pk to pk mV)	AC Output of Amplifier (pk to pk V)
100	1	0.642	50	1.08
100	2	1.18	95	2.02
100	4	2.24	175	4.08
100	6	3.23	270	6.13
200	1	0.653	46	0.974
200	2	1.24	92.3	2.09
200	4	2.26	175	4.14
200	6	3.42	270	6.42
300	1	0.724	42	0.814
300	2	1.43	77	1.75
300	4	2.73	156	3.63
300	6	4.21	221	5.2
400	1	0.72	55	1.18
400	2	1.41	103	2.34
400	4	2.72	202	4.73
400	6	4.07	297	7

The signal from the function generator to the vibration exciter was first adjusted to the correct driving frequency. The amplitude of the vibration exciter signal was then adjusted so that the output voltage from the displacement sensor system at the low pass butterworth filter was at a certain magnitude. These magnitudes were chosen to be 1V, 2V, 4V, and 6V peak to peak output displacements. The feedback was then supplied to the PMN amplifier, and the input gain was manually adjusted by hand until maximum vibration without instability was obtained, and the voltage level of the gain (the input voltage to the PMN amplifier) was recorded. The AC voltage to the PMN amplifier versus the initial amplitude without feedback is graphed at the various frequencies as shown in Fig. 5-6.

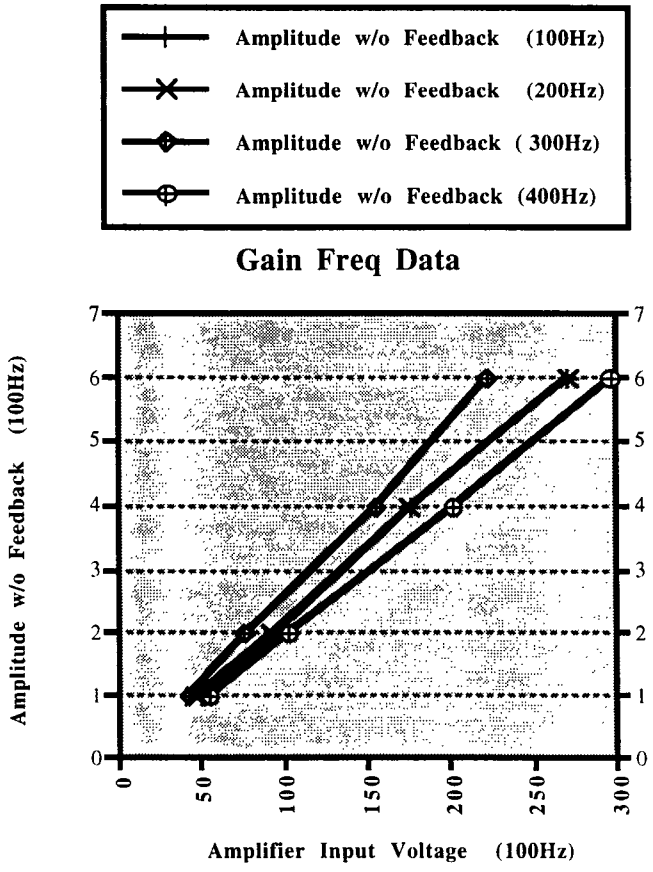

Figure 5-6 PMN Amplifier Voltage vs. Frequency and Feedback Amplitude

As can be seen in Fig. 5-6, the input voltage to the PMN amplifier for vibration compensation is linearly proportional to the initial feedback amplitude. A frequency dependency can also be seen. To determine the extent of the frequency dependency, the input voltage to the PMN amplifiers was tested at various frequencies for the same initial displacement. The data are shown in Table 5-3, and are graphed in Fig. 5-7.

Table 5-3 Amplifier Input Voltage Frequency Dependency

Frequency	Amplitude without Feedback (V)	Amplitude with Feedback (V)	AC Voltage to Amplifier (pk to pk mV)	AC Output of Amplifier (pk to pk V)
100	2	1.06	90.7	2.08
150	2	1.2	87.3	2.01
200	2	1.29	79.9	1.75
250	2	1.32	80.7	1.81
300	2	1.38	82.2	1.84
350	2	1.39	84.2	1.88
400	2	1.48	88.4	1.97

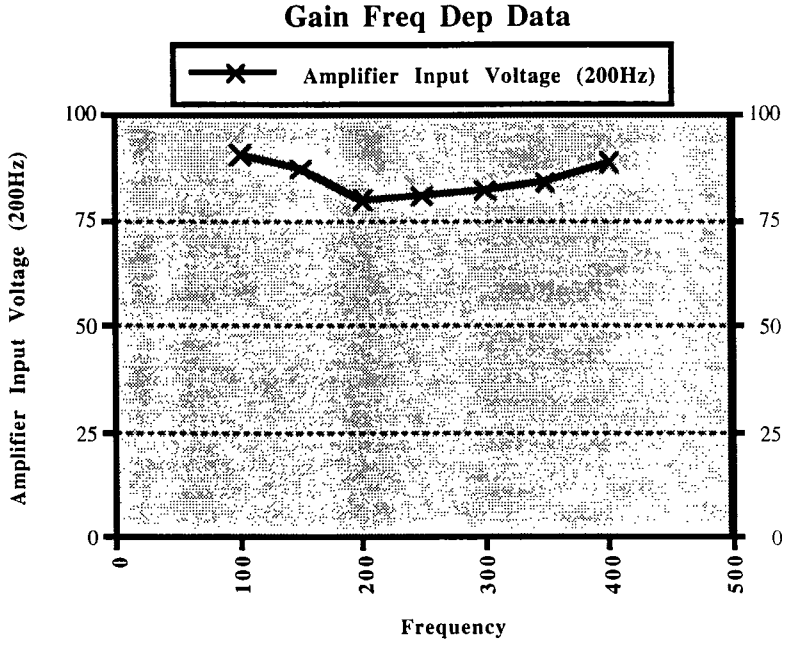

Figure 5-7 Frequency Dependence of Amplifier Input Voltage

As can be seen, there is a slight frequency dependency on the required amplifier input voltage, with a change in the required voltage approximately 10%.

5.4.2 Framework for Automatic Gain Control

The block diagram for the automatic gain control circuit is shown in Fig. 5-8.

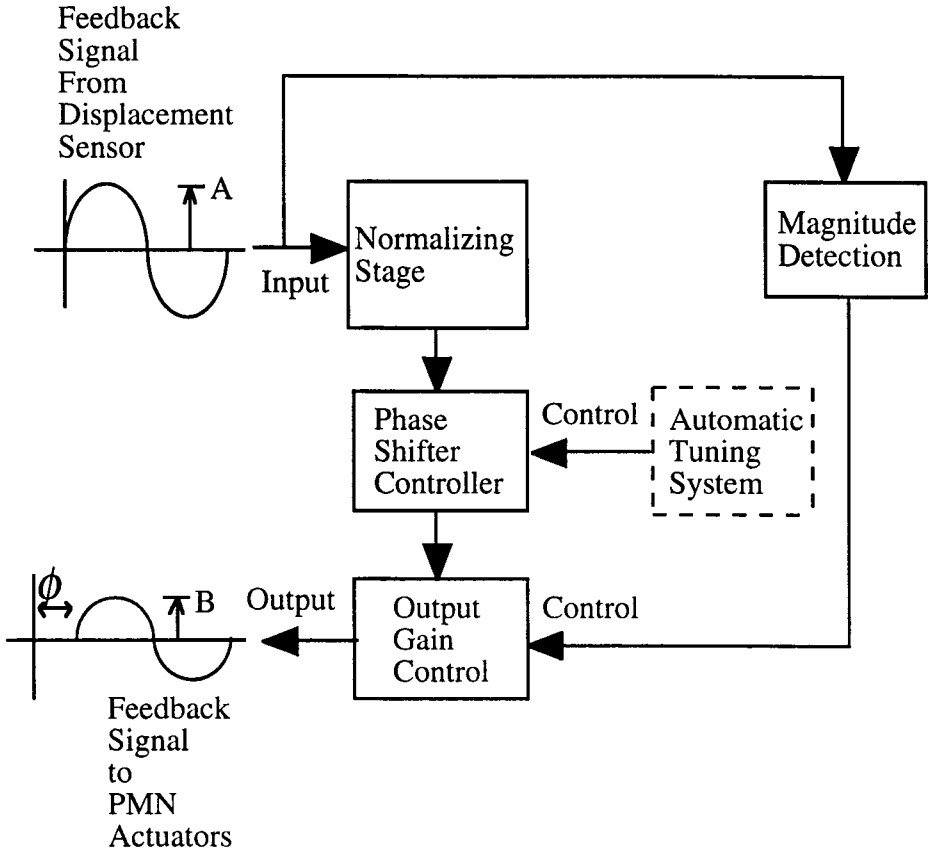

Figure 5-8 Block Diagram of Automatic Gain Control System

The system consists of two variable gain amplifier sections, with the gain being controlled by digital potentiometers. The digital potentiometers are adjusted by a microprocessor.

5.4.2.1 Normalizing Stage

The input stage of the gain control circuit is shown in Fig. 5-9.

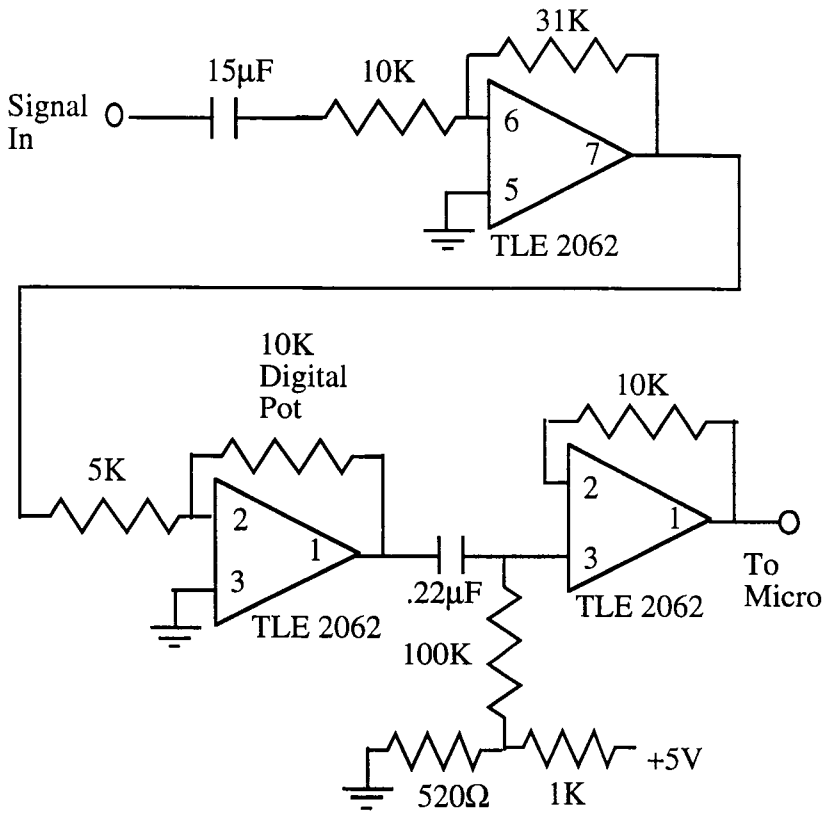

Figure 5-9 Input Amplifier Stage of Gain Control System

The input stage is used to normalize the input signal to a standard peak-to-peak level to be input to the microprocessor controlled phase shifter. The A/D converter used in the Motorola MC68HC11F1 microprocessor is an eight bit converter, with an input voltage range is from 0V to 5V. Therefore, each bit value for the converted signal corresponds to 19.6 mV. This is the least significant bit (LSB) value. To insure the best possible signal to noise ratio, the full dynamic range of the A/D converter should be used to convert the signal. If

the signal level is too low, the converted signal will not be an accurate representation. This is shown in Fig. 5-10.

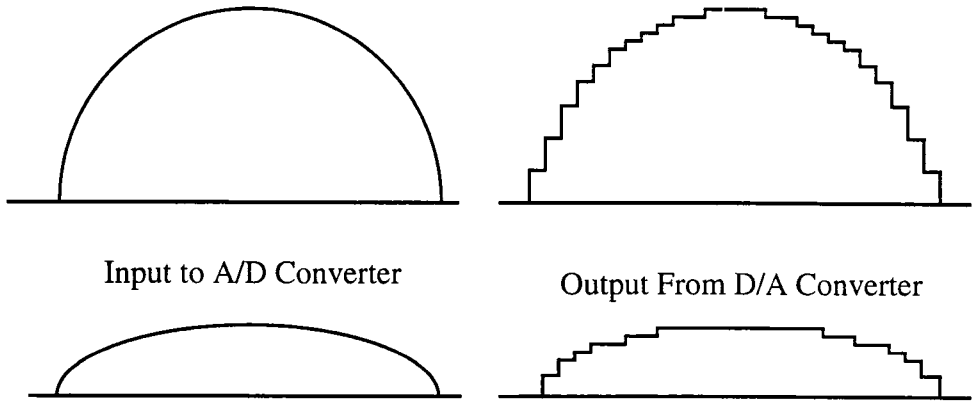

Figure 5-10 Resolution of Input Signal Compared with LSB Value

To make most effective use of the A/D converter, the input signal is adjusted with a normalization process so that the peak-to-peak voltage entering the microprocessor A/D converter always maintains a certain value. The 15μF capacitor and 10K resistor combination are used to AC couple the input signal at 1 Hz. The signal then goes through an inverting amplifier with a gain of 3.1. The signal then goes to the next inverting amplifier, which has a XICOR X9C103P 10K digital potentiometer in the feedback loop. The XICOR X9C103P digital potentiometer is a solid state nonvolatile potentiometer is a resistor array composed of 99 resistive elements. Between each element and at either end are tap points accessible to the wiper element. The position of the wiper element is adjusted by a three wire TTL control, which is readily controlled by the microprocessor. For the 10K digital resistor, each resistive element is equal to 101Ω, which is the value (10,000)/(99).

The A/D converter has a range of 0 to 5V, so the input signal has to be centered about a point so that the peak-to-peak voltage swing is inside this range.

Also, to keep the input signal less than five volts without using a clipping circuit, the amplifiers used were supplied with +/- 5V. There is approximately 1.2V to 1.3V of headroom required by the amplifier. Therefore, the output voltage range from the amplifiers is from -3.7V to 3.7V. For single sided operation, the voltage range becomes 0V to 3.7V. The midpoint of this range is 1.85V. The third amplifier used in the input stage is a buffer amplifier, with an AC-couple centered at 1.71V.

5.4.2.2 Input Stage Normalization Calculation

The control system program for the input normalization routine was designed using the model shown in Fig. 5-11.

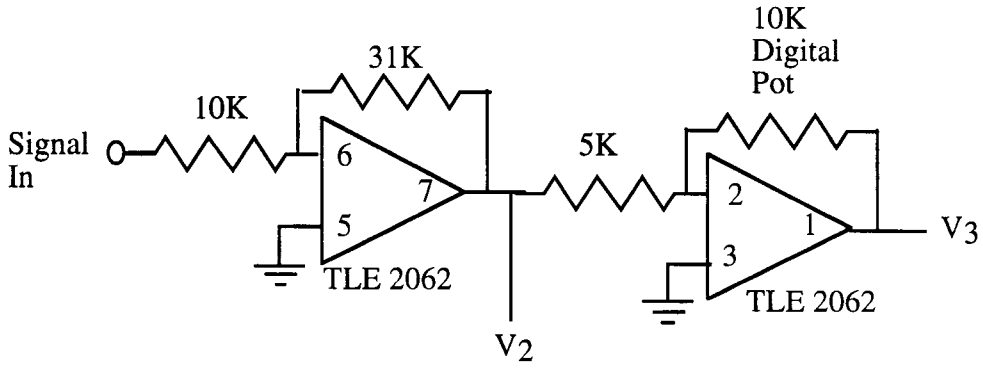

Figure 5-11 Circuit for Calculation of Parameters of Input Gain Control System

The system is designed to keep the voltage V_3 at a peak-to-peak level of 3V. Since the voltage level is 3V peak-to-peak, it is 1.5V 0-to-peak.

$$V_3 = -(\frac{R_F}{R_A})V_2 \qquad (5\text{-}1)$$

R_F is the resistance of the digital potentiometer. Its resistance is equal to (101Ω)(I), where (I) is the current increment value of the wiper position. Inserting this into equation (5-1) and solving for (I) produces

$$I = \frac{-9.9V_3}{V_2} \approx \frac{-10V_3}{V_2} \tag{5-2}$$

The microprocessor samples the voltage V_2 using one of the eight-bit A/D converters. The eight-bit A/D converter has 255 positions, and the input range is 0V to 5V, so each bit in the conversion corresponds to .0196V, or approximately .02V. Substituting in V_3 =-1.5V and V_2 =(.02)(BIT),

$$I = \frac{(10)(1.5)}{(.02)(BIT)} = \frac{750}{BIT} \tag{5-3}$$

The wiper position has to be between 0 and 100. The maximum value for BIT equals 255, so (I) will never be less than zero. To find the smallest value of BIT, we let

$$\frac{750}{BIT} \leq 100 \quad \therefore \quad BIT \geq 7.5 \text{ or } BIT \geq 8 \tag{5-4}$$

The microprocessor samples the voltage at V_2, and then adjust the digital potentiometer so that the voltage at V_3 is at a predetermined constant level.

5.4.2.3 Peak Detector and Sample and Hold

The input signal is a time varying signal, so a peak detector circuit, shown in Fig. 5-12, was implemented to accurately record the peak voltage of the feedback signal, shown as V_2 is Fig. 5-11.

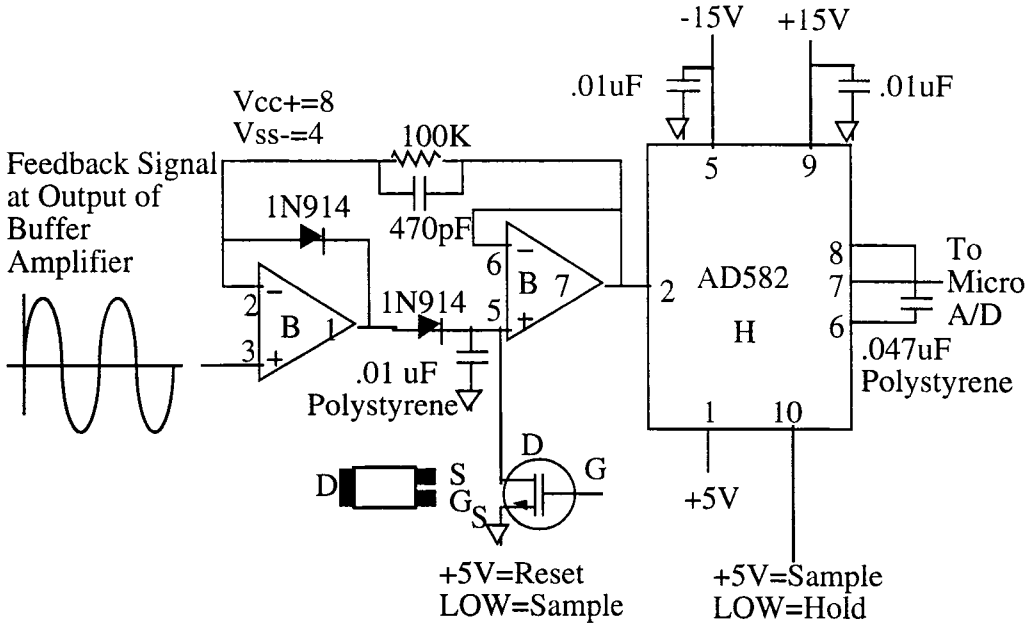

Figure 5-12 Peak Detector and Sample and Hold Circuit

The reset FET and sample or hold control line of the AD582 were controlled in software by the microprocessor.

5.4.2.4 Output Attenuation and Gain Stage

The input voltage to the PMN amplifiers, given in Table 5-2, is given by the equation

$$V_{PMN} = [(43.559)(V_{FEEDBACK}) + 5.932]mV \qquad (5\text{-}5)$$

This equation is a linear approximation of the average of the values for the input voltage versus initial displacement given in Table 5-2. This equation does not take into account any frequency dependency, since the effect of the frequency dependency was small. The output stage is shown in Fig. 5-13.

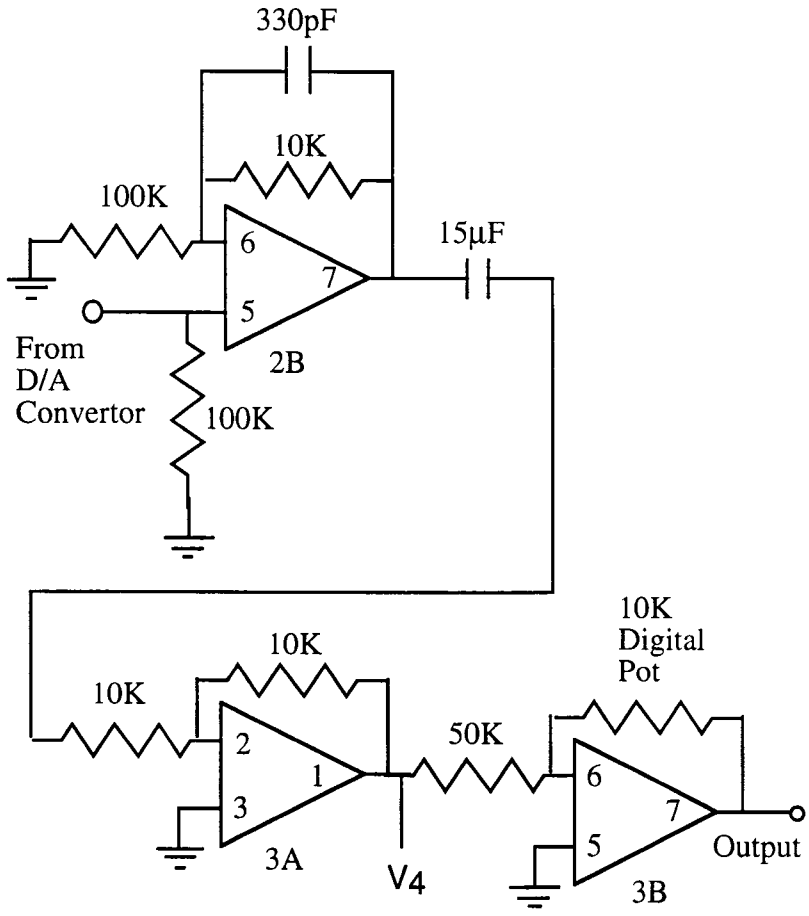

Figure 5-13 Output Gain Control Amplifier Stage

The first amplifier is a filter to reduce the staircase signal supplied from the D/A converter. As in the first stage, a 1Hz AC-couple is used to center the signal about 0V. The second amplifier is an inverter with unity gain. The third amplifier uses a digital potentiometer to attenuate or magnify the output signal.

To determine the output of the gain control system required for the input of the PMN amplifier, the voltage V_4, shown in Fig. 5-13, was first measured. The input stage of the gain control keeps the input level to the microprocessor constant, so the voltage level at V_4 is also held constant. The digital potentiometer parameters were calculated using the circuit shown in Fig. 5-14.

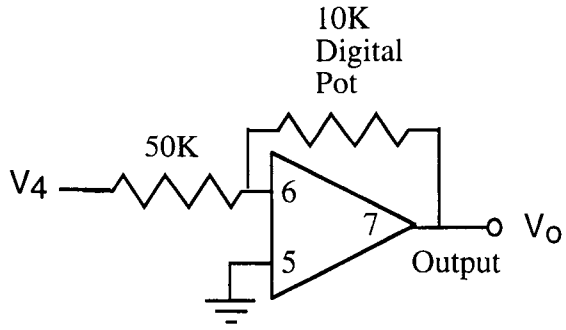

Figure 5-14 Circuit for Calculation of Parameters of Output Gain Control

The output is given as

$$V_O = -(\frac{R_F}{R_A})V_4 \tag{5-6}$$

The peak value of V_4 was measured as 1.64V. (Note: The peak-to-peak voltage swing is 3.28V). R_F is again given by

$$R_F = (101)(I_2) \tag{5-7}$$

where (I) is the increment value of the wiper position. Substituting these values into equation 5-6,

$$V_O = \frac{(101)(I_2)}{50000}(1.64) = (.00331)(I_2) = (3.31)(I_2) \text{ Volts} \tag{5-8}$$

The input voltage to the PMN amplifier, given by Equation 5-5, is equal to the voltage V_O. Equating Equation 5-5 and 5-8,

$$(.00331)(I_2) = (43.559)(V_{FEEDBACK}) + 5.932 \tag{5-9}$$

$V_{FEEDBACK}$, given as voltage V_2, has already been converted by the microprocessor, and its digital value is stored in the register BIT. Therefore, solving for the wiper increment position I_2,

$$I_2 = (.258)(BIT) + 1.79 \tag{5-10}$$

This value gives only the zero-to-peak voltage, the peak-to-peak voltage is twice this amount. Therefore,

$$I_2 = (.516)(BIT) + 3.58 \tag{5-11}$$

The 68HC11 microprocessor has two types of divide instructions, an integer divide and a fractional divide. The integer divide was used due to its faster implementation time and the simpler mathematics involved. Therefore, to compute equation 4-15 with the microprocessor, the right side is multiplied and divided by 100. The index wiper position equation is then calculated as

$$I_2 = \frac{(51.6)(BIT) + 358}{100} \approx \frac{(52)(BIT) + 358}{100} \tag{5-12}$$

5.4.2.5 Microprocessor Code Implementation

There are two microprocessors used in the control system. The phase shifter controller is a dedicated microprocessor. The automatic tuning controller is incorporated with a separate microprocessor. To implement the gain control system, a third microprocessor could have been added to the system. Instead, the code is implemented in the automatic tuning microprocessor. The timing of this code had to be such that it did not interfere with the automatic tuning program.

The feedback signal and comparator output for the automatic tuning circuit is shown in Fig. 5-15.

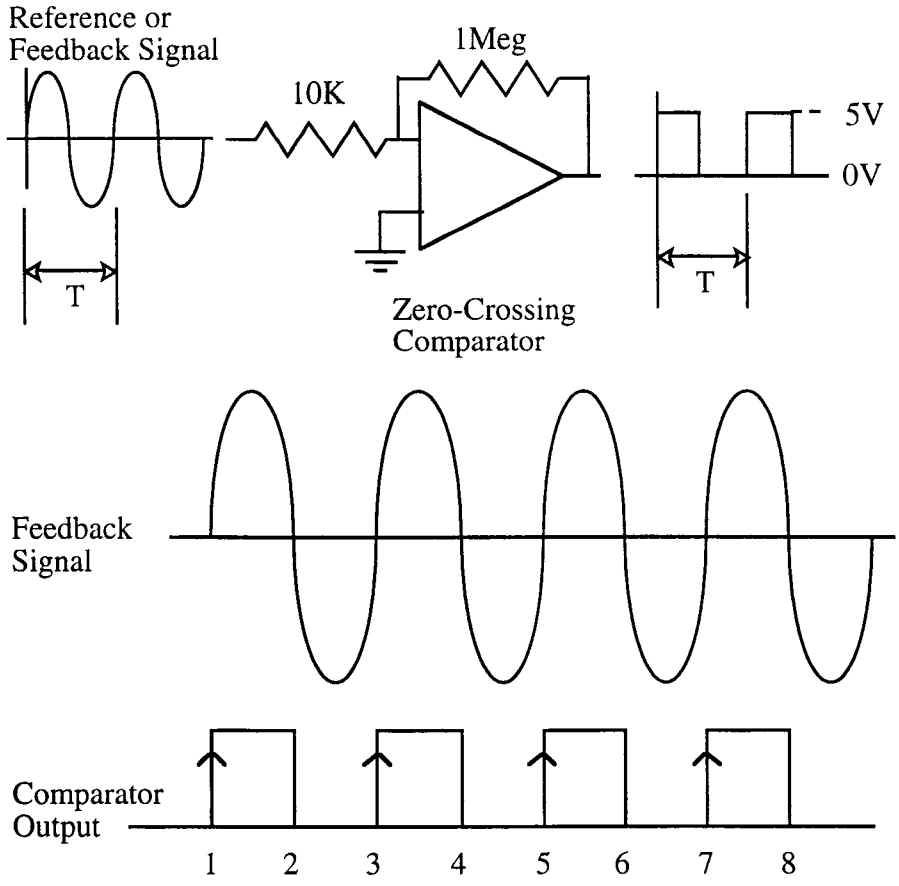

Figure 5-15 Comparator Output with Feedback Signal Input

The program for the automatic tuning system synchronized to the rising edge of the comparator output, and is given as follows:

1. Point 1. This is the first rising edge. The microprocessor loads the free-running counter (described in section 3.3.2.1) and stores this information.
2. Point 3. This is the second rising edge. The microprocessor loads the free-running counter again, and the information for the phase shifter is then calculated and transferred to the phase shifter.
3. Point 5. This now becomes the first rising edge again, and the timing process is initiated again.

In between point 2, the falling edge of the comparator signal, and point 3, the rising edge, the microprocessor is in a wait status. The gain control algorithm was implemented in this time window. The microprocessor sets a flag at the first rising edge (point 1), and starts checking to see when the comparator output goes low, after the falling edge (point 2). The automatic gain control program is then initiated. There is only 1.25 milliseconds to execute the program, which made it necessary to streamline the code as much as possible.

The complete circuit diagram for the adaptive control system is shown in Fig. 5-16.

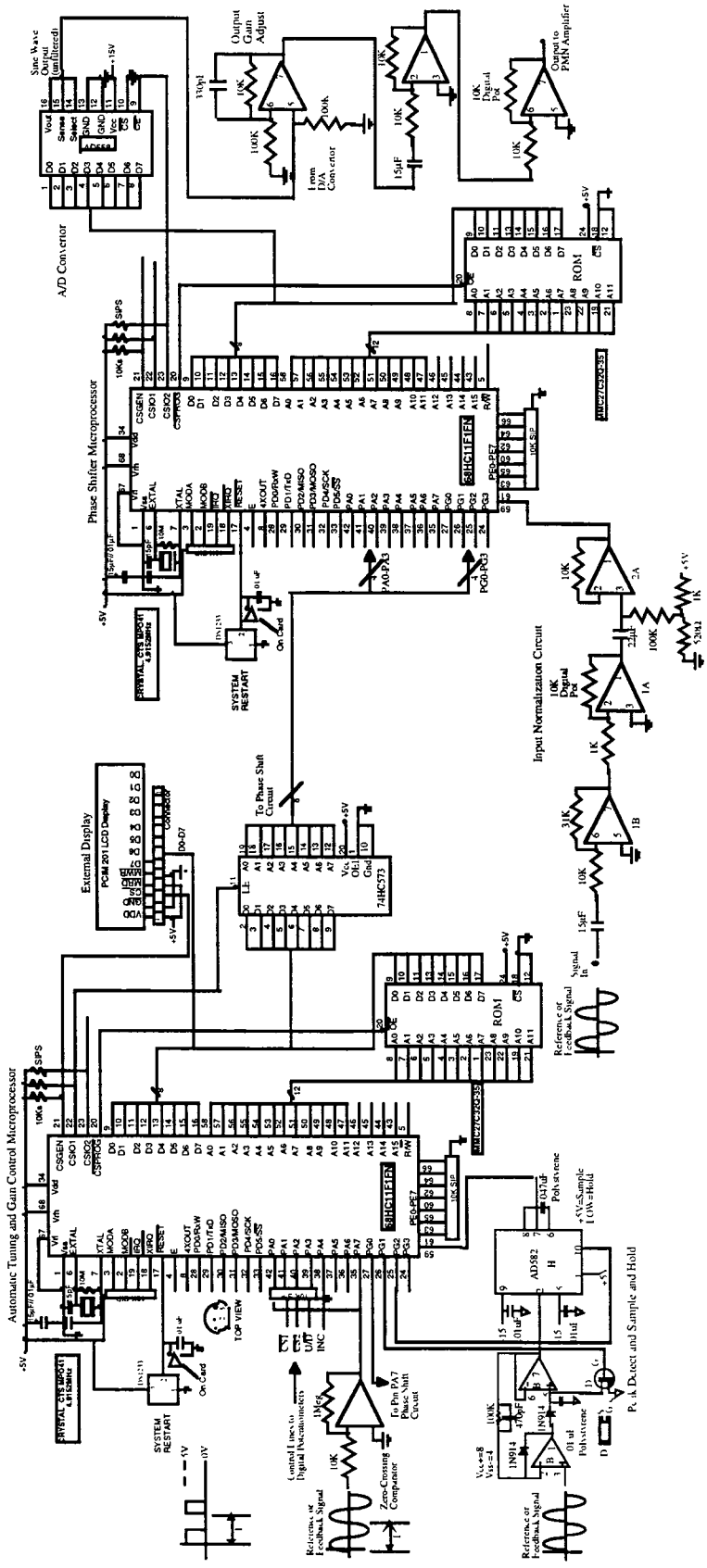

Figure 5-16 Complete Adaptive Control System

5.5 Discussion of Oscilloscope Plots

To determine the operating parameters for the phase shifter and the self-tuning gain control, an oscilloscope was used to monitor various outputs. The oscilloscope, a Phillips PM3384E 200MHz digitizing oscilloscope was equipped with FFT capabilities.

5.5.1 Phase Shift Output

As is given in Equation 4-5, the phase shift is modeled as a linear function of the frequency. The program designed for the automatic tuning circuit computes the incoming frequency and then calculates the phase shift necessary. Figs. 5-17(a) through 5-17(h) show the output of the phase shifter at various frequencies.

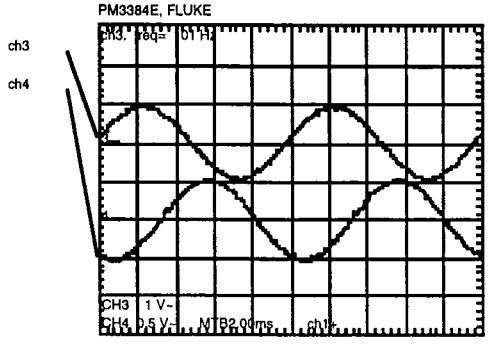

Figure 5-17 (a) 100 Hz

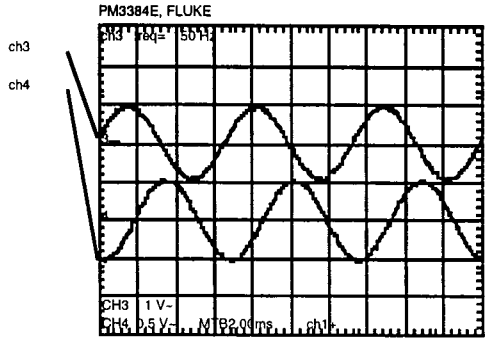

Figure 5-17 (b) 150 Hz

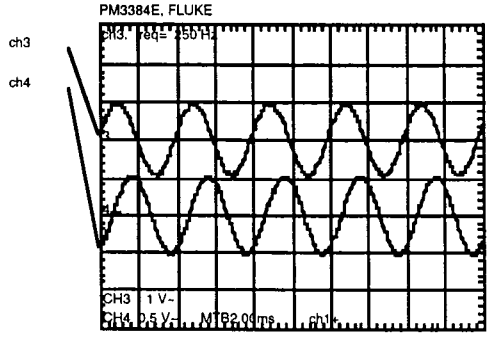

Figure 5-17 (c) 200 Hz

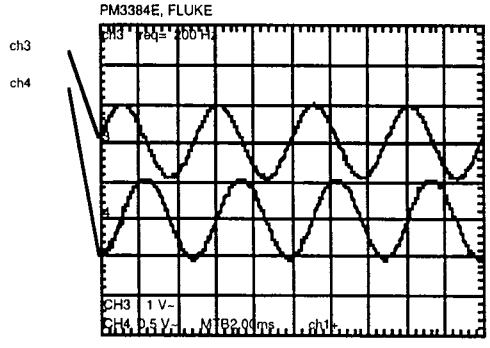

Figure 5-17 (d) 250 Hz

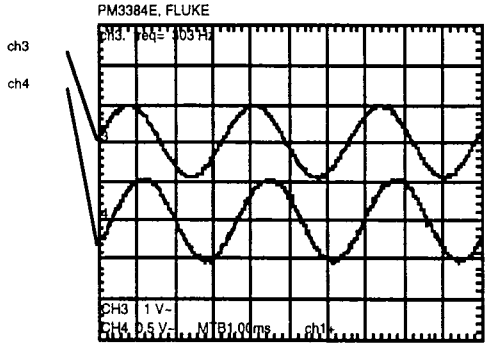

Figure 5-17 (e) 300 Hz

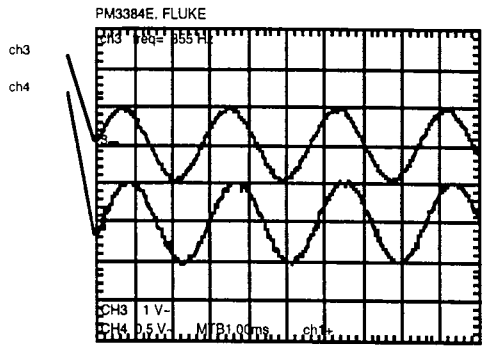

Figure 5-17 (f) 350 Hz

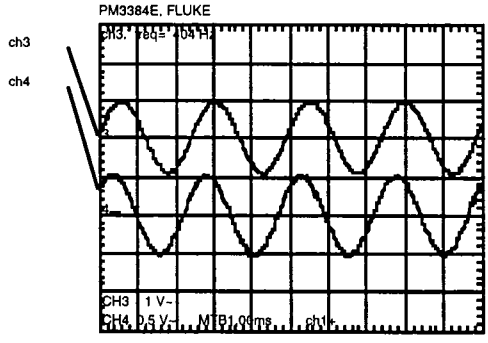

Figure 5-17 (g) 400 Hz

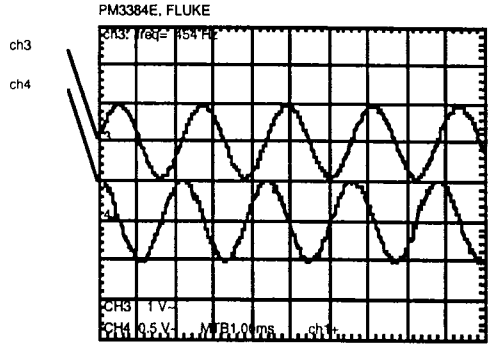

Figure 5-17 (h) 450 Hz

Figure 5-17 Phase Shifts at Various Frequencies

In Fig. 5-17, ch.3 denotes the sensor feedback signal, and ch.4 denotes the shifted feedback signal, as shown in Fig. 5-18.

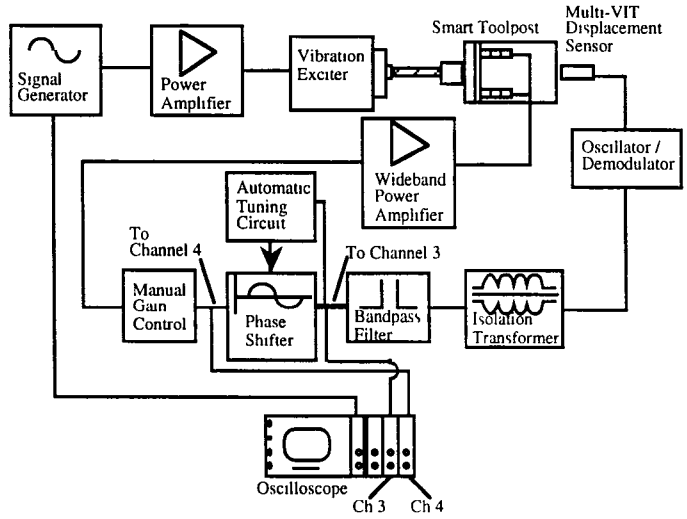

Figure 5-18 Oscilloscope Connections for Measuring Phase Shift

As can be seen in Figs. 5-17(a) through 5-17(h), the phase shift successively becomes less as the frequency increases from 100Hz to 350Hz. At 350Hz, the phase shift is almost zero. At 400Hz, the phase shift appears to be leading the sensor feedback signal, and then continues to decrease.

5.5.2 Reduction of Vibration

Figure 5-19 shows the output of the sensor feedback on channel 3 and the phase shifted sensor feedback on channel 4. This signal is with the system being driven at 125 Hz, with no active feedback. The peak to peak displacement of the sensor signal is approximately 0.9V. Figure 5-20 shows the output of the sensor and the phase shifted signal, on channels 3 and 4 respectively, but with active feedback. Figure 5-21 shows the difference between the feedback signal without active feedback , on m1.4, and with active feedback, given on channel 4. The reduction that is possible can be seen here.

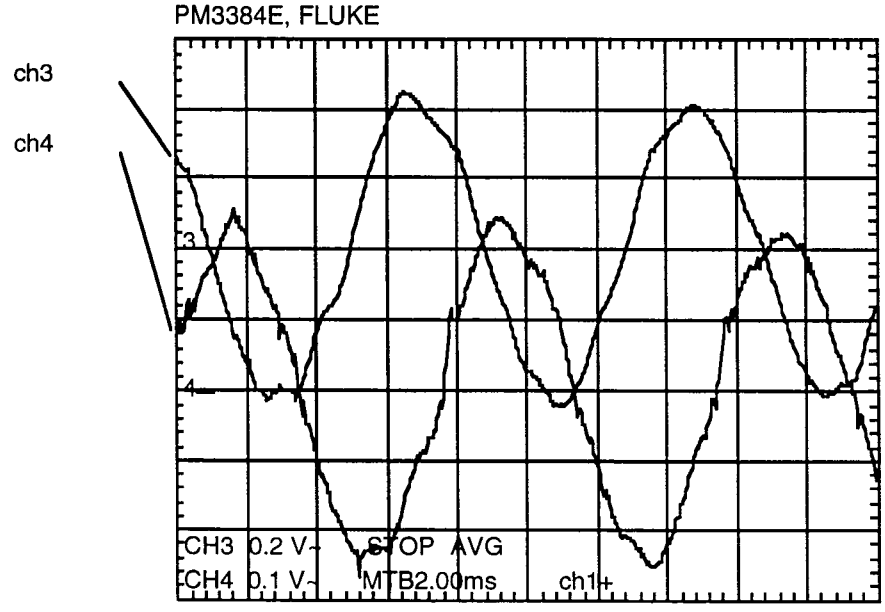

Figure 5-19 Output of Sensor Without Active Feedback

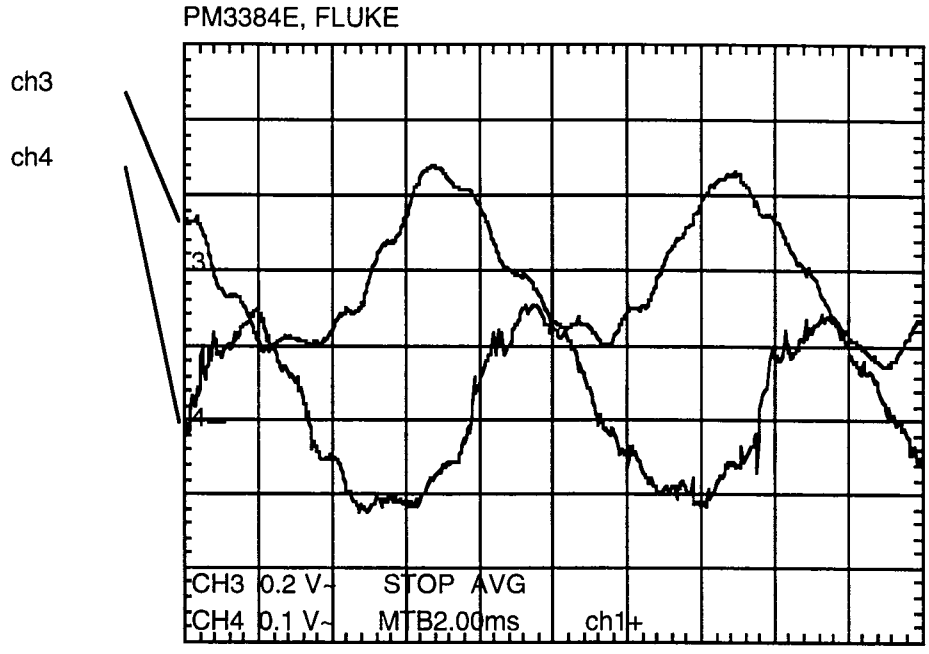

Figure 5-20 Output of Sensor With Active Feedback

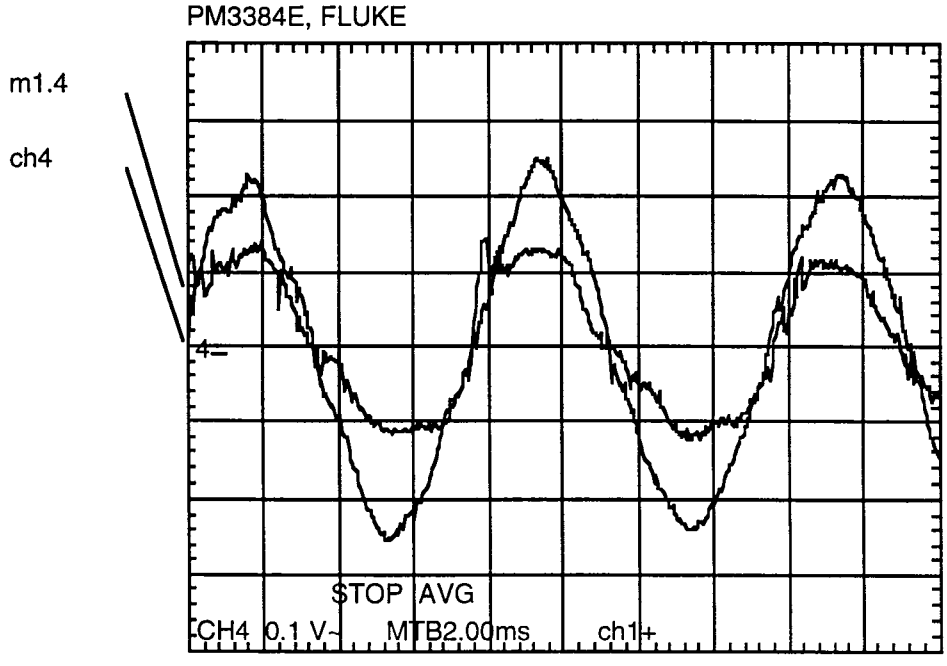

Figure 5-21 Comparison between Sensor Signal with and without Feedback

5.5.3 Discussion of Automatic Gain Control and Instability

As with any closed loop system, the amount of gain in the feedback loop is a critical factor in the stability of the system. It also accounts for the rate at which the system settles to an equilibrium state. During this thesis work, the feedback gain was always adjusted by hand to insure stability. The amplifier for the PMN actuators has a gain control knob, and a connect / disconnect switch, which controls whether the output is on or off. At a certain amplitude of displacement vibration being induced by the vibration exciter, the amplifier output could be disconnected, the frequency changed, and the amplifier output could be connected again without changing the gain control knob, with the system staying stable. Fine adjustment of the gain control always resulted in more reduction of the oscillation. Too much feedback resulted in complete loss of stability.

The onset of instability can be predicted by careful inspection of the feedback signal. The sensor feedback signal would start to oscillate slowly at a lower frequency. In other words, the sensor feedback signal would begin to "ride" on a lower frequency carrier signal. This is explained progressively in Figs. 5-22 through 5-26. These figures show the sensor feedback signal on channel 3, the shifted feedback signal on channel 4, and a FFT of the sensor feedback signal on m1.1. Figure 5-22 shows the signals with no active feedback. The FFT trace shows the major frequency in the signal, 250 Hz, with a clear peak. Figure 5-23 shows the system signals with feedback active. The gain is not adjusted for maximum reduction of vibration, as can be measured on channel 3, which has a peak to peak voltage of approximately 0.7V. The FFT trace now has two peaks, however, one at 250Hz and one at a lower frequency, approximately 50Hz. If the feedback gain is now raised, the displacement of the system becomes less, as can be seen in Fig. 5-24. The peak-to-peak output of

the sensor signal is now at 0.6V. This is the point of maximum reduction without instability.

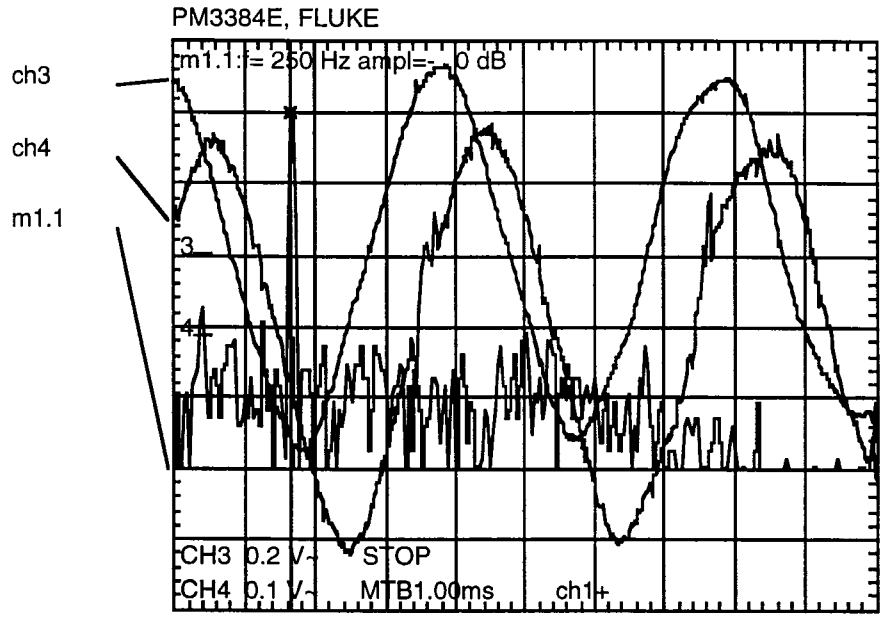

Figure 5-22 Output of Sensor without Active Feedback, FFT included

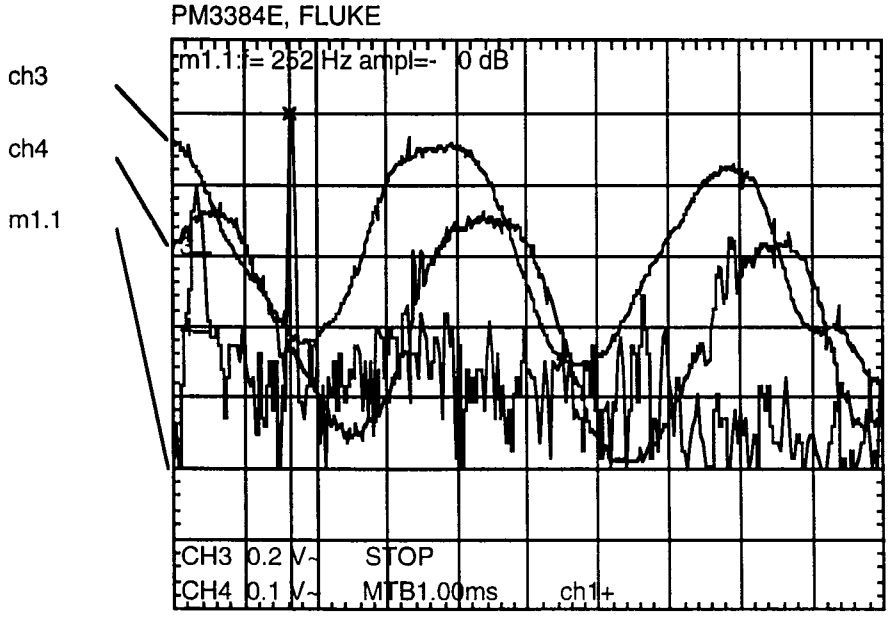

Figure 5-23 Active Feedback Present, Two Peaks on FFT

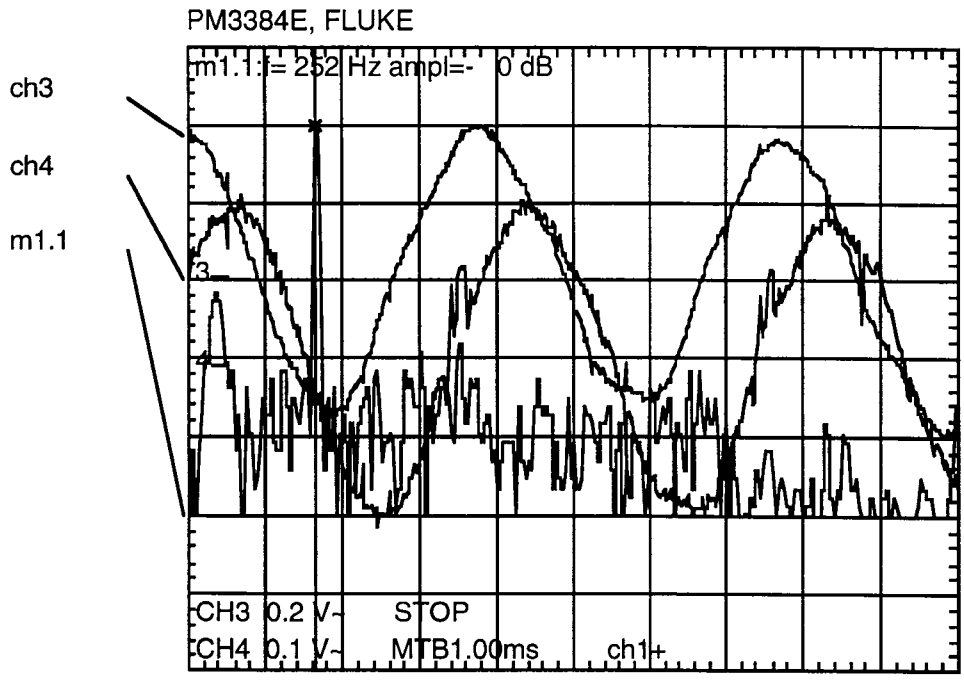

Figure 5-24 Maximum Reduction Before Instability

If the feedback signal gain is increased too much, the system becomes unstable. Fig. 5-25 shows the onset of instability.

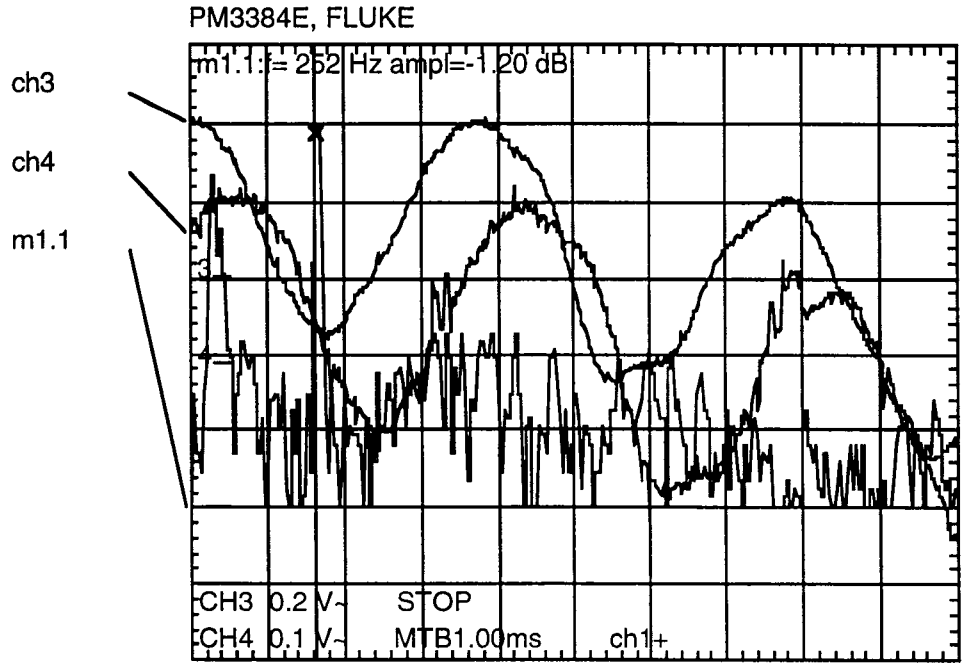

Figure 5-25 Onset of Instability

The lower peak on the FFT signal has become much higher, and inspection of the sensor feedback signal and shifted feedback signal shows a skew downwards in voltage. The system is becoming unstable. If the gain is not adjusted, the signal will continue a slow oscillation. Figure 5-26 shows the output of the system if the gain is set too high. The sensor feedback signal undergoes very large oscillations. The FFT trace now shows one major peak, at around 50Hz, not at 250Hz. The system is completely unstable.

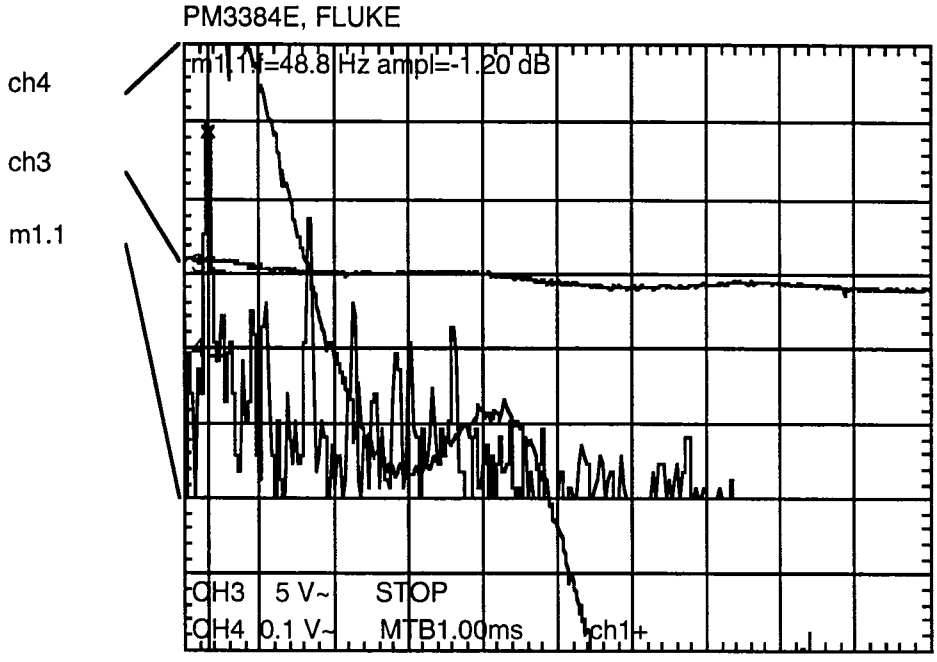

Figure 5-26 Unstable System

Chapter 6 Conclusions and Recommendations

6.1 Conclusions

The overriding goal of this thesis has been the design of an intelligent controller for vibration compensation during machining. Special emphasis is given to utilizing PMN actuators which are made of lead magnesium niobate, a type of smart material. Smart material is new to the engineering community and its applications are still in an exploratory stage. Difficulties in their engineering applications arise from understanding the material behavior, both mechanically and electronically, and the interaction between the mechanical and electronic systems. However, the two-year efforts have resulted in significant achievements and an adaptive controller has been designed and implemented. Important findings and practical significance of this thesis are summarized as follows:

1. In this thesis study, we have formulated an architecture which integrates a mechanical system and an electronic system to constitute a mechatronic system. The designed mechanical system serves as the test bed for performance evaluation of the entire mechatronic system. Recognizing the fact that the behavior of the mechatronic system is dominated by the mechanical system design in terms of the system rigidity, the resonance nature, and damping characteristics, the control action has to follow the behavior of the designed mechanical structure for vibration compensation. Fortunately, the design of the mechanical system has offered an excellent working environment for the controller to play.

Regarding the electronic system, a mechatronic system will not be able to function properly without the control action which responds to the performance need. It is the controller which serves as the central commander to coordinate the activities at the system level to achieve the design objectives of the mechatronic system.

2. The research work involved in this thesis work focuses on the controller design. Recognizing complexity of the system dynamics under a variety of machining conditions, it is neither possible nor economical to make a thorough investigation of the nonlinear dynamics of the machining system. However, introduction of nonlinear compensation is essential, leading to the design of an adaptive control system for the smart tool post structure The two key issues are the phase relationship between the excitation and the anti-vibration action; and the magnitude relationship between them. An effective control of these relationships ensures the synchronization between the system input and system output. Consequently, the maximum compensation can be achieved while the system stability during the compensation is maintained.

3. In this thesis research, the difference between the phase angle of the excitation and the phase angle of the compensation action is selected as one of the control variables. The phase difference variable characterizes: 1) the dynamic nature of the mechanical system in response to the variation of the excitation frequency, and; 2) the time lag caused by computation delay because of the analog-to-digital and digital-to-analog conversions. Control of the phase difference variable is further complicated by the fact that the tool post structure is a multi-degree-

freedom system and displays non-linear behavior even under harmonic excitation. Consequently, mathematical modeling of the phase relationship between the system input and output becomes extremely difficult. In this thesis, a new approach which is integration of microprocessor control and information modeling is developed.

4. The motivation of utilizing microprocessor chips comes from the need to synchronize the system excitation and the control action within a limited and allowable time duration. The Bucket Bridge algorithm and the self-tuning circuit, which are implemented using two 68HC11F1FN processors, keep the realization of phase shift and gain adjustment within 45 μsec. On the other hand, information modeling of the phase shift required for vibration compensation is characterized by the use of look-up table. Information stored in the table is based on the experimental data during the system calibration, thus taxing the needed computation time before the machining operation starts. In this thesis work, the maximum time lag is controlled within one cycle of the excitation, which ranges from 0.05 sec to 0.0025 sec.

5. In the hardware realization, other unique contributions of this thesis work include:

   (1) Introduction of the Kaman Smμ–9100 system, which consists of a variable impedance transducer and a special signal conditioning unit. The sensing system ensures the detection of the tool displacement, which is used as the feedback signal for the controller, with high accuracy.

(2) Implementation of a Self-Tuning Gain Adapter, which consists of a peak detector, gain control amplifier, and a microprocessor-based coding system for self tuning to optimizing the gain adjustment while maintaining the system stability.

The implemented controller system has been tested under a variety of excitation conditions. Vibration compensation has been achieved ranging from 40% at frequency between 120 Hz and 140 Hz, to 25% at frequency between 250 Hz and 280 Hz. Such reduction has met the design objective for on-line vibration compensation, which has never been achieved during machining.

6.2 Recommendations

Although the accomplishments have been significant, there is still a lot of work to be done in order to build a truly smart tool post structure to carry out active vibration control during machining. Several suggestions are listed as follows:

1. Vibration compensation under excitation with multi-frequency components. On the shop floor, the cutting force generated during machining may not be a harmonic signal with a single frequency. It is expected that the cutting force signal covers a wide range of frequency. Under such circumstances, selection of the targeted frequency range for vibration compensation becomes critical. There exist several choices, namely targeting the frequency component with the maximum magnitude, targeting the lowest or highest frequency component. It should be recognized that the phase shift compensation has its limitation to balance the need to synchronize two frequency components. A detailed study,

both experimentally and analytically, is needed to gain a basic understanding on on-line compensation under multi-frequency excitation.

2. On-site stability protection mechanism. Having a smart or an intelligent system to carry out machining operations has been a dream for the machining community. The research effort exerted in this project is a step forward to realizing the dream. However, a protection mechanism is needed for almost every automated system. For mechatronic systems, the protection mechanism will ensure that the mechatronic system will stop its operation immediately when system instability occurs. There is a need to design a detection and protection mechanism, which monitors the system stability, and strengthens safe operations whenever something goes wrong during machining.

3. Computer-tool post controller networking. Desk-top computers are very popular and easily accessible. It is natural to consider the utilization of a desk-top computer to replace the self-tuning gain adapter microprocessor used in the control system. Such replacement not only offers a faster computation speed and a large memory storage for the information model, but also create a unique working environment under which commercial software packages can be utilized in the controller design. Software of FFT spectrum analyzers, and digital signal processing-based amplifiers and filters are unique candidates for further improvement of this research work.

Appendix A Feedback Control System Definitions

Fig. A-1 presents a block diagram for the following set of definitions:

1. System: A combination of components that act together, which can be represented through a common mathematical symbolism.

2. Command Input: The motivating input signal to the system, which is independent of the output of the system.

3. Reference Selector (reference input element): The unit that establishes the value of the reference input. The reference selector is calibrated in terms of the desired value of the system output.

4. Reference Input: The reference signal produced by the reference selector. It is the actual signal input to the control system.

5. Control unit (dynamic element): The unit that reacts to an actuating signal to produce a desired output. This unit does the work of controlling the output.

6. Output (controlled variable): The quantity that must be maintained at a prescribed value.

7. Open-loop Control System: A system in which the output has no effect upon the input signal.

8. Feedback element: The unit that provides the means for feeding back the output quantity, or a function of the output, in order to compare it with the reference input.

9. Actuating Signal: The signal that is the difference between the reference input and the feedback signal. It actuates the control unit in order to maintain the output at the desired value.

10: Closed-loop Control System: A system in which the output has an effect upon the input quantity in such a manner as to maintain the desired output value.

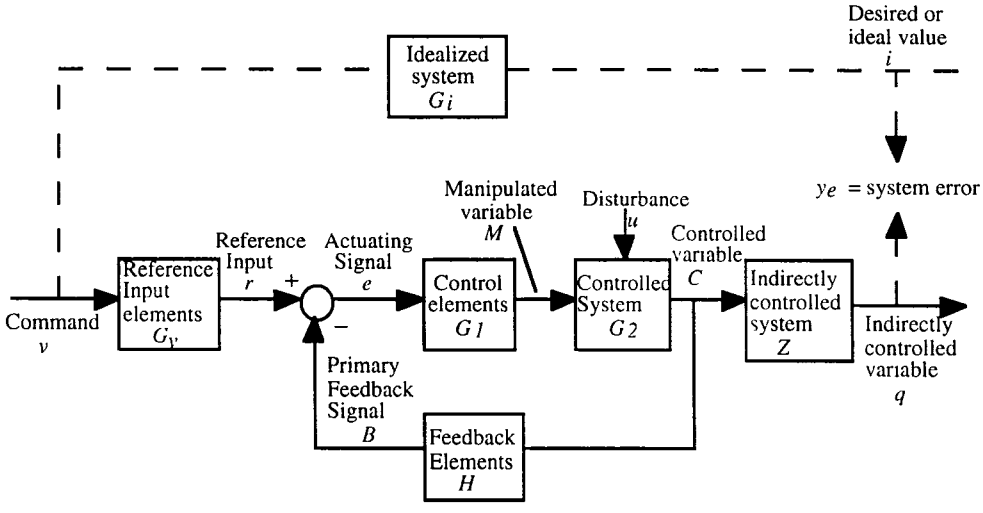

Figure A-1 Block Diagram of Feedback Control System Containing all Basic Elements

Appendix B

Eight Pole Butterworth Frequency and Step Response

The low-pass filter used for anti-aliasing and noise reduction in the system design is an eight-pole butterworth filter. The theoretical response is given in Fig. B-1 [Active 1986].

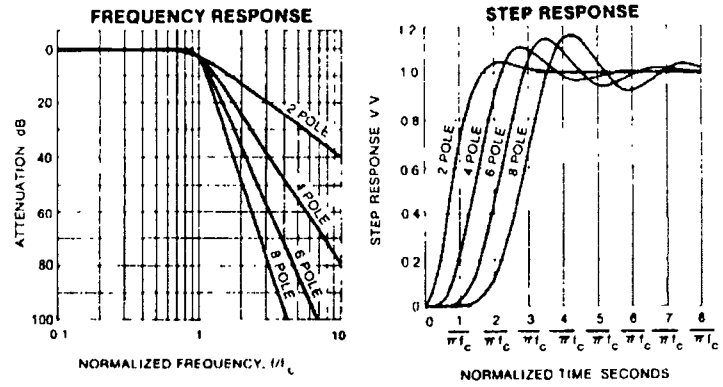

NORMALIZED FREQUENCY RESPONSE TABLE

f/f_c	2 POLE		4 POLE		6 POLE		8 POLE	
	A(dB)	ψ(°)	A(dB)	ψ(°)	A(dB)	ψ(°)	A(dB)	ψ(°)
0.00	0 00	0 0	0 00	0.0	0.00	0 0	0 00	0.0
0.10	0 00	-8 1	0 00	-15.0	0 00	-22.0	0 00	-29.4
0 20	0 01	-16.4	0 00	-30.1	0 00	-44 5	0 00	-59.0
0 30	0 04	-25.0	0 00	-45 5	0 00	-67 2	0 00	-89.1
0.40	0 11	-34.0	0.00	-61.4	0.00	-90 4	0 00	-119.8
0 50	0 26	-43 3	0 02	-78 0	0 00	-114 5	0.00	-151.7
0.60	0.53	-53 0	0 07	-95.7	0.01	-140.0	0.00	-185.0
0 65	0.71	-57 9	0 14	-105 1	0.02	-153 4	0 00	-202 6
0.70	0.93	-62 7	0.24	-114.9	0.06	-167.5	0 01	-220.9
0 75	1 19	-67 6	0 41	-125 2	0 14	-182.4	0.04	-240 2
0.80	1.49	-72 3	0 67	-135 9	0 29	-198 2	0 12	-260 8
0.85	1 82	-77 0	1 05	-146.9	0.58	-215.2	0 31	-283 2
0.90	2.19	-81 5	1.55	-158.1	1.08	-233.1	0 74	-307.4
0.95	2 59	-85 8	2 21	-169 2	1 88	-251 6	1 59	-333.5
1 00	3 01	-90 0	3 01	-180 0	3 01	-270 0	3 01	-360.0
1 10	3 92	-97 7	4 97	-199.9	6 17	-303.6	7 48	-407 9
1.20	4 88	-104 5	7.24	-216 8	9.96	-330 6	12 90	-444 5
1 30	5 86	-110 6	9 62	-230.8	13 86	-351 7	18 30	-472 1
1.40	6 85	-115 9	11 98	242 2	17 61	-368.4	23 40	-493 7
1 50	7 83	-120.5	14 25	-251.7	21 16	-382.0	28 18	-511 4
2 00	12 30	-136 7	24 10	-282 0	36 12	-425 5	48 16	-56[illegible] 3
2 50	16 03	-146 0	31.84	-298 6	47 75	-449 6	63 67	-60[illegible] ?
3 00	19 14	-152.1	38.17	-309 3	57 25	-465 2	76 34	-620 8
3 50	21 79	-156 3	43.53	-316 7	65.29	-476 1	87 05	-635 3
4 00	24 10	-159 3	48 16	-322 2	72.25	-484 2	96 33	-646 0
5.00	27 97	-163.6	55.92	-329 9	83 88	-495 5	111 84	-661 0
6 00	31 13	-166 4	62.25	-334 9	93.38	-503 0	124 50	-670 9
7 00	33 81	-168 3	67 61	-338 6	101 41	-508 3	135 22	-677 9
8 00	36.12	-169 8	72 25	-341 2	108 37	-512 3	144 49	-683 2
9 00	38 17	-171 0	76 34	-343 3	114 51	-515 4	152 68	-687 3
10.00	40 00	-171 9	80 00	-345 0	120 00	-517 8	160 00	-690 6

Figure B-1 Theoretical Butterworth Filter Response

References

"Active Filter Products Design and Selection Guide," Frequency Devices, 1986.

Agogino, A. M., et al., "Concept Database: A Design Information System for Concurrent Engineering with Application to Mechatronic Design," Proceedings fo the 1996 NSF Design and Manufacturing Grantees Conference, Alberquerque, New Mexico, 1996, P. 1-2.

Astrom, K. J., and Wittenmark, B., "Adaptivce Control," 2nd Edition, Addison-Wesley Publishing, 1995.

D'Azzo, J. J., C.H. Houpis, "Feedback Control System Analysis and Synthesis," McGraw-Hill Book Company, 1966.

Graeme, J.G., Tobey, G.E., Huelsman, L.P., "Operational Amplifiers Design and Applications," McGraw-Hill Book Company, 1971.

"HC11," M68HC11 Reference Manual, Motorola, 1990.

"How to Run a Lathe," South Bend Lathe, 1966.

Inman, D. J., "Engineering Vibration," Prentice-Hall, 1994.

Jaffe, B., W. R. Cook, H. Jaffe, "Piezoelectric ceramics," Academic Press London, 1971, P. 1-4.

Ko, W.F., "A Systems Engineering Approach to Design a Smart Tool Post Structure," M.S. Thesis, University of Maryland, 1995.

Kuo, B. C., "Automatic Control Systems," 4th Edition, Prentice-Hall, 1982.

Merchant, M.E., "Basic Mechanics of the Metlaal -Cutting Process," Journal of Applied Mechanics, Vol. 11, Transactions of the ASME, Vol. 66, 1944, P.A-168.

Merritt, H.E., "Theory of Self-Excited Machine-Tool Chatter'" Journal of Engineering for Industry, November 1965, P.447-454.

Phillips, C. L., Harbor, R. D., "Feedback Control Systems," 3rd Edition, Prentice Hall, 1996.

Rogers, C., "Intelligent Material Systems," Center for Intelligent Material Systems and Structures, 1992.

Tansel, I., "Simulation of Turning Operations," Journal of Machine Tools Manufacturing, Vol. 30, No. 4, 1990, P. 535-547.

Zhang, G.M., Yerramareddy, S., Lee, S.M., Lu, S. C-Y., "Simulation of intermittent Turning Processes," Journal of Dynamic Systems, Measurement, and Control, September 1991, P. 458-466.